TRIESKOVÉ A BEZTRIESKOVÉ OBRÁBANIE DREVA 2026

CHIP AND CHIPLESS WOODWORKING PROCESSES 2026

Vedecký časopis // Scientific journal

TECHNICKÁ UNIVERZITA VO ZVOLENE // TECHNICAL UNIVERSITY IN ZVOLEN
DREVÁRSKA FAKULTA // FACULTY OF WOOD SCIENCES AND TECHNOLOGY
KATEDRA OBRÁBANIA DREVA // DEPARTMENT OF WOODWORKING

TECHNICKÁ UNIVERZITA VO ZVOLENE // TECHNICAL UNIVERSITY IN ZVOLEN
DREVÁRSKA FAKULTA // FACULTY OF WOOD SCIENCES AND TECHNOLOGY
KATEDRA OBRÁBANIA DREVA // DEPARTMENT OF WOODWORKING

TRIESKOVÉ A BEZTRIESKOVÉ OBRÁBANIE DREVA 2026

CHIP AND CHIPLESS WOODWORKING PROCESSES 2026

Vedecký časopis // Scientific journal

drevársky kongres

ZVÄZ SLOVENSKÝCH VEDECKOTECHNICKÝCH SPOLOČNOSTÍ

Trieskové a beztrieskové obrábanie dreva - ISSN 1339-8350 (online)
je vedecký časopis uverejňujúci recenzované pôvodné vedecké práce, z oblasti technického a technologického výskumu trieskového delenie a obrábanie dreva, procesu tvorby triesky, kvality vytváraného povrchu a fyzikálno-mechanických vlastnostiach triesky. Súčasťou zamerania časopisu je i problematika termickej a hydrotermickej úpravy drevnej hmoty teplom a realizácie týchto procesov. Časopis vychádza s dvojročnou periodicitou v elektronickej a printovej forme.

Chip and chipless woodworking processes - ISSN 1339-8350 (online)
is a scientific journal publishing the reviewed original scientific works focusing on the technical and technological research of chip separation and wood processing, the process of making chips, the quality of created surface as well as the physico-mechanical chips characteristics. The journal focuses also on the issue of thermal and hydrothermal modification of the wood pulp by heat and how these processes are realized. The journal is published in a twoyear periodicity in an electronic and a print form.

Redakcia/Editorial office
Technická univerzita vo Zvolene/ Technical university in Zvolen
Drevárska fakulta/ Faculty of Wood Sciences and Technology
Katedra obrábania dreva/ Departmen of Woodworking
T. G. Masaryka 24
960 01 Zvolen

Vydavateľ/Publisher
Technická univerzita vo Zvolene/Technical university in Zvolen,
T. G. Masaryka 24
960 01 Zvolen, IČO 00397440, 2026
Rozsah (Pages) 153 strán
Vydanie I. – september
Periodikum s periodicitou raz za dva roky. Za vedeckú úroveň tejto publikácie zodpovedajú autori.

ISSN 1339-8350 (online)

CONTENTS

ADAMČÍK Lukáš – HALIM Engindzhan:
Study of kerf depth in CO_2 laser cutting of solid beech wood 7

ADAMČÍK Lukáš – KMINIAK Richard – BANSKI Adrián:
Mechanisms of surface irregularities in CNC-milled SOLID wood and wood composite materials 15

BANSKI Adrián – NEMEC Lukáš – ŠUSTEK Ján:
Color homogenization of pine wood by pressure steaming 21

BEDNÁROVÁ Dagmara – MORAVČÍKOVÁ Bianka – IGAZ Rastislav – ŠUSTEK Ján – RICHVALSKÁ Jana – SCHMIDTOVÁ Jarmila – NĚMEC Miroslav:
Evaluation of Noise Exposure and Cutting-Zone Temperature in CNC processing of PLYWOOD 29

BORYSIUK Piotr – KOZAKOW Aleksy – PŁATKOWSKI Mikołaj – DANECKI Leszek – SUMIONKA Mikołaj – AURIGA Radosław:
Expanded Plant-Based Materials as Fillers for Lightweight Particleboards 35

DUDIAK Michal – BANSKI Adrián:
The effect of steaming on the acidity of pine wood 45

DZURENDA Ladislav – DUDIAK Michal:
Hardness of steamed beech sapwood and false heartwood determined by Leeb hardness tester ISH-SPHA 55

DZURENDA Ladislav – DUDIAK Michal:
Activation energy value of the color unification of beech sapwood and false heartwood in the steaming process 61

GEJDOŠ Miloš – LIESKOVSKÝ Martin – TOMČÍK Daniel:
Airborne Particulate Emissions from Woodchip Handling: Implications for Worker Safety in Biomass-Based Heating Plants 67

HANINCOVÁ Luďka – PROCHÁZKA Jiří – NOVÁK Vít – KYSELKA David:
Relationship between cutting forces and surface roughness in edge milling of particleboard 75

KUBOVSKÝ Ivan – KÚDELA Jozef – ANDREJKO Michal:
The influence of CO_2 laser engraving parameters on colour changes of wood surface 81

MICHALAK Dorota – PRAŁAT Barbara – WIADEREK Krzysztof – ROGOZIŃSKI Tomasz:
Working time utilization in upholstered furniture manufactoring 89

OČKAJOVÁ Alena – KUČERKA Martin – DADO Miroslav:
Effectiveness of wood dust extraction system of hand-held belt sander 95

SHARMA Varun – CHUCHALA Daniel:
Effect of feed speed on immediate spring back in densified wood surface 103

ŠUGÁROVÁ Veronika – ADAMČÍK Lukáš – KMINIAK Richard:
Methodology for quantifying edge delamination in CNC milling of plywood 109

VILKOVSKÁ Tatiana – KLEMENT Ivan – VILKOVSKÝ Peter:
Analysis of the effect of drying conditions and hygrothermal treatment on the processing of beech blanks containing reaction wood 121

WIADEREK Krzysztof – PRAŁAT Barbara – MICHALAK Dorota – ROGOZIŃSKI Tomasz:
Digital transformation as a driver of technological process modernization in furniture manufacturing 133

RUŽIAK Ivan – KUBOVSKÝ Ivan – GAJTANSKA Milada – KMINIAK Richard – ŠTEFANČIN Lukáš – ADIJANS Imants – DER Oguzhan – TODARO Luigi – LO-GIUDICE Valentina – TUDOR Eugenia Mariana
Energy density of CO_2 laser cutting leading to acceptable kerf taper of spruce, beech and oak wood 139

DARABOŠOVÁ Anna – BUBENÍKOVÁ Tatiana – ČABALOVÁ Iveta:
Thermal influence on VOC emissions from particleboards incorporating recycled plastic waste 147

AREKO

... dodávateľ najvyššej kvality...

... sme tu pre Vás viac ako 30 rokov...

MERACIA TECHNIKA A SNÍMAČE

... univerzálna meracia technika
... presná digitálna technológia snímačov
... spoľahlivé kezkontaktné pyrometre
... bezdrôtové a IoT technológie
... riešenie všetkých meracích aplikácií

ROBOTIKA A PRIEMYSELNÁ AUTOMATIZÁCIA

... riešenia a realizácie „na kľúč“
... vizuálna kontrola kvality
... aplikácie v rôznych priemyselných odvetviach
... odborné poradenstvo a servis
... simulácie a testovanie

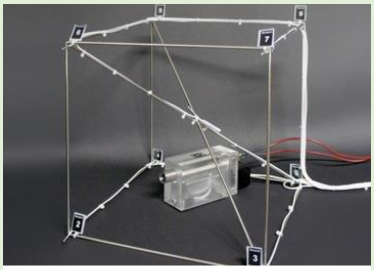

AKREDITOVANÉ KALIBRAČNÉ LABORATÓRIUM

... akreditácia podľa normy ISO/IEC 17025:2018
... kalibrované veličiny: teplota, vlhkosť, tlak, objem
... odborné akreditované merania
... validácia skladových priestorov
... kalibrácia klimatických komôr
... odborné poradenstvo a konzultácie

PROTIKORÓZNA OCHRANA

... striekané polyuretánové protikorózne materiály
... viskózno-elastické protikorózne hmoty
... zariadenia na povrchové úpravy potrubí
... plynovody, ropovody produktovody, armatúry
... rehabilitácia potrubných línií
... poradenstvo v oblasti protikoróznej ochrany

AREKO, s.r.o.
Tomanova 35, 831 07 Bratislava – Vajnory
www.areko.sk

STUDY OF KERF DEPTH IN CO_2 LASER CUTTING OF SOLID BEECH WOOD

Lukáš Adamčík[1] – Engindzhan Halim[2]

Abstract
This paper presents the results of experimental investigations into the variation in kerf depth (z_{max}) during laser cutting of solid beech wood (Fagus sylvatica L.) using a universal ZnSe lens with a focal length of F = 50.8 mm, suitable for detailed laser engraving and cutting up to 10 mm. The experiments were conducted on a CO_2 laser machine, AEON MIRA 9, at three laser beam power levels (P = 30 W, 60 W, 90 W), three feed rates (v_f = 9 mm.s^{-1}, 11 mm.s^{-1}, 13 mm.s^{-1}), and three focal point positions relative to the surface of the processed material (ΔF = -2 mm, 0 mm, 2 mm). A Keyence VHX–7000 digital microscope was used to determine the kerf depth (z_{max}) and the kerf widths ($s_1 - s_2$) of the experimental specimens.
It was established that the laser beam power (P) had the strongest effect on kerf depth (z_{max}), followed by the focal point position (ΔF) and the feed rate (v_f). The obtained mathematical model can be used to predict kerf depth (z_{max}) and to optimize technological parameters in CO_2 laser cutting of solid beech wood (Fagus sylvatica L.).

Key words: *CO2 laser cutting, kerf depth, solid beech wood, cutting parameters, ANOVA, digital microscope*

INTRODUCTION
CO_2 laser cutting is a modern, chipless machining process widely used for processing solid wood and a variety of other materials, including plywood, particleboard, acrylic (PMMA), textiles, and others. The process provides high cutting accuracy, a narrow kerf width, a high degree of automation, and minimal mechanical impact on the workpiece. The absence of tool wear and the need for tool sharpening represents a significant advantage over conventional cutting technologies. Despite these advantages, the quality of the machined surface and the kerf geometry (width and depth) are strongly influenced by the selected processing parameters as well as by the anatomical structure of the wood itself.
Solid wood species such as beech (*Fagus sylvatica* L.), oak (*Quercus robur*.), Norway spruce (*Picea abies*), and aspen (*Populus tremula*), among others, have attracted considerable interest in CO_2 laser cutting research. In the furniture industry, solid beech wood (*Fagus sylvatica* L.) is increasingly preferred for both structural and decorative components due to its favorable mechanical and aesthetic properties. Owing to its relatively high density and homogeneous diffuse-porous structure, beech wood may respond differently to CO_2 laser cutting than softwoods or other hardwood species with ring-porous anatomical structures.

[1] Technical University in Zvolen, T. G. Masaryka 24, 960 01 Zvolen
e-mail: lukas.adamcik@tuzvo.sk
[2] Department of Woodworking Machines, University of Forestry, Sofia, Bulgaria,
e-mail: e_halim@ltu.bg

Previous studies (Gochev et al. 1994; Gochev 1996; Gochev et al. 1996; Dinkov et al. 1996; Gurau et al. 2017, 2024; Kúdela et al. 2020, 2022, 2024; Adamčík et al. 2023, 2025; Halim et al. 2025) have demonstrated that the outcome of laser processing of wood and wood-based materials depends not only on the laser beam power (*P*), but also on the feed/scanning speed (v_f), the focal position relative to the workpiece surface (ΔF), the energy input per unit area, the material density, and other processing- and material-related factors.

In laser cutting, kerf depth (z_{max}) is one of the primary indicators of process efficiency. It is directly related to the amount of absorbed laser energy and the interaction time between the laser beam and the wood. A lower feed rate (v_f) increases the interaction time and generally results in greater material removal; however, it may also lead to more severe charring and increased irregularities along the kerf walls. Conversely, a higher feed rate (v_f) reduces the thermal input but may limit the achievable kerf depth (z_{max}). Adamčík et al. (2023) reported that, during CO_2 laser cutting, surface irregularities increase with increasing laser beam power and decreasing feed rate. Laser processing induces not only geometric changes but also significant physicochemical modifications in wood. In CO_2 laser engraving of beech wood, substantial surface darkening, a reduction in lightness (L*), and changes in the chemical structure of lignin and hemicelluloses, particularly in carbonyl (C=O) functional groups, have been reported. These findings indicate that laser irradiation promotes thermal degradation and the formation of new chromophoric structures, thereby explaining the observed darkening and charring of the processed zone (Jurek et al. 2021; Kúdela et al. 2024). Regarding surface roughness, the findings of several studies (Gurau et al. 2007; Eltawahni et al. 2011, 2013; Rezaei et al. 2022; Adamčík et al. 2023) demonstrate that both the feed rate (v_f) and the laser beam power (*P*) have a significant influence on the surface roughness of laser-machined materials.

Establishing the relationship between laser beam power (*P*), feed rate (v_f), focal position (ΔF), and the resulting kerf depth (z_{max}) would facilitate process optimization to achieve sufficient cutting depth while minimizing charring and maintaining acceptable kerf wall quality. This is particularly important in the machining of solid wood, where the anatomical structure, material density, and thermal behavior have a significant influence on the efficiency and quality of the CO_2 laser cutting process.

MATERIAL AND METHODS

For the experimental investigation, specimens of solid beech wood (*Fagus sylvatica* L.) with dimensions of h = 15 mm, b = 20 mm, l = *200* mm were prepared (Fig. 1A, B). The specimen width and length were selected to ensure optimal material yield from pre-calibrated and sanded beech boards used as the raw material. The wood moisture content, maintained at 8–10%, corresponds to the equilibrium moisture content commonly encountered in the furniture industry. Moisture content was determined using a digital moisture meter (Model MD, China) with a measurement range of 5% to 50% for wood.

The experiments were conducted using an AEON MIRA 9 CO_2 laser cutting and engraving machine (China) with a maximum output power of 100 W. A universal ZnSe lens with a focal length of F = 50.8 mm, suitable for precision laser engraving and cutting of materials up to 10 mm in thickness, was employed. The cutting path was generated using the LightBurn software. For each combination of the experimental design matrix (Table 2), three kerfs were produced on the solid beech wood (*Fagus sylvatica* L.) specimens
(Fig. 1B). The kerf measurements were subsequently averaged, and the arithmetic mean was used for further analysis.

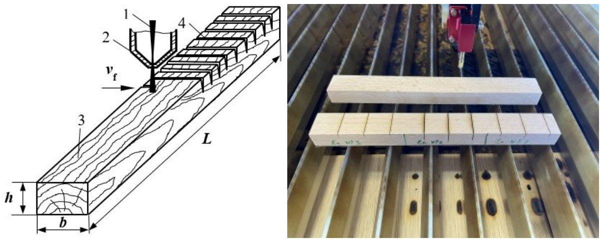

A B

Figure 1. *Experiment scheme: 1 – laser beam, 2 – laser head, 3 – material, 4 – kerf; L – length; b – width; h – thickness*

The values of the independent variables—focal position relative to the workpiece surface (ΔF, mm), laser beam scanning (feed) rate (V_f , mm.s^{-1}), and laser beam power (P, W) – in both actual and coded form are presented in Table 1. The design matrix of the three-factor experiment is shown in Table 2. The experimental data were evaluated using analysis of variance (ANOVA) according to the methodology described by Vuchkov et al. (1986), implemented in the QStatLab statistical software.

Table 1. *Values of variable factors ΔF, v_f u P*

Variable factors	Minimum value		Average value		Maximum value	
	Open form	Coded form	Open form	Open form	Coded form	Open form
Focus position $\Delta F = x_1$ [mm]	-2	-1	0	0	2	1
Laser beam feed rate $V_f = x_2$ [mm.s^{-1}]	9	-1	11	0	13	1
Laser beam power $P = x_3$ [W]	30	-1	60	0	90	1

Table 2. *Plan for conducting a three-factor experiment*

Exper. №	**Variable factors**					
	$x_1 = \Delta F$, mm		**$x_2 = v_f$, mm.s^{-1}**		**$x_3 = P$, W**	
1	-	-2	-	9	-	30
2	-	-2	-	9	+	90
3	-	-2	+	13	-	30
4	-	-2	+	13	+	90
5	+	2	-	9	-	30
6	+	2	-	9	+	90
7	+	2	+	13	-	30
8	+	2	+	13	+	90
9	-	-2	0	11	0	60
10	+	2	0	11	0	60
11	0	0	-	9	0	60
12	0	0	+	13	0	60
13	0	0	0	11	-	30
14	0	0	0	11	+	90
15	0	0	0	11	0	60
16	0	0	0	11	0	60
17	0	0	0	11	0	60
18	0	0	0	11	0	60
19	0	0	0	11	0	60
20	0	0	0	11	0	60

After a total of 60 kerfs had been produced, they were scanned using a Keyence VHX-7000 digital microscope (Keyence Corporation, Osaka, Japan). For each kerf, the depth (z_{max}) and widths ($s_1 - s_2$), as shown in Fig. 2, were measured.

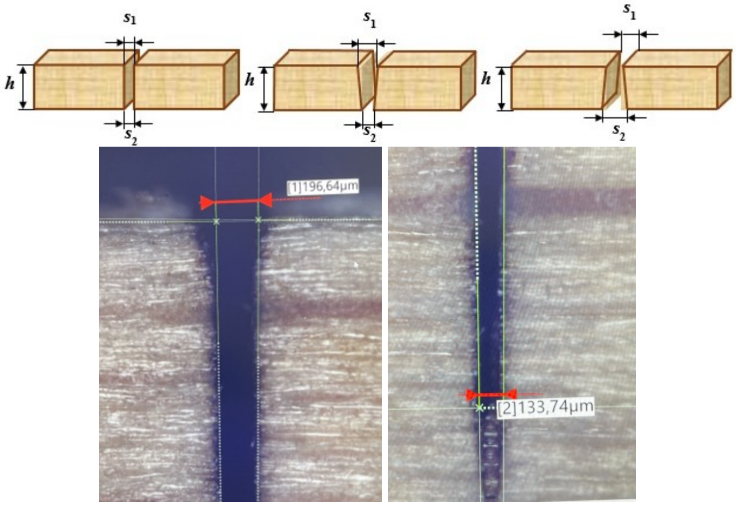

Figure 2. *Schematic representation of the geometric parameters of the kerf*

RESULTS

Table 3 presents the arithmetic mean values of the kerf depth (z_{max}) and kerf widths ($s_1 - s_2$) obtained for all experimental runs according to the three-factor experimental design matrix (Tables 1 and 2).

Table 3. *Results obtained for Z_{max}, S_1 and S_2*

Exper. №	Average, Z_{max}, **mm**	Average, S_1, **mm**	Average, S_2, **mm**
1	4,20	0,22	0,12
2	9,30	0,34	0,18
3	3,23	0,17	0,08
4	7,87	0,29	0,10
5	2,69	0,63	0,21
6	7,07	0,83	0,16
7	1,72	0,66	0,09
8	3,62	0,64	0,14
9	6,77	0,29	0,11
10	4,71	0,81	0,13
11	7,35	0,46	0,13
12	6,00	0,42	0,10
13	2,73	0,40	0,17
14	7,60	0,49	0,20
15	6,69	0,46	0,18
16	6,10	0,51	0,21
17	7,68	0,50	0,23
18	8,92	0,49	0,21
19	8,51	0,49	0,20
20	7,11	0,43	0,21

As a result of the three-factor experimental study conducted to evaluate the effects of the focal position relative to the workpiece surface (ΔF, mm), laser beam scanning (feed) rate (V_f, mm.s^{-1}), and laser beam power (P, W) on the maximum kerf depth (z_{max}) during CO_2 laser cutting of solid beech wood (*Fagus sylvatica* L.), a second-order quadratic regression model (Equation 1) was developed. The model includes linear terms, quadratic effects, and two-factor interaction terms. The resulting regression equation is expressed as follows:

$$Y = 7{,}1546 - 1{,}156x_1 - 0{,}817x_2 + 2{,}089x_3 - 0{,}894x_1^2 + 0{,}0409x_2^2 - 1{,}469x_3^2 - 0{,}2525x_1x_2 - 0{,}3675x_2x_3 - 0{,}4325x_1x_3 \quad (1)$$

where:
Y – Predicted kerf depth in coded form (z_{max}), mm;
x_1 – Focus position in coded form ΔF, mm;
x_2 – Laser beam feed rate in coded form V_f, mm.s^{-1};
x_3 – Laser beam power in coded form P, W.

The analysis of variance presented in Tables 4 and 5 indicates that the model is statistically significant at a significance level of $\alpha = 0.05$. The coefficient of determination (R^2) shows that approximately 90.6% of the variation in the maximum kerf depth (z_{max}) is explained by the factors included in the model.

Table 4. *Summary of Results for Solid Beech Wood (Fagus sylvatica L.)*

Source	Sqr. sum	DOF	Variance	F	P
Model	88,86186	9	9,87354	10,70837	0,00047
Residual	9,22039	10	0,92204		
Total	98,08226	19			

Table 5. *Analysis of Variance (ANOVA) for Solid Beech Wood (Fagus sylvatica L.)*

T(0,025,10) = 2,22814	F(0,050,9,10) = 3,02038	
Residual StDev = 0,96023	R-sq = 0,90599	Radj-sq = 0,82139
PRESS = 32,82324	R-sq(pred) = 0,66535	

The analysis of the regression coefficients (Equation 1) revealed that the linear effects of all three investigated factors are statistically significant. Among them, laser beam power (P) exhibited the strongest influence on kerf depth (z_{max}) (Fig. 3A), as indicated by its positive regression coefficient with the largest absolute value ($x_3 = 2.089$). This result demonstrates that increasing the laser beam power increases the energy input into the cutting zone, thereby producing a greater kerf depth. From a physical perspective, this finding is expected, since higher laser power increases the intensity of laser–material interaction, promoting heating, thermal degradation, charring, and vaporization of the wood material.
The focal position relative to the workpiece surface (ΔF) also had a statistically significant effect on kerf depth (z_{max}). The negative regression coefficient ($x_1 = -1.156$) indicates that shifting the focal position in the positive direction from the center level decreases the kerf depth, as illustrated in Fig. 3B. This behavior can be attributed to changes in the laser spot diameter, resulting in a reduction in energy density at the material surface and within the cutting zone. When the focal position deviates from its optimum, the laser beam is unable to concentrate its maximum energy at the cutting zone, thereby reducing the efficiency of the ablation process and consequently decreasing the kerf depth.

As shown in Fig. 3C, increasing the laser beam scanning (feed) rate (V_f) results in a decrease in kerf depth (z_{max}). This behavior is consistent with the expected physical mechanism, as a higher scanning speed reduces the interaction time between the laser beam and the material. Consequently, less energy is delivered per unit length of the kerf, limiting the extent of thermal degradation and material removal, and resulting in a shallower kerf.

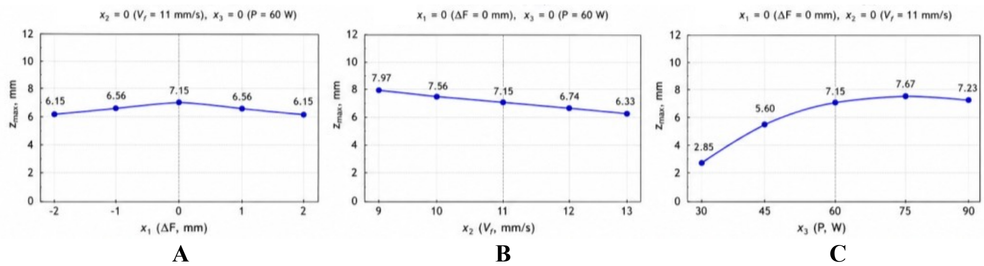

Figure 3. *Variation in kerf depth (z_{max}) as a function of (A) the focal position relative to the workpiece surface (ΔF), (B) the laser beam scanning (feed) rate (V_f), and (C) the laser beam power (P) for solid beech wood (Fagus sylvatica L.) specimens.*

CONCLUSION

1. Laser beam power (*P*) exerted the greatest influence on kerf depth (z_{max}), with increasing power resulting in a substantial increase in kerf depth. The statistically significant quadratic effect of laser power indicates a nonlinear relationship and the existence of an optimal operating range, beyond which further increases in power do not produce a proportional increase in kerf depth.
2. The laser beam scanning (feed) rate (V_f) and the focal position (ΔF) exhibited statistically significant linear effects on the maximum kerf depth (z_{max}). An increase in the feed rate reduced the kerf depth because of the shorter interaction time between the laser beam and the material, whereas proper positioning of the focal point ensured a higher energy density at the cutting zone, resulting in more efficient laser penetration into the wood.
3. The optimal conditions for achieving the maximum kerf depth (z_{max}) in solid beech wood (*Fagus sylvatica* L.) were obtained at a focal position of $\Delta F \approx -1.5$ mm, a feed rate of $V_f = 9$ mm.s^{-1}, and a laser beam power of $P \approx 88$ W. Under this combination of parameters, the model predicted a maximum kerf depth of approximately 9.5 mm, which is in close agreement with the maximum experimentally measured value of 9.3 mm.

REFERENCES

1. Adamčík, L., Igaz, R., Štefančin, L., Kubovský, I., & Kminiak, R. (2023). *Evaluation of the Surface Irregularities of the Cross-Section of the Wood after CO_2 Laser Cutting*. **Materials, 16**, 7175. https://doi.org/10.3390/ma16227175
2. Adamčík, L., Kminiak, R., Kyselica, K., Igaz, R., & Kubovský, I. (2025). *Optimisation of CO_2 Laser Technological Parameters and Their Impact on the Surface Quality of Cut Wood*. **Forests, 16**(5), 785. https://doi.org/10.3390/f16050785

3. Dinkov, B., Gochev, Zh., & Barnekov, V. (1996). *Optimizing the Influence of Main Factors for the Formation of Cutting Kerf in the Interaction of a Laser Beam with Wood and Wood-Based Materials*. In **Proceedings of the International Scientific Conference**, University of Forestry, Section Mechanical Technology of Wood (November 21–23, 1996, Sofia, Bulgaria) (pp. 305–311). Publishing House at the University of Forestry. (in Bulgarian)

4. Eltawahni, H. A., Olabi, A. G., & Benyounis, K. Y. (2011). *Investigating the CO_2 Laser Cutting Parameters of MDF Wood Composite Material*. **Optics & Laser Technology, 43**, 648–659.

5. Eltawahni, H. A., Rossini, N. S., Dassisti, M., Alrashed, K., Aldaham, T. A., Benyounis, K. Y., & Olabi, A. G. (2013). *Evaluation and Optimization of Laser Cutting Parameters for Plywood Materials*. **Optics and Lasers in Engineering, 51**, 1029–1043.

6. Gochev, Zh. (1996). *Investigation of the Laser Cutting Process of Furniture Details from Wood Particle Boards*. PhD thesis, University of Forestry, Sofia, Bulgaria, 200 p. (in Bulgarian)

7. Gochev, Zh., & Dinkov, B. (1996). *Specific Cutting Energy in Interaction of a Laser Beam with Wood and Wood-Based Materials*. In **Proceedings of the International Scientific Conference**, University of Forestry, Section Mechanical Technology of Wood (November 21–23, 1996, Sofia, Bulgaria) (pp. 298–304). Publishing House at the University of Forestry.

8. Gotchev, J. V., Barnekov, B., & Dinkov, B. (1994). *Modeling the Laser Cutting of Particleboard*. In **Proceedings of the 2nd International Conference on Automated Lumber Processing Systems and Laser Machining of Wood and Composites** (pp. 71–81). Michigan State University, East Lansing, MI, USA.

9. Gurau, L., Angelescu, A. M., & Timar, M. C. (2024). *Surface Morphology and Chemical Changes of Maple and Beech Cut Through by CO_2 Laser Under Different Angles Relative to the Wood Grain*. **Forests, 15**(10), 1767. https://doi.org/10.3390/f15101767

10. Gurau, L., Petru, A., Varodi, A., & Timar, M. C. (2017). *The Influence of CO_2 Laser Beam Power Output and Scanning Speed on Surface Roughness and Colour Changes of Beech (Fagus sylvatica)*. **BioResources, 12**(4), 7395–7412.

11. Gurau, L., Williams, H. M., & Irle, M. (2007). *Separation of Processing Roughness from Anatomical Irregularities and Fuzziness to Evaluate the Effect of Grit Size on Sanded European Oak*. **Forest Products Journal, 57**, 110–115.

12. Halim, E., Gochev, Zh., & Vitchev, P. (2025). *Research on the Specific Cutting Energy of CO_2 Laser Beam Interaction with Solid Wood and Plywood*. In **Proceedings of the 33rd International Conference on Wood Science and Technology (ICWST 2025): Unleashing the Potential of Wood-Based Materials** (December 4–5, Zagreb, Croatia) (pp. 73–88). ISBN 978-953-292-094-9.

13. Jurek, M., & Wagnerová, R. (2021). *Laser Beam Calibration for Wood Surface Colour Treatment*. **European Journal of Wood and Wood Products, 79**(5), 1097–1107.

14. Kúdela, J., Kubovský, I., & Andrejko, M. (2020). *Surface Properties of Beech Wood after CO_2 Laser Engraving*. **Coatings, 10**(1), 77. https://doi.org/10.3390/coatings10010077

15. Kúdela, J., Kubovský, I., & Andrejko, M. (2022). *Influence of Irradiation Parameters on Structure and Properties of Oak Wood Surface Engraved with a CO_2 Laser*. **Materials, 15**(23), 8384. https://doi.org/10.3390/ma15238384

16. Kúdela, J., Kubovský, I., & Andrejko, M. (2024). *Discolouration and Chemical Changes of Beech Wood after CO_2 Laser Engraving*. **Forests, 15**(12). https://doi.org/10.3390/f15122211

17. Rezaei, F., Wimmer, R., Gaff, M., Gusenbauer, C., Frybort, S. F., Sethy, A. K., Corleto, R., Ditommaso, G., & Niemz, P. (2022). *Anatomical and Morphological Characteristics of Beech Wood after CO_2-Laser Cutting*. **Wood Material Science & Engineering, 17**, 459–468.

18. Vuchkov, I., & Stoyanov, S. (1986). *Mathematical Modelling and Optimization of Technological Objects*. Tehnika, Sofia, 341 p. (in Bulgarian).

CHIP AND CHIPLESS WOODWORKING PROCESSES, 15(1): 15–20, 2026
Zvolen, Technical University in Zvolen, ISSN 1339-8350 (online)

MECHANISMS OF SURFACE IRREGULARITIES IN CNC-MILLED SOLID WOOD AND WOOD COMPOSITE MATERIALS

Lukáš Adamčík – Richard Kminiak – Adrián Banski

Abstract

This study investigates the influence of feed speed and rotational speed on the surface quality of CNC-milled solid wood (spruce, oak, and beech wood) and birch plywood. Milling experiments were performed on a 5-axis CNC machining centre using a solid carbide spiral mill. Surface roughness was evaluated with a Keyence VHX-7000 digital microscope, complemented by microscopic observations of machining defects. Feed speed was identified as the dominant factor affecting surface irregularities, whereas higher rotational speeds generally improved the machined surface. Microscopic analysis revealed that protruding fibres, cutter marks, and material anatomy were the primary sources of surface defects.

Key words: *surface roughness; microscopic analysis; CNC milling; solid wood; VHX-7000*

INTRODUCTION

CNC milling of solid wood and wood-based materials is widely used in modern manufacturing. Surface quality can be evaluated from both macroscopic and microscopic perspectives, as machining defects reduce the aesthetic appearance and functional performance of the final product. Macroscopic defects mainly include fibre tear-out, splintering, and delamination, particularly in plywood and laminated wood-based materials (Babu et al., 2015). Their occurrence depends on several factors, including tool geometry, milling strategy, fibre orientation, feed speed, rotational speed, feed per tooth, and the mechanical properties of wood such as density, hardness, and anisotropy (Garrido et al., 2024). At the microscopic level, machining quality is characterised by surface irregularities, including roughness and waviness. Typical milling defects include kinematic tool marks, local fibre tearing, and surface fuzziness (Brenci and Gurău, 2024). Numerous studies have shown that feed speed is a dominant technological factor affecting surface roughness and waviness, primarily through its influence on feed per tooth (Aykac and Sofuoglu, 2021; Gochev, 2018; Pinkowski et al., 2024). Increasing feed per tooth generally increases surface roughness. Rotational speed usually has the opposite effect by improving surface quality through higher cutting speeds (Demir et al., 2022), although excessive rotational speeds may increase vibration and consequently worsen the machined surface (Vitchev and Gochev, 2018).
The present study investigates the influence of feed speed and rotational speed on the surface roughness and waviness of spruce, oak, and beech during CNC milling. Besides

Technical University in Zvolen, T. G. Masaryka 24, 960 01 Zvolen
e-mail: lukas.adamcik@tuzvo.sk

evaluating selected roughness and waviness parameters, microscopic analysis is used to identify the dominant machining defects.

MATERIAL AND METHODS

Sample preparation

The experiment was conducted on two groups of wood materials: native wood and plywood. Native wood was represented by Norway spruce (*Picea abies* L.), European beech (*Fagus sylvatica* L.), and oak wood (*Quercus robur* L.), representing softwood, diffuse-porous hardwood, and ring-porous hardwood, respectively. In addition, 13-layer birch plywood (18 mm thickness, BB quality) was included to compare the influence of machining parameters on a wood-based composite material. The plywood panels (1525 mm × 1525 mm) were conditioned until reaching an equilibrium moisture content of approximately 8 – 10%. Solid wood boards were kiln-dried (12 ± 3%) and conditioned to an equilibrium moisture content of approximately 9%. Test specimens measuring 20 mm × 70 mm × 400 mm were prepared from solid wood and 18 × 70 × 400 mm from plywood.

CNC milling of the samples

CNC milling was performed on a 5-axis SCM Tech Z5 machining centre (SCM Group, Rimini, Italy). A Klein T143 solid carbide finishing spiral end mill (Sistemi S.r.l., Pesaro, Italy) with a diameter of 20 mm, three cutting edges, and a positive helix was used throughout the experiment. The positive helix promoted upward chip evacuation and improved the quality of the machined edge. Finishing milling was performed in climb-cutting mode with a radial depth of cut of 1 mm. A full factorial design was applied with two machining factors: feed speed (10 $m \cdot min^{-1}$, 14 $m \cdot min^{-1}$, and 18 $m \cdot min^{-1}$) and rotational speed (16,000 rpm and 20,000 rpm). Each combination was repeated six times for each wood species, resulting in 162 specimens.

Surface irregularities measurements

Before measurement, the machined surfaces were cleaned using compressed air to remove loose particles without affecting the surface morphology. Surface quality was evaluated using a Keyence VHX-7000 digital microscope (Keyence Corporation, Osaka, Japan), which enabled both three-dimensional optical surface measurement and microscopic observation of machining defects. Measurements were performed using λc = 2.5 mm and λs = 8 µm filters. For each specimen, five surface areas (2.5 mm × 18 mm) were scanned, and four profile traces were evaluated from every scanned image, resulting in twenty measurements per specimen.

RESULTS AND DISCUSSION

Surface irregularities measurements

Table 1 demonstrates that increasing rotational speed generally resulted in a significant reduction in surface roughness in both measurement directions, which is consistent with previous studies (Demir et al., 2022). This behaviour is primarily attributable to the reduction in feed per tooth as rotational speed increases. Consequently, the cutting load decreases, resulting in a smoother machined surface. (Pinkowski et al., 2024) observed that increasing rotational speed decreases chip thickness, leading to lower Ra values. At higher rotational speeds, finer and smaller chips are produced, which have been identified as another important factor contributing to improved surface finish. The formation of smaller chips promotes more gradual material removal and reduces the occurrence of pronounced surface irregularities. In addition, increasing rotational speed proportionally increases cutting speed, which has also been shown to reduce surface roughness (Yu et al. 2023a,b). According to the results in Table 1, the *R*a parameter decreased with increasing rotational speed and increased with increasing feed speed. The lowest values of these parameters were obtained at a rotational speed of 16,000 rpm and a feed speed of 10 $m \cdot min^{-1}$, whereas the highest values occurred at the same rotational speed with a feed speed of 18 $m \cdot min^{-1}$.

Table 1. Values of the surface roughness parameters of plywood at different feed speeds and rotational speeds (values in parentheses represent standard deviation)

Material	Feed Speed ($m \cdot min^{-1}$)	Rotational Speed (rpm)	*R*a (μm)	*R*z (μm)	*R*p (μm)	*R*v (μm)
Plywood	10	16,000	12.6	60.05	26.79	33.26
			(1.90)	(12.48)	(4.48)	(10.02)
Plywood	10	20,000	10.9	51.20	22.34	28.85
			(1.41)	(10.70)	(4.13)	(8.24)
Plywood	14	16,000	12.42	68.86	30.49	38.37
			(2.27)	(14.62)	(6.69)	(9.86)
Plywood	14	20,000	12.30	63.46	27.70	35.76
			(1.68)	(10.64)	(4.72)	(8.36)
Plywood	18	16,000	15.73	84.04	37.00	47.04
			(2.94)	(20.02)	(9.32)	(14.79)
Plywood	18	20,000	13.8	67.53	31.1	36.52
			(2.59)	(15.47)	(7.05)	(10.95)

The results presented in Table 2 indicate that the highest surface roughness was obtained for spruce wood at a rotational speed of 16,000 rpm and a feed speed of 18 $m \cdot min^{-1}$. This behaviour can be explained by the relatively low density of spruce, which promotes the formation of protruding fibres and surface fuzziness during CNC milling. The effect became increasingly evident at higher feed speeds, where roughness increased markedly. In contrast, the smoothest surface was achieved for oak wood at a feed speed of 10 $m \cdot min^{-1}$ and a rotational speed of 20,000 rpm. Denser wood species generally produced smoother machined surfaces. Accordingly, the measured roughness values followed the density of the investigated species, with oak exhibiting the lowest roughness, followed by beech and spruce. For all wood species, surface roughness increased with increasing feed speed, whereas a slight reduction was generally observed with increasing rotational speed. Statistical analysis confirmed that feed speed had a significant effect on surface roughness in most cases, while the influence of rotational speed was considerably weaker. The increase in roughness with feed speed is consistent with the fundamental principles of wood machining. Higher feed speeds result in a greater feed per tooth, causing each cutting edge to remove a larger volume of material and generating higher cutting forces. Consequently, the cutting tool is subjected to greater mechanical loading and vibration, which promotes the formation of more pronounced surface irregularities. This trend was reflected in both the *R*a and *R*z roughness parameters, indicating not only an increase in average roughness but also in the height of surface irregularities. Microscopic examination further revealed that higher feed speeds intensified machining marks and surface fuzziness, confirming these mechanisms as the dominant factors affecting surface roughness during CNC milling.

Table 1. Values of the surface roughness parameters of oak, beech, and spruce wood at different feed speeds and rotational speeds (values in parentheses represent standard deviation)

Material	Feed Speed ($m \cdot min^{-1}$)	Rotational Speed (rpm)	*R*a (µm)	*R*z (µm)	*R*p (µm)	*R*v (µm)
Oak	10	16,000	5.41 (1.98)	21.18 (6.40)	6.78 (1.89)	14.39 (4.71)
Oak	10	20,000	4.96 (2.07)	19.40 (7.93)	6.05 (2.06)	13.35 (6.29)
Oak	14	16,000	5.73 (1.81)	23.86 (7.48)	8.42 (2.33)	15.46 (5.33)
Oak	14	20,000	5.69 (1.82)	22.86 (7.19)	7.76 (2.34)	15.12 (5.36)
Oak	18	16,000	6.72 (1.43)	29.55 (8.31)	11.11 (2.47)	18.44 (6.38)
Oak	18	20,000	6.46 (1.77)	28.64 (9.87)	9.74 (2.66)	18.90 (7.86)
Spruce	10	16,000	5.55 (2.08)	23.34 (8.60)	9.80 (5.20)	13.63 (4.51)
Spruce	10	20,000	5.71 (1.92)	24.11 (8.12)	9.89 (4.75)	14.06 (4.41)
Spruce	14	16,000	7.78 (2.81)	36.08 (16.55)	15.81 (10.79)	20.14 (7.74)
Spruce	14	20,000	6.85 (2.23)	31.44 (12.24)	14.51 (8.74)	16.95 (4.80)
Spruce	18	16,000	8.19 (2.94)	37.66 (17.81)	16.75 (12.22)	20.93 (7.24)
Spruce	18	20,000	7.49 (2.98)	34.92 (16.81)	16.33 (11.36)	18.35 (7.55)
Beech	10	16,000	6.39 (1.29)	26.56 (4.73)	9.78 (2.58)	16.77 (3.11)
Beech	10	20,000	6.36 (1.87)	27.20 (8.05)	9.45 (3.05)	17.72 (5.56)
Beech	14	16,000	6.64 (1.41)	28.80 (5.59)	10.84 (2.75)	17.90 (3.71)
Beech	14	20,000	7.22 (1.39)	31.68 (5.84)	11.56 (2.83)	20.04 (4.28)
Beech	18	16,000	7.40 (1.53)	32.52 (6.64)	11.69 (3.10)	20.81 (4.54)
Beech	18	20,000	7.46 (1.56)	33.25 (6.39)	11.45 (2.63)	21.76 (4.56)

Microscopic analysis of the milled surface

Microscopic analysis confirmed the trends observed in the roughness measurements. Under the least favourable machining conditions (16,000 rpm and 18 $m \cdot min^{-1}$), the machined surfaces of solid wood and plywood were characterised by pronounced fuzziness, protruding fibres, and kinematic ripples produced by the cycloidal motion of the cutting edge (Fig. 1a – 1d). These defects explain the increase in *R*-parameters values and the deterioration of surface quality with increasing feed speed. Although higher rotational speed generally improves surface finish. In contrast, the combination of high rotational speed and low feed speed produced the smoothest surface, with fewer protruding fibres and reduced ripple height due to the lower feed per tooth. For spruce wood, microscopy revealed that the highest roughness resulted primarily from fibre pull-out and surface fuzziness. Consequently, spruce wood exhibited the highest roughness among all investigated materials due to surface fuzziness located in the earlywood zone. Oak wood showed lower surface roughness than beech despite the presence of characteristic earlywood vessels. Under unfavourable machining conditions, cutter marks and surface fuzziness were still visible; however, their intensity was lower than in beech wood, likely due to the higher density of oak wood. Under the optimal machining conditions (20,000 rpm and 10 m·min^{-1}), the characteristic ripples were substantially reduced, and tool marks became visible only under microscopic observation. In the case of plywood, the unevenness was mainly caused by the height difference between the cross and lengthwise veneers. It was also caused by the tearing of wood fibres from the cross veneer.

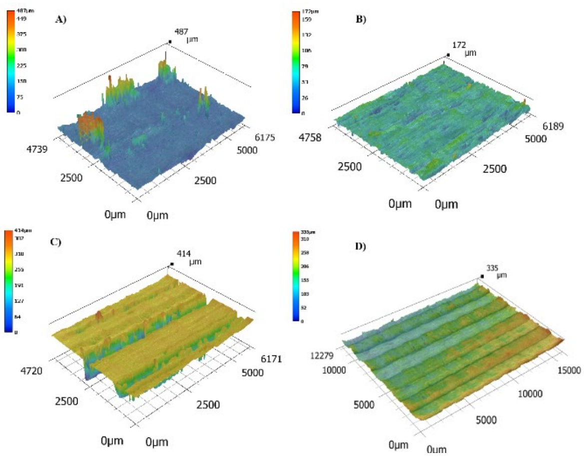

Fig. 1 Microscopic analysis of the milled surface of spruce wood (A), beech wood (B), oak wood (C), and plywood (D) at the feed speed of 18 m·min^{-1} and at the rotational speed of 16,000 rpm

CONCLUSION

This study investigated the effects of feed and rotational speeds on the surface roughness of CNC-milled spruce, beech, oak, and birch plywood. The results confirmed that feed speed was the dominant machining parameter affecting surface quality, while the influence of rotational speed was less pronounced within the investigated range. Increasing feed speed increased all evaluated roughness parameters due to higher feed per tooth, greater cutting forces, and more intensive formation of machining defects.

Microscopic analysis demonstrated that the deterioration of surface quality was mainly associated with kinematic tool marks, protruding fibres, and surface fuzziness. These defects were particularly pronounced in spruce, probably because of its lower density,

whereas oak produced the smoothest surfaces owing to its higher density and greater resistance to fibre deformation. For plywood, the measured roughness reflected the combined influence of surface fuzziness and height differences between longitudinal and transverse veneer layers, resulting in different behaviour of some amplitude parameters.
Overall, the combination of a low feed speed (10 $m \cdot min^{-1}$) and a high rotational speed (20,000 rpm) provided the best surface quality for all investigated materials. The findings contribute to a better understanding of the mechanisms responsible for the formation of surface irregularities during CNC milling and provide practical guidance for selecting machining parameters to improve surface quality in both solid wood and wood-based composite materials.

Acknowledgement:
This experimental research was prepared within the KEGA 015TU Z4/2025 project Creation of support tools for further and update training of workers in the woodworking industry for the needs of Industry 4.0.

REFERENCES

1. Aykac, E., Sofuoglu, S.D. (2021). Investigation of the Effect of Machining Parameters on Surface Quality in Bamboo. Tehnički vjesnik 28, 684–688. https://doi.org/10.17559/TV-20200102202928
2. 2. Babu, J., Philip, J., Zacharia, T., Davim, J.P. (2015). 5. Delamination in composite materials: measurement, assessment and prediction, in: Davim, J.P. (Ed.), Machinability of Fibre-Reinforced Plastics. De Gruyter, pp. 139–162. https://doi.org/10.1515/9783110292251-006
3. Brenci, L.-M., Gurău, L. (2024). A Stratified Characterization of Surface Quality of Beech Processed by Profile Milling. Applied Sciences 14, 129. https://doi.org/10.3390/app14010129
4. Demir, A., Cakiroglu, E.O., Aydin, I. (2022). Effects of CNC Processing Parameters on Surface Quality of Wood-Based Panels Used in Furniture Industry. Drv. ind. (Online) 73, 363–371. https://doi.org/10.5552/drvind.2022.2109
5. Garrido, N., Martins, J., Davim, J.P., Carvalho, L. (2024). Influence of machining parameters on edge quality of particleboards: modeling and optimization. Int J Adv Manuf Technol 133, 5463–5482. https://doi.org/10.1007/s00170-024-14033-5
6. Gochev, Z. (2018). Examination the Process of Longitudinal Solid Wood Profile milling. Part II: Influence of the Revolution Frequency and Feed Rate on the Roughness of the Treated Surfaces. Innovations in Woodworking Industry and Engineering Design 5, 48–54.
7. Pinkowski, G., Piernik, M., Wołpiuk, M., Krauss, A. (2024). Effect of chip thickness and tool wear on surface roughness and cutting power during up-milling wood of different density. BioRes 19, 9234–9248. https://doi.org/10.15376/biores.19.4.9234-9248
8. Vitchev, P., Gochev, Z. (2018). Study on quality of milling surfaces depending on the parameters of technological process, in: Implementation of Wood Science in Woodworking Sector. Presented at the 29th ICWST International Conference on Wood Science and Technology, University of Zagreb - Faculty of Forestry, Zagreb, pp. 195–201.

COLOR HOMOGENIZATION OF PINE WOOD BY PRESSURE STEAMING

Adrián Banski – Lukáš Nemec – Ján Šustek

Abstract
*This study evaluates the color homogenization of pine (Pinus sylvestris L.) sapwood and heartwood pressure steaming. Lumber was treated at 105°C and 120 °C for 6 and 18 h, and evaluated using the color space CIE L*a*b*. Both parameters significantly affected all color coordinates, with temperature being the dominant factor. Steaming accelerated darkening and increased redness (a*). Mode I (105°C) at 18h proved optimal for visual homogenization. At this point, the lightness confidence intervals of sapwood (71.0 ± 0.9) and heartwood (73.9 ± 1.5) overlap, rendering the macro-anatomical boundary indistinguishable to the human eye. Due to different chemical sensitivities, customized industrial control is essential for uniform surface quality.*

Key words: pine wood, sapwood, heartwood, saturated water steam, color wood, total color difference

INTRODUCTION

Pine wood (*Pinus sylvestris* L.) represents a cornerstone raw material for the European woodworking sector. Its widespread industrial utilization is driven not only by its abundance within our climatic zone, but also by its distinct microstructural and chemical attributes (Fengel – Wegener, 2003). These properties render it an excellent substrate for advanced technological processing and surface treatment applications. Within the coating industry, pine serves as an essential model for investigating the interactions between natural wood texture and rigorous industrial specifications. The macroscopic architecture of pine wood is defined by a sharp anatomical differentiation between the sapwood and heartwood zones (Fengel and Wegener, 2003; Rowell 2012). While the sapwood exhibits high permeability, making it ideal for deep impregnation, the heartwood region is characterized by the accumulation of secondary metabolites (Hill 2006; Ekeberg *et al.,* 2006). This elevated concentration of resins and hydrophobic extractives within the core forms a natural diffusion barrier, which substantially alters sorption behavior and can compromise the adhesion of coating systems (Budakçı *et al.,*2019; Bergström 2003).

The density and distinctive structural pattern of the pine matrix dictate both the aesthetic value of the surface and its optical permanence. Reflectance and color fastness are directly governed by the photochemical stability of the lignin-carbohydrate complex. Consequently, maintaining the visual integrity of the wood surface depends on the chemical resistance of its macromolecular constituents, particularly the stability of lignin against ultraviolet (UV) photo-degradation and oxidative reactions (George *et al.,*2005; Tolvaj *et al.,* 2005).

Technical University of Zvolen, T.G.Masaryka 24, 96053, Zvolen, SLOVAKIA
e-mail: banski@tuzvo.sk

Wood steaming is a controlled process of exposing the material to saturated water steam in pressure devices (autoclaves). The primary goal of this technology is to optimize rheological properties, eliminate internal stresses, and achieve color homogeneity of wood. When exposed to temperatures in the range of 100–140 °C, partial hydrolysis of cell wall biopolymers occurs. The process is initiated by the degradation of hemicelluloses associated with the release of water-soluble extractive substances. The kinetics of these transformations is determined by the thermal mode and exposure, leading to the progressive decomposition of polysaccharides. The autocatalytic effect of the re-leased acetic and formic acids induces the oxidation of carbohydrates and pectins; subsequent dehydration of pentoses produces 2-furaldehyde (Fengel and Wegener, 2003; Sundqvist 2006; Hill 2006; Wilems *et al.,* 2015; Vilkovský *et al.* 2022; Dzurenda 2024).

Color performance stands as a primary physical-aesthetic parameter governing the utilization of wood in interior architecture and furniture manufacturing. The resulting visual appearance is determined by the presence of chromophoric groups in the lignin, tannins, and specific extractive compounds distributed throughout the cellular matrix (Tolvaj *et al.,* 2009; Molnár *et al.,* 2009).

The aim of this study is to investigate the color changes of pine sapwood and heartwood during the technological process of steaming with saturated water vapor at temperatures from 105 °C to 125 °C for 18 hours. Also, to evaluate the total color difference (ΔE*) in the CIE L*a*b* color space recorded during the steaming process and to demonstrate the effect of steaming on achieving color uniformity between sapwood and heartwood.

MATERIALS AND METHODS

For the research, 25 pine trunks with a length of 6.3 m with a clearly visible sap-wood and heartwood zone (Fig.1) were selected from the Štiavnické vrchy locality (GPS. 48.4161247N, 18.8593111E, Central Slovakia region).


Figure 1. View of the front cut of pine wood before sawing (left), view of the sawn lumber before entering the autoclave (right).

The center lumber with a width of 300–400 mm and a thickness of 50 mm was produced by cutting along the edge, which was subsequently divided into two asymmetric parts by longitudinal sawing. By transverse shortening of these parts, a 2 m long lumber was produced, which was randomly divided into 5 groups. The semi-finished products of the 1st group, in the number of 15 pieces, were not steamed. The other semi-finished products were steamed in mode I/t = 105 °C and pressure p = 0.12 MPa; and in mode II/t = 125 °C and pressure p = 0.23 MPa. Individual groups of steamed semi-finished products were taken from the pressure autoclave after τ = 6 h and τ = 18 h of steaming. The technological process was carried out in a pressure autoclave APDZ 240 (Himmasch AD, Chaskovo, Bulgaria) in the company Sundermann s.r.o. in Banská Štiavnica (Slovakia). The conditions for steaming pine core wood in a saturated water vapor environment, including the time intervals for sampling individual groups of steamed semi-finished products, are shown in the diagram in Fig. 2.

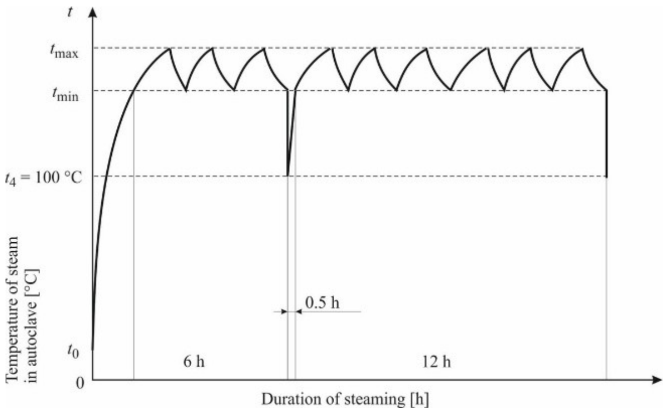

Figure 2. Diagram of the process of steaming pine wood.

Table 1. Technological conditions for steaming wood.

Steaming modes	t_{min}	t_{max}	t_4	Time of the technological process of steaming wood	
Mode I	102.5	107.5	100	τ_1 = 6 h	τ_2 = 12 (+0.5[a]) h
Mode II	117.5	122.5	100		

Note: [a] After the specified period of wood treatment, exactly according to the specified diagram (course), 0.5 h must be added to the basic steaming time of pine wood. This time between individual treatment periods serves to reduce the pressure and for safe opening of the autoclave and manipulation when selecting one group of treated semi-finished products from the autoclave, closing and pressurizing the autoclave with saturated water steam.

The surface chromatic parameters of native and steamed pine wood samples were determined in the three-dimensional color space CIE L*a*b* using a tristimulus colorimeter Color Reader CR-10 from Konica Minolta, Japan. This color system, which covers the entire range of human perception, is based on the Hering model of opposing colors, where the L* coordinate defines lightness in the range from 0 for black to 100 for white. The a* chromatic axis represents the relative position between green and red, with negative values indicating a shift towards green and positive values towards red, while the b* axis expresses the relationship between blue and yellow, with negative numbers pointing towards blue and positive numbers pointing towards yellow. The measurement was performed using a normalized D65 light source through an 8 mm optical sensor hole, and data were recorded on the radial surfaces of the pine samples before and after the steaming process. Due to the nature of the transformations, this space is characterized as a chromatic value color space, which allows even subtle visual changes in wood color to be accurately quantified. The total color difference was calculated using the following equation:

$$\Delta E^* = \sqrt{(L_2^* - L_1^*)^2 + (a_2^* - a_1^*)^2 + (b_2^* - b_1^*)^2} \quad (1)$$

Where: L^*_1, a^*_1, b^*_1 values in the color space coordinates of the surface of dried milled native wood;

L^*_2, a^*_2, b^*_2 values in the color space coordinates of the surface of dried milled steamed wood.

RESULTS AND DISCUSSION

In the color space CIE L*a*b*, untamed dry pine sapwood exhibits a highly luminous, whitish-yellow shade, defined by the coordinate parameters: L* = 84.8 ± 1.5; a* = 7.9 ± 1.0; b* = 21.9 ± 0.9 (Tab. 2). Conversely, the inherent coloration of pine heartwood displays a marginally deeper and more intense reddish-yellow tint, which is quantified by the following color space values: L* = 82.9±1.5; a* = 9.3±1.1; b* = 23.8±1.1 (Tab. 3). These baseline measurements align with previously documented optical profiles typical for heartwood-forming conifers (Meints *et al.* 2017; Suchta *et al.,* 2024). Subjecting pine wood to hydrothermal treatment triggers substantial modifications in both its physical and chemical attributes. The overall kinetics and the degree of color development in the steamed material are crucially governed by the treatment temperature, processing time, and the respective anatomical region (sapwood/heartwood), as illustrated in Fig. 3.

Figure 3. The color of pine wood in the steaming process.

Detailed information on the development of pine wood color coordinates during steaming focusing on the lightness coordinate L*, red chromaticity a*, and yellow chromaticity b* is comprehensively summarized in Table 3 for pine sapwood and Table 3 for pine heartwood.

Table 2. Average values of the color of pine sapwood in the color space CIE L*a*b* (mean ± SD).

Pine sapwood	Number of measurements [-]	Steaming Time [h]	Values in the Color Space CIE L*a*b*		
			L*	a*	b*
Unsteamed	60	0	84.8 ± 1.5	7.9 ± 1.0	21.9 ± 0.9
Steamed Mode I./t_I = 105 ± 2.5°C	60	6	82.5 ± 1.0	9.3 ± 0.9	23.6 ± 0.8
	60	18	71.0 ± 0.9	10.5 ± 0.8	25.2 ± 0.7
Steamed Mode II./t_{II} = 120 ± 2.5°C	60	6	72.8 ± 1.1	10.9 ± 0.9	25.7 ± 1.0
	60	18	61.1 ± 0.9	14.4 ± 0.7	26.8 ± 0.8

Table 3. Average values of the color of pine heartwood in the color space CIE L*a*b* (mean ± SD).

Pine sapwood	Number of measurements [-]	Steaming Time [h]	Values in the Color Space CIE L*a*b*		
			L*	a*	b*
Unsteamed	60	0	82.9 ± 1.5	9.3 ± 1.1	23.8 ± 1.1
Steamed Mode I./t_I = 105 ± 2.5°C	60	6	80.4 ± 1.6	11.4 ± 0.9	25.0 ± 1.0
	60	18	73.9 ± 1.5	11.9 ± 0.8	26.6 ± 0.9
Steamed Mode II./t_{II} = 120 ± 2.5°C	60	6	73.8 ± 1.5	12.5 ± 0.9	26.7 ± 1.2
	60	18	67.7 ± 1.6	13.6 ± 0.7	27.4 ± 1.0

The experimental data for untamed and hydrothermally modified pine wood within the color space CIE L*a*b*, as detailed in Tab. 2 and Tab. 3, demonstrate that steaming temperature and duration exert a profound influence on the materials final visual appearance. The baseline lightness (L*) of the reference wood varied by anatomical zone; sapwood displayed a higher initial lightness (L* = 84.8±1.5) than heartwood (L* = 82.9 ±1.5), representing an inherent difference of 2.24%.Under Mode I conditions (105 °C), a 6h exposure reduced the lightness of sapwood by 2.71% (dropping to 82.5) and heartwood by 3.02% (dropping to 80.4). Extending this treatment to 18 hours resulted in a cumulative lightness reduction of 16.27% in sapwood (L* = 71.0) and 10.86% in heartwood (L* = 73.9). In Mode II (120 °C), the elevated thermal energy accelerated the darkening kinetics. After just 6 h, the L^ values fell by 14.15% in sapwood (L* = 72.8) and by 10.98% in heartwood (L* = 73.8). At the 18h mark, the total decrease reached 27.95% for sapwood (L* = 61.1±0.9) and 18.34% for heartwood (L* = 67.7±1.6). The chromatic coordinate a* (redness) exhibited a linear upward trend across both anatomical zones, visually reflecting a shift toward warm brown hues. Unmodified heartwood possessed an initial red component 17.72% higher (a* = 9.3) than that of sapwood (a* = 7.9). Following an 18h exposure in Mode II, the a* value surged by 82.28% in sapwood (reaching 14.4 ± 0.7) and by 46.24% in heartwood (reaching 13.6±0.7). Concurrently, the yellowness coordinate (b*) increased steadily under both treatment modes. In Mode II after 18 h, sapwood b* values shifted upward by 22.37% (from 21.9 to 26.8±0.8), while heartwood values recorded a total increase of 15.13% (from 23.8 to 27.4±1.0).Analysis of variance (ANOVA) confirmed that both "steaming temperature" and "exposure time" have a statistically highly significant impact ($p < 0.001$) on all three color coordinates (L*, a*, b*). Lightness (L*): Post-hoc testing indicated that the decrease in sapwood lightness between 6 h (L* = 82.5) and 18 h (L* = 71.0) in Mode I is statistically significant ($p < 0.05$), with an even more pronounced statistical shift observed under Mode II (120 °C).Chromaticity (a* and b*): Regarding the a* coordinate in heartwood, the analysis revealed that the difference between the 6h (a* = 11.4) and 18 (a* = 11.9) intervals in Mode I is not statistically significant ($p > 0.05$). This indicates that prolonged steaming at 105 °C does not significantly increase the red hue fraction in heartwood. Conversely, Mode II (120 °C) yielded a statistically significant increase to 13.6±0.7, confirming that higher thermal thresholds are required to trigger deeper chemical alterations in heartwood chromaticity. Although the mean L* values of sapwood and heartwood were significantly different in their native state (t-test; $p < 0.05$), an intersection of their statistical profiles occurred after 18 h of treatment in Mode I. The overlapping confidence intervals of sapwood (71.0±0.9) and heartwood (73.9±1.5) mathematically define this parameters as the optimal point of visual homogenization, where the human eye can no longer differentiate the macro-anatomical boundary between the two zones (Meints *et al.* 2017; *Klement et al.,* 2018; Suchta *et al.,* 2024).

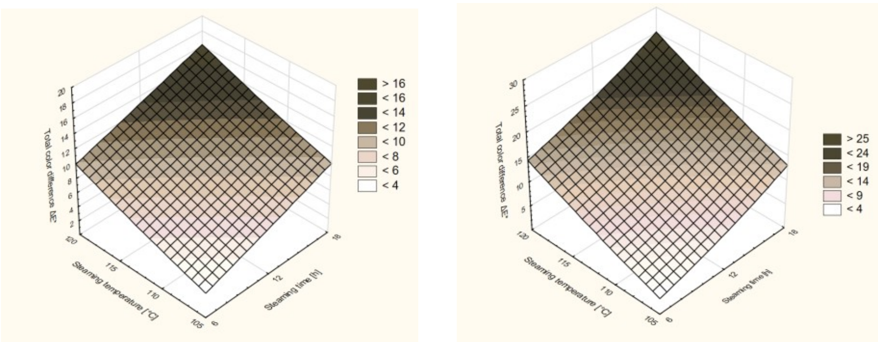

Figure 4. 3D graphs of total color difference of heartwood (left), sapwood (right).

CONCLUSIONS

In this study, the effects of pressure steaming parameters (temperature and time) on moisture dynamics, color coordinates of pine sapwood and heartwood (*Pinus sylvestris* L.) were comprehensively evaluated. Based on experimental results and statistical analyses, the following main conclusions can be formulated.

Increasing the steaming temperature from 105°C to 120°C and extending the time to 18 h significantly accelerated the wood darkening process. While in the native state there is a demonstrable optical difference between sapwood and heartwood, mode I (105°C) at 18 h exposure represents the optimal technological point for visual homogenization. At this point, the lightness confidence intervals (L*) overlap, making the human eye unable to perceive the boundary between the sapwood and heartwood zones.

Since heartwood and sapwood show different chemical sensitivity and different maxima of total color difference (ΔE*), it is essential to approach both zones individually in industrial management to ensure optimal adhesion of subsequent coating systems and surface quality.

REFERENCES

1. Fengel, D.; Wegener, G. Wood: Chemistry, Ultrastructure, Reactions; Walter de Gruyter: Berlin, Germany, 2003; pp. 25–60.
2. Rowell, R.M. Handbook of Wood Chemistry and Wood Composites, 2nd ed.; CRC Press: Boca Raton, FL, USA, 2012; pp. 55–92.
3. Hill, C.A.S. Wood Modification: Chemical, Thermal and Other Processes; John Wiley & Sons: Chichester, UK, 2006; pp. 15–43.
4. Ekeberg, D.; Flæte, P.-O.; Eikenes, M.; Fongen, M.; Naess-Andresen, C.F. Qualitative and quantitative determination of extractives in heartwood of Scots pine (*Pinus sylvestris* L.) by gas chromatography. J. Chromatogr. A 2006, 1110, 120–127.

5. Budakçı, M.; Saygin, E.; Şenol, S. ffect of resin cleaning process on adhesion strength of water-based varnishes. BioResources 2019, 14(1), 1317-1332.
6. Bergström, B. Chemical and structural changes during heartwood formation in *Pinus sylvestris*. Wood Sci. Technol. 2003, 37, 221–233.
7. George, B.; Suttie, E.; Merlin, A.; Deglise, X. Photodegradation and photostabilisation of wood—The state of the art. Polym. Degrad. Stab. 2005, 88, 268–274.
8. Tolvaj, L.; Mitsui, K. Light source dependence of the photo-induced discoloration of wood. J. Wood Sci. 2005, 51, 468–473. 10.1007/s10086-004-0693-4
9. Sundqvist, B.; Karlsson, O.; and Westremark, U. Determination of formic-acid and acid concentrations formed during hydrothermal treatment of birch wood and its relation to color, strength and hardness. Wood Sci. Technol. 2006, 40, 549–561.
10. Hill, C.A.S. Wood Modification: Chemical, Thermal and Other Processes; John Wiley & Sons: Chichester, UK, 2006; pp. 1–239.
11. Willems, W.; Altgen, M.; Militz, H. Comparison of EMC and durability of heat treated wood from high versus low water vapour pressure reactor systems. Int. Wood Prod. J. 2015, 6, 12–18. https://doi.org/10.1179/2042645314Y.0000000083
12. Dzurenda, L. Colouring of Beech Wood during Thermal Treatment using Saturated Water Steams. Acta Fac. Xylologiae Zvolen 2014, 56, 13–22.
13. Dzurenda, L.; Dudiak, M. Homogenization of the Color of Beech Sapwood and False Heartwood by the Steaming Process. Forests 2024, 15, 1009.
14. Vilkovský, P.; Vilkovská, T.; Klement, I.; Čunderlík, I. The Analysis Effect of Selected Factors on the Shear Strength of Woodbark at Different Wood Species. Forests 2022, 13, 637. https://doi.org/10.3390/f13050637
15. Tolvaj, L.; Molnár, S.; Varga, D. Range of Color Changes of Beech Wood in the Steaming Process. BioResources 2009, 4, 1335–1345.
16. Molnar, S.; Tolvaj, L.; Colour homogenisation of different wood species by steaming. Interaction of Wood with Various Forms of Energy; Technical University in Zvolen, Slovakia, 2002; pp. 119–122.
17. ISO/CIE 11664-4:2019. Colorimetry — Part 4: CIE 1976 L*a*b* Colour Space; International Organization for Standardization: Geneva, Switzerland, 2019.
18. Meints, T.; Teischinger, A.; Stingl, R.; Hassmann, C. Wood colour of central European wood species: CIELAB characterisation and colour intensification. Eur. J. Wood Prod. 2017, 75, 499–509.
19. Suchta, A.; Barański, J.; Vilkovská, T.; Klement, I.; Vilkovský, P. The impact of drying conditions on the surface color changes of pine wood. BioResources 2024, 19(1), 656–669.
20. Klement, I.; Vilkovská, T.; Baranski, J.; Konopka, A. The impact of drying and steaming processes on surface color changes of tension and normal beech wood. Dry. Technol. 2018, 36, 1490–1497. https://doi.org/10.1080/07373937.2018.1509219

ACKONWLEDGEMENT:

This paper was prepared within the grant project: VEGA 1/0423/25 as the result of work of the authors and the considerable assistance of the agencies.

EVALUATION OF NOISE EXPOSURE AND CUTTING-ZONE TEMPERATURE IN CNC PROCESSING OF PLYWOOD

Dagmara Bednárová – Bianka Moravčíková – Rastislav Igaz – Ján Šustek – Jana Richvalská – Jarmila Schmidtová – Miroslav Němec

Abstract

This paper addresses noise exposure and cutting-zone temperature in the tool–workpiece interaction zone at the TECH Z5 CNC machining centre operated at the Technical University in Zvolen. The study evaluates the equivalent A-weighted sound pressure level in the operator's working area and the temperature in the tool–workpiece interaction zone under selected feed rates and depths of cut at a constant spindle speed during milling of plywood. The equivalent A-weighted sound pressure level was measured by a single-channel arrangement and cutting-zone temperature was monitored by a non-contact method. The proposed approach enables a joint comparison of acoustic and thermal process responses under identical technological conditions. A measurable increase in equivalent sound pressure levels and temperature was observed with increasing depth of cut, while the influence of feed rate was not strictly linear under the tested conditions. The results are presented in a generalized form and provide a basis for further optimization of operating modes with respect to workplace safety and process loading.

Keywords: *CNC machining centre; noise exposure; cutting-zone temperature; occupational noise*

INTRODUCTION

The operation of CNC machining centres is associated with noise that may represent a health risk during long-term exposure (Axelsson et al., 1987). Occupational noise assessment can be performed according to STN EN ISO 9612 (2025). In addition to noise exposure, the thermal loading of the cutting zone is an important technological aspect of CNC machining. Heat generated by friction and material deformation affects tool loading, process stability, and surface quality (Igaz et al., 2018; Guimarães et al., 2022). For this reason, assessment of machining conditions should include both acoustic and thermal aspects. However, acoustic and thermal responses are often evaluated separately, although their combined monitoring may provide a more comprehensive indication of process loading during CNC machining.
The selected TECH Z5 CNC machining centre (Figure 1) was used for milling operations. Noise at this workplace is generated mainly during active machining, axis movement, and auxiliary operations. During milling, heat is generated in the cutting zone, and the resulting temperature depends on the combination of machining parameters, material properties, and tool geometry. Previous studies indicate that spindle speed, feed rate, and depth of cut may

Technical University in Zvolen, T. G. Masaryka 24, 960 01 Zvolen
e-mail: xhlavcakova@is.tuzvo.sk

influence both acoustic emission and thermal loading in the process (Kminiak et al., 2023; Igaz et al., 2018; Nasir et al., 2020; Guimarães et al., 2022).
The aim of this paper is to evaluate the noise exposure of a CNC machine operator in three selected model work scenarios during plywood machining. The assessment is complemented by monitoring the cutting-zone temperature as an indicator of thermal process loading under the evaluated cutting conditions.

Figure 1 CNC machining center SCM TECH Z5

MATERIAL AND METHODS

Measurements of the equivalent A-weighted sound pressure level under different operating conditions were carried out in the Development Workshops and Laboratories of the Technical University in Zvolen. The measurement was performed under conditions corresponding to the normal operation of the workplace so that the results would reflect the real working environment as closely as possible. The Brüel & Kjær Type 2270 (Figure 2) sound level meter was used to measure the sound pressure level. Before the measurement, the sound level meter was calibrated using a Brüel & Kjær 4231 calibrator, and after the measurement, a control calibration was performed.

Figure 2 Measuring device with microphone and microphone cover

The machined material was a plywood board. The cutting conditions corresponded to practical operating modes and included selected levels of feed rate, depth of cut, and spindle speed during finishing. The experiment was designed as a broader set of machining tests; however, the present contribution reports only a partial evaluation focused on a selected reference spindle speed. The material is wood-based and can be processed under normal milling conditions. A monolithic spiral cutter with a positive helix angle and a diameter of 20 mm was used as the tool, and the selected process parameters were determined in cooperation with CNC machine operators so that they reflected commonly applied finishing regimes. For the combined evaluation of the equivalent sound pressure level at the operator's workstation and cutting-zone temperature, the measurements were evaluated at a spindle speed of 9,000 min^{-1}. The cutting parameters are given in Table 1.

Table 1 Evaluated milling parameters

Parameter	**Value**
Feed rate (v_f) ($m \cdot min^{-1}$)	5; 7; 10
Depth of cut (u) (mm)	1; 2; 3
Spindle speed (n) (min^{-1})	9,000
Milling direction	Conventional milling
Milling strategy	Finishing

The microphone was placed at a height of approximately 1.5 m above the floor in the vicinity of the CNC operator's workstation so that its position corresponded to the approximate height of the worker's ear. The measurement and subsequent evaluation of noise exposure were performed in accordance with the STN EN ISO 9612 (2025) standard.
Based on the experimentally obtained data, three model work scenarios were created to represent selected 8-hour work shifts of a CNC machine operator. Each scenario consisted of 7.5 hours of work divided into three 2.5-hour work blocks and a 30-minute lunch break without noise exposure. The scenarios were defined by constant feed rates of 5 $m \cdot min^{-1}$, 7 $m \cdot min^{-1}$, and 10 $m \cdot min^{-1}$. Within each scenario, the depth of cut was varied between 1 mm, 2 mm, and 3 mm in the individual work blocks, while the spindle speed remained constant at 9,000 min^{-1}. Each machining condition was measured repeatedly 9-times, and the evaluation of daily noise exposure followed the task-based strategy defined in STN EN ISO 9612. The definition of operating conditions and model work scenarios was based on previous experimental measurements carried out at the same CNC workstation by Moravčíková (2026).
Temperature in the tool–workpiece interaction zone was monitored by a non-contact method using infrared sensing on the machined material surface (Figure 3) (Igaz et al., 2018; Guimarães et al., 2022). This made it possible to compare cutting-zone temperature with acoustic response under the same operating conditions. Repeated measurements were carried out for different combinations of feed rate and depth of cut, and the maximum temperature in the tool–workpiece interaction zone was evaluated.

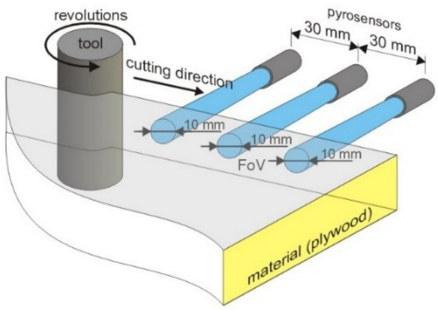

Figure 3 Schematic model of non-contact temperature measurement in the tool–workpiece interaction zone during CNC machining

RESULTS AND DISCUSSION

Sound pressure level measurements were performed in the operator's working area to assess the acoustic conditions directly relevant to worker exposure. The microphone position corresponded approximately to the height of the operator's ear; therefore, the evaluation reflects the acoustic conditions to which the worker was exposed during CNC machining.

A more detailed analysis (Figure 4 Dependence of the equivalent sound pressure level on the feed rate at different depths of cutFigure 4) showed that the lowest equivalent A-weighted sound pressure level, 81.3 dB, was recorded at the smallest depth of cut (1 mm) and a feed rate of 7 m·min⁻¹. At this depth of cut, the values ranged narrowly between 81.3 dB and 82.0 dB, indicating only limited variation in sound pressure level. With an increase in the depth of cut to 2 mm, the sound pressure level increased, reaching values between 84.1 dB and 84.9 dB. A moderate increase was observed particularly at a feed rate of 7 m·min⁻¹, which may be associated with less favourable cutting conditions and a more intensive cutting process. The highest sound pressure levels were recorded at the maximum depth of cut (3 mm), where the sound pressure level ranged from 84.3 dB to 85.4 dB. The maximum value of 85.4 dB was again observed at a feed rate of 7 m·min⁻¹. The influence of feed rate was not strictly linear under the tested conditions, as the highest sound pressure level was not recorded at the maximum feed rate of 10 m·min⁻¹, but rather at the intermediate value of 7 m·min⁻¹.

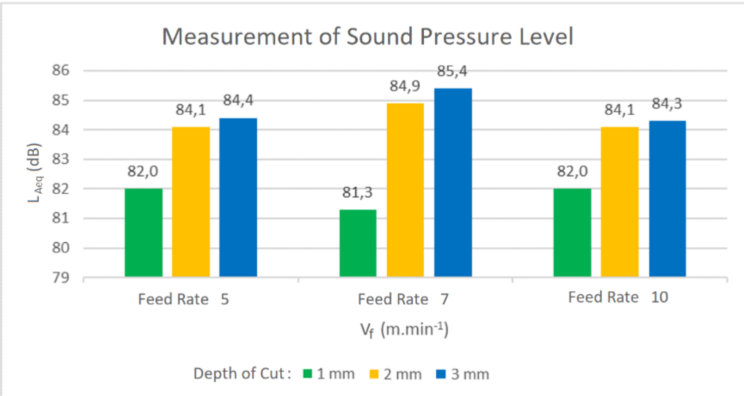

Figure 4 Dependence of the equivalent sound pressure level on the feed rate at different depths of cut

Overall, the measured sound pressure levels varied depending on the selected combination of feed rate and depth of cut under the tested operating conditions (Moravčíková, 2026). In accordance with STN EN ISO 9612, the daily noise exposure level of the operator was calculated for an 8-hour working shift under three model scenarios with constant feed rates and varying depths of cut (Table 2). For a feed rate of 5 m·min⁻¹, the daily noise exposure level was $L_{AEX,8h}$ = 83.3 dB. For a feed rate of 7 m·min⁻¹, the daily noise exposure level increased to $L_{AEX,8h}$ = 83.9 dB, while for a feed rate of 10 m·min⁻¹ it was again $L_{AEX,8h}$ = 83.3 dB. When the expanded measurement uncertainty of 2.1 dB was included, the corresponding assessment values ranged from 85.4 dB to 86.0 dB.

Table 2 Daily noise exposure levels and assessment values including expanded measurement uncertainty

Scenario	$L_{AEX,\,8h}$ (dB)	U (dB)	$L_{AEX,\,8h} + U$ (dB)
1	83.3	2.1	85.4
2	83.9	2.1	86.0
3	83.3	2.1	85.4

These results indicate that, although the measured sound pressure levels varied depending on the cutting parameters, the overall daily noise exposure remained within a relatively narrow range under the tested operating conditions. When the expanded measurement uncertainty was included, the assessment values exceeded the upper action value but remained below the exposure limit value of 87 dB (Government Regulation No. 115/2006). This finding points to the need for systematic noise control measures and consistent use of hearing protection, especially in situations where additional noise sources may be present or where the worker spends the entire shift at the CNC workstation.

In addition to acoustic measurements, the temperature in the tool–workpiece interaction zone was also evaluated under identical cutting conditions (Figure 5).

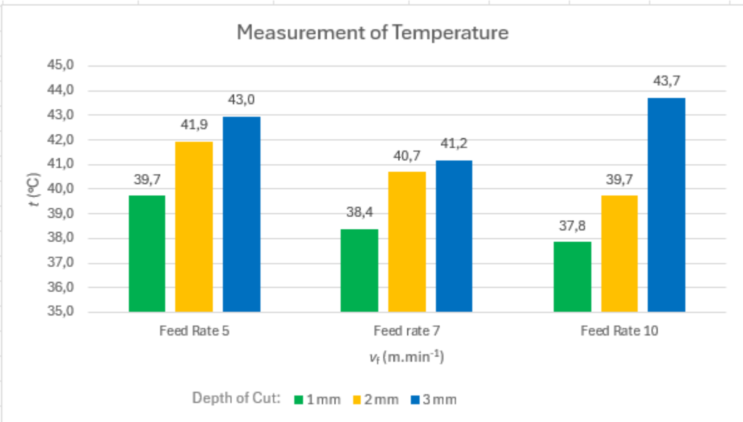

Figure 5 Dependence of temperature on the feed rate at different depths of cut

For the reference spindle speed of 9,000 min⁻¹, the maximum cutting-zone temperature typically ranged between approximately 38 °C and 44 °C. Increasing the radial depth of cut from 1 mm to 3 mm resulted in an increase in the maximum cutting zone temperature in all cases, indicating increased thermal loading on the process at higher depths of cut. Overall, the temperature results complemented the acoustic measurements and provided additional information on process loading under the evaluated cutting conditions.

Taken together, the present observations suggest that the evaluated cutting conditions, particularly feed rate and depth of cut, affected both noise exposure and cutting-zone temperature during CNC machining. Non-contact temperature monitoring complemented acoustic measurements by providing information on the thermal loading of the tool–workpiece interaction zone. More intensive cutting conditions may lead to higher sound pressure levels and increased thermal loading of the cutting zone.

CONCLUSION

The paper evaluated the noise exposure of a CNC machine operator during plywood machining in three selected model work scenarios. When the expanded measurement uncertainty was included, the assessment values ranged from 85.4 dB to 86.0 dB. These assessment values exceeded the upper action value but remained below the exposure limit value. The acoustic evaluation was complemented by monitoring of cutting-zone temperature under the same cutting conditions. The maximum temperature in the tool–workpiece interaction zone varied depending on the selected combinations of feed rate and depth of cut, indicating that the cutting conditions also affected the thermal loading of the process.

The combined evaluation of noise exposure and cutting-zone temperature provides useful information for assessing CNC machining conditions from both occupational and technological viewpoints. Further work may focus on a more detailed evaluation of cutting parameters, material type, tool characteristics, and work scenarios.

ACKNOWLEDGMENTS

This research was funded by VEGA 1/0179/25, KEGA 003TU Z-4/2024, and VEGA 1/0027/24.

REFERENCES

AXELSSON, A.; HAMERNIK, R.P. Acute acoustic trauma. *Acta Otolaryngologyca*, 1987 Sep-Oct;104(3-4), 225-233. DOI: 10.3109/00016488709107322.

GUIMARÃES, B. M. P.; FERNANDES, C. M. S.; FIGUEIREDO, D. A.; PEREIRA DA SILVA, F. S. C.; MIRANDA, M. G. M. Cutting temperature measurement and prediction in machining processes: comprehensive review and future perspectives. *The International Journal of Advanced Manufacturing Technology*, 2022, 120(5-6), 2849–2878. DOI:10.1007/s00170-022-08957-z

IGAZ, R.; KMINIAK, R.; KRIŠŤÁK, Ľ.; NĚMEC, M.; GERGEĽ, T. Methodology of temperature monitoring in the process of CNC machining of solid wood. *Sustainability,* 2019, *11*, 95. https://doi.org/10.3390/su11010095

KMINIAK, R.; NĚMEC, M.; IGAZ, R.; GEJDOŠ, M. Advisability-selected parameters of woodworking with a CNC machine as a tool for adaptive control of the cutting process. *Forests,* 2023, *14*, 173. https://doi.org/10.3390/f14020173

MORAVČÍKOVÁ, B. Noise of a CNC machine under different operating conditions. Technical University in Zvolen, Faculty of Ecology and Environmental Sciences, 2026. Bachelor's thesis.

NARIADENIE VLÁDY SR č. 115/2006 Z. z. o minimálnych zdravotných a bezpečnostných požiadavkách na ochranu zamestnancov pred rizikami súvisiacimi s expozíciou hluku.

NASIR, V.; KOOSHSKBAGHI, M.; COOL, J.; FERNANDES, C. Cutting tool temperature monitoring in circular sawing: measurement and multi-sensor feature fusion-based prediction. *The International Journal of Advanced Manufacturing Technology*, 2020, 112, 2413-2424. DOI:10.1007/s00170-020-06473-6

STN EN ISO 9612:2025. Akustika – Stanovenie expozície hluku v pracovnom prostredí – Technická metóda. Bratislava: Úrad pre normalizáciu, metrológiu a skúšobníctvo SR, 2025.

EXPANDED PLANT-BASED MATERIALS AS FILLERS FOR LIGHTWEIGHT PARTICLEBOARDS

Piotr Borysiuk[1] – Aleksy Kozakow[1] – Mikołaj Płatkowski[1] – Leszek Danecki[2] – Mikołaj Sumionka[2] – Radosław Auriga[1]

Abstract
The growing demand for wood-based materials and the limited availability of wood raw materials have intensified the search for alternative components for the production of lightweight particleboards. The aim of this study was to compare the effects of expanded rice and expanded spelt, used as partial substitutes for wood particles in the core layer, on the physical and mechanical properties of lightweight three-layer particleboards. Particleboards with a target density of 550 kg/m³ were manufactured from industrial pine particles by replacing 10%, 15%, and 20% of the core-layer particles with expanded rice or expanded spelt. The manufactured boards were evaluated in terms of density, density profile, MOR, MOE, IB, TS and WA. The results showed that increasing the content of expanded rice above 10% reduced both MOR and MOE, whereas expanded spelt had a considerably smaller effect on bending properties. The addition of both expanded materials increased thickness swelling and water absorption, with a more pronounced effect observed for expanded rice. All manufactured boards satisfied the requirements of EN 16368 for LP2 lightweight particleboards.

Key words: *lightweight particleboards, expanded rice, expanded spelt, plant-based fillers, agricultural biomass*

INTRODUCTION

Particleboards are among the most important wood-based materials used in the modern furniture and construction industries. In recent years, increasing pressure has been placed on reducing wood consumption due to both the rising cost of raw materials and the necessity of sustainable forest resource management. Consequently, considerable efforts have been devoted to developing technologies that enable the production of wood-based composites with reduced wood consumption while maintaining satisfactory performance characteristics (Boruszewski *et al*. 2016; Martyniak *et al*. 2025).
One of the most promising approaches is the development of low-density particleboards. According to EN 16368, particleboards with a density below 600 kg/m³ are classified as lightweight. Reducing board density decreases wood consumption, lowers the weight of

[1]Institute of Wood Sciences and Furniture, Warsaw University of Life Sciences – SGGW, 159 Nowoursynowska Str, 02-776 Warsaw, Poland
e-mail: piotr_borysiuk@sggw.edu.pl, radoslaw_auriga@sggw.edu.pl
[2]Research & Development Centre for Wood-Based Panels Ltd. in Czarna Woda, 10a Mickiewicza Str, 83-262 Czarna Woda, Poland
e-mail: leszek.danecki@obrppd.com.pl, mikolaj.sumionka@obrppd.com.pl

furniture components, and reduces transportation and storage costs. However, lowering density generally results in deterioration of mechanical properties; therefore, new structural solutions and lightweight filler materials are required (Lengyel *et al.* 2018; Luo *et al.* 2020a; Röllig *et al.* 2024).

Various approaches to manufacturing lightweight particleboards have been proposed. One solution involves the use of low-density wood species, such as paulownia and poplar (Boruszewski *et al.* 2016; Röllig *et al.* 2024). Another strategy is the partial replacement of wood particles with lignocellulosic agricultural materials, including rapeseed straw, sunflower stalks, kenaf core, and corn cobs (Dziurka *et al.* 2015; Xu *et al.* 2004; Faustino *et al.* 2012; Taghiyari *et al.* 2017). These materials contribute to reducing board density while simultaneously supporting the principles of the circular economy through the utilization of agricultural by-products.

Increasing attention has also been given to expanded materials used as lightweight fillers in the core layer of particleboards. Kharazipour and Bohn (2007) were among the first to propose the use of expanded cereal grains in the production of wood-based composites. Subsequently, Czechowska *et al.* (2010) demonstrated the feasibility of using popcorn as a filler in particleboards. Another alternative is expanded polystyrene (EPS), which improves the structural integrity of boards while enabling further reductions in density (Luo *et al.* 2020b; Shupin *et al.* 2020).

Expanded plant-based fillers incorporated into lightweight particleboards generally reduce density, improve thermal and acoustic insulation, and exert varying effects on strength and stiffness (Boruszewski *et al.* 2022; Karua *et al.* 2023; El Hajam *et al.* 2025). Their influence on mechanical performance depends on the filler type, particle size, expansion degree, and the quality of interfacial bonding with the wood particle matrix (Perez-Pacheco *et al.* 2024; Barczewski *et al.* 2024). Previous studies have shown that while some expanded fillers (e.g., perlite, expanded clay, or coconut fibre) may enhance strength and insulation performance, others may reduce bending strength, highlighting the importance of proper filler selection (Karua *et al.* 2023; Doleželová *et al.* 2021).

Despite growing interest in the application of expanded materials in wood-based panel technology, studies investigating cereal-based expanded products other than popcorn remain limited. In particular, there is a lack of information regarding the use of expanded spelt as a lightweight core-layer filler in particleboards. Therefore, the objective of the present study was to compare the effects of expanded rice and expanded spelt on the physical and mechanical properties of lightweight particleboards and to evaluate their potential as alternative renewable components in wood-based composites.

MATERIALS AND METHODS

Pine industrial particles were used for the production of particleboards. The moisture content of the particles was 5.5% for the face layers and 7.5% for the core layer. Expanded rice (P.P. "Prepar" Józef Sidor, Chojnice, Poland) and expanded spelt (Pro Natura Sp. z o.o., Chwiram, Poland) were used as additive materials.

Three-layer particleboards with a thickness of 15 mm and a target density of 550 kg/m³ were manufactured in seven variants: three levels of expanded particle content (10%, 15%, and 20%) in the core layer for both rice and spelt, and a control variant (0%) (Table 1). The proportion of face layers was 35%. Urea–formaldehyde (UF) resin was used as the adhesive. The resin content was 12% for the face layers and 8% for the core layer. A 10% aqueous ammonium sulfate solution was used as a hardener. Adhesive application was performed in a pneumatic spraying mixer. Mat formation was carried out manually according to the designed variants.

Table 1. Manufactured particleboard variants.

Variant	Face layer particles	Core layer particles	Expanded particles
10 R	35 %	55 %	10 % rice
15 R	35 %	50 %	15 % rice
20 R	35 %	45 %	20 % rice
10 O	35 %	55 %	10 % spelt
15 O	35 %	50 %	15 % spelt
20 O	35 %	45 %	20 % spelt
K (control)	35 %	65 %	0 %

Pressing was carried out in a single-opening hot press at a maximum specific pressure of 2.5 MPa. Pressing time was 270 s, and pressing temperature was 200°C. After production, the boards were conditioned for 7 days under laboratory conditions (20 ± 2°C and 65 ± 5% relative humidity).
The following properties were evaluated:

- Density – according to PN-EN 323:1999
- Density profile – measured using a DA-X profilometer (GreCon), measurement step 0.02 mm, speed 0.05 mm/s
- MOR and MOE – according to PN-EN 310:1994
- Internal bond (IB) – according to PN-EN 319:1999
- Thickness swelling and water absorption – after 2 h and 24 h immersion in water according to PN-EN 317:1999.

Each test was performed in 10 replicates for each board variant. Statistical analysis of the results was performed using Statistica 13 software. A multifactorial ANOVA was applied. Tukey's post hoc test was used to determine statistically homogeneous groups.

RESULTS

The mean densities of the manufactured particleboard variants ranged from 529 to 577 kg/m³, remaining close to the target density of 550 kg/m³. The variation in mean density did not exceed 10% of the nominal value. The density profiles presented in Fig. 1 reveal a similar distribution for all board variants, exhibiting the characteristic U-shaped profile typical of three-layer particleboards (Thoemen *et al*. 2010). The obtained density profiles were independent of the type of lightweight filler used. Similar observations were reported by Boruszewski *et al*. (2016) for low-density particleboards and by Lengyel *et al*. (2018), who demonstrated that replacing part of the wood particles with low-density materials does not significantly alter the density profile provided that appropriate pressing conditions are maintained.
The results of the modulus of rupture (MOR) and modulus of elasticity (MOE) tests are presented in Figs. 2 and 3. In general, the incorporation of expanded particles (rice or spelt) into the core layer at levels exceeding 10% resulted in lower MOR and MOE values, with the reduction being more pronounced for expanded rice. In boards containing expanded rice, the decreases in MOR and MOE were generally statistically significant, as confirmed by different homogeneous groups. In contrast, although boards containing expanded spelt

exhibited slightly lower MOR and MOE values than the control boards, these differences were not statistically significant. According to EN 16368, lightweight particleboards of type LP2 with a thickness of 13–20 mm should exhibit a minimum MOR of 7 N/mm^2 and a minimum MOE of 950 N/mm^2.

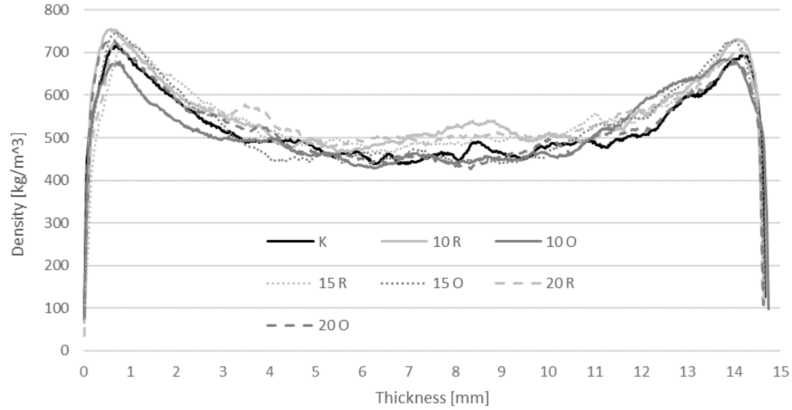

Fig. 1. Density profiles of the manufactured particleboards.

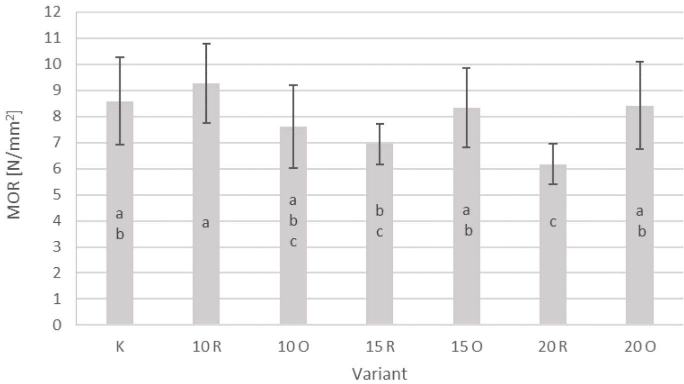

Fig. 2. MOR results; a, b, c – homogeneous groups according to Tukey's test.

The reduction in bending properties observed in boards containing expanded rice can be attributed to differences in particle geometry between wood particles and expanded rice. Partial replacement of wood particles with rice particles most likely affected resin distribution and particle bonding, resulting in weaker cohesion within the board structure and consequently lower MOR and MOE values compared with the control boards. This phenomenon was not observed in boards containing expanded spelt, whose larger particle size appeared to promote more effective interaction with wood particles. The reduction in bending performance with increasing content of lightweight fillers is consistent with previous findings. Luo *et al*. (2020a) reported that increasing the proportion of lightweight materials in the core layer reduces the effective contact area between wood particles, thereby impairing stress transfer within the composite. Similar relationships were described by Regmi *et al*. (2022) for particleboards incorporating agricultural biomass. The results obtained in the present study indicate that the larger particles of expanded spelt interact more effectively with wood particles than the finer expanded rice particles, resulting in a considerably smaller reduction in MOR and MOE.

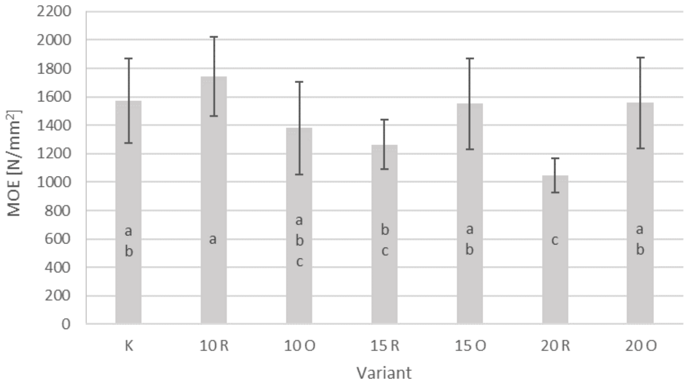

Fig. 3. MOE results; a, b, c – homogeneous groups according to Tukey's test.

The multifactor analysis of variance (Table 1) demonstrated that the proportion of expanded particles had a statistically significant effect on MOR and MOE, accounting for 10.4% and 11.3% of the total variation, respectively. The particle type (rice or spelt) alone did not significantly affect MOR or MOE, contributing only 0.1% and 0.4%, respectively. However, the interaction between particle content and particle type was statistically significant, explaining 27.3% of the variation in MOR and 30.1% of the variation in MOE. A relatively large proportion of unexplained variation (Error) was also observed, accounting for 62.2% and 58.2% of the variation in MOR and MOE, respectively. This variation may be attributed to factors not included in the analysis, such as adhesive distribution and the uniformity of expanded particle dispersion within the board.

Table 1. Analysis of variance (ANOVA) of the mechanical properties of particleboards.

Factor	MOR		MOE		IB	
	p	X	p	X	p	X
particle content	0.010691	10.4	0.004856	11.3	0.474468	2.3
particle type	0.775993	0.1	0.503608	0.4	0.000001	26.8
particle content × particle type	0.000008	27.3	0.000001	30.1	0.241358	4.0
Error		62.2		58.2		66.8

p – significant with α=0.05; X – percentage of contribution

The results of the internal bond strength (IB) measurements are presented in Fig. 4. The addition of expanded rice to the core layer (variants 10 R, 15 R, and 20 R) resulted in higher IB values compared with the control boards. However, although these differences were apparent, they were not statistically significant, as all variants belonged to the same homogeneous group. In contrast, the incorporation of expanded spelt (variants 10 O, 15 O, and 20 O) led to a reduction in IB, with additions exceeding 10% causing statistically significant decreases. The higher IB values observed for boards containing expanded rice indicate stronger internal cohesion than in boards containing expanded spelt. Nevertheless, all manufactured boards satisfied the requirements of EN 16368 for LP2 lightweight particleboards, which specifies a minimum IB value of 0.35 N/mm² for boards with a thickness of 13–20 mm. A similar increase in IB with the incorporation of expanded fillers was reported by Shupin *et al*. (2020) for lightweight particleboards containing expanded polystyrene in the core layer. Those authors also obtained higher IB values than for control boards manufactured exclusively from wood particles. The increase in IB observed for expanded rice may indicate improved densification of the core layer and more effective filling of voids between wood particles. Comparable mechanisms have been reported by Shupin *et al*. (2020) for expanded polystyrene-filled boards and by Monteiro *et al*. (2016) for lightweight particleboards bonded with starch-based adhesives. Conversely, the reduction in IB observed in boards containing expanded spelt may be associated with the larger particle size, which likely hindered uniform adhesive distribution and the formation of effective internal bonds.

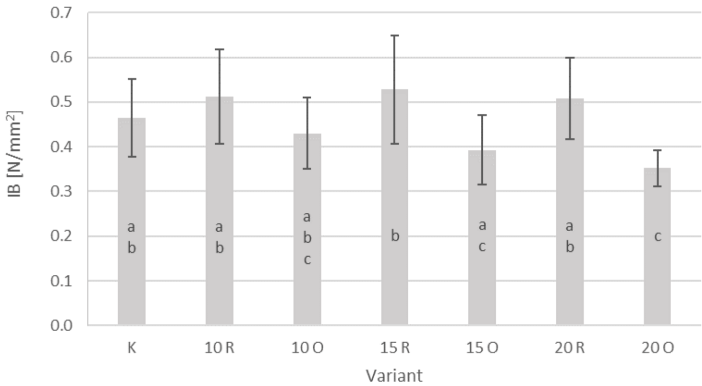

Fig. 4. IB results; a, b, c – homogeneous groups according to Tukey's test.

The multifactor ANOVA (Table 1) further indicated that particle type was the principal factor affecting IB, accounting for 26.8% of the total variation. The proportion of expanded particles and the interaction between particle proportion and particle type explained only 2.3% and 4.0%, respectively. In this case, the largest contribution originated from unexplained factors (Error = 66.8%).

The results of thickness swelling (TS) and water absorption (WA) are presented in Figs. 5 and 6. Increasing the content of expanded rice or expanded spelt consistently increased both TS and WA, indicating deterioration in water-related properties. All observed differences were statistically significant. It is noteworthy that, regardless of board variant, approximately 90% of the final thickness swelling and nearly 95% of the final water absorption recorded after 24 h were already reached after only 2 h of water immersion. The increase in TS and WA is most likely associated with weaker bonding between expanded particles and wood particles, facilitating water penetration into the board structure. Furthermore, expanded rice exhibited lower water resistance than expanded spelt. This was particularly evident in the statistically significant difference in TS between variants 20 R and 20 O. The deterioration in water resistance with increasing proportions of lightweight fillers has been widely reported in the literature. Dziurka *et al*. (2015) and Luo *et al*. (2020a) demonstrated that replacing part of the wood particles with more porous materials increases the number of internal voids and facilitates water penetration into the board. The present findings suggest that expanded spelt provides greater dimensional stability than expanded rice, which is likely related to differences in particle structure and lower water affinity. The multifactor ANOVA (Table 2) showed that the proportion of expanded particles explained 52.1% of the variation in TS after 2 h and 54.4% after 24 h. The interaction between particle proportion and particle type accounted for 25.3% and 25.0%, respectively, while unexplained factors (Error) contributed 22.2% and 20.1%. For water absorption, the proportion of expanded particles explained 58.7% of the variation after 2 h and 59.0% after 24 h, whereas unexplained factors accounted for 39.4% and 39.5%, respectively. In contrast to TS, neither the particle type nor the interaction between particle proportion and particle type had a statistically significant effect on WA.

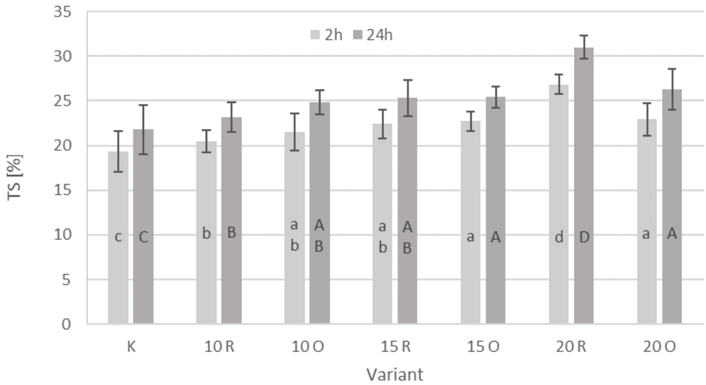

Fig. 5. TS results; a, b, c, d, A, B, C, D – homogeneous groups according to Tukey's test.

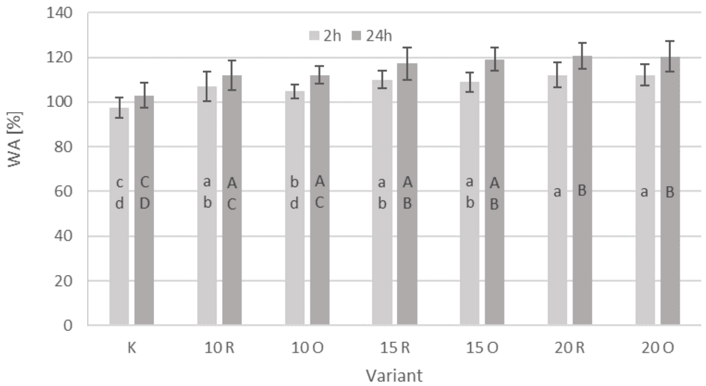

Fig. 6. WA results; a, b, c, d, A, B, C, D – homogeneous groups according to Tukey's test.

Table 2. Analysis of variance (ANOVA) of the physical properties of particleboards.

Factor	TS				WA			
	2h		24h		2h		24h	
	p	X	p	X	p	X	p	X
particle content	0.000000	52.1	0.000000	54.4	0.000000	58.7	0.000000	59.0
particle type	0.218203	0.5	0.224564	0.4	0.950649	0.0	0.313839	0.6
particle content × particle type	0.000000	25.3	0.000000	25.0	0.339195	1.9	0.672826	0.8
Error		22.2		20.1		39.4		39.5

p – significant with α=0.05; X – percentage of contribution

CONCLUSION

Based on the tests of lightweight particleboards with the addition of expanded particles in the core layer, the following conclusions can be drawn:

1. Both expanded rice and expanded spelt can be successfully used as fillers in the core layer of lightweight particleboards.
2. Increasing the content of expanded rice above 10% significantly reduced the modulus of rupture (MOR) and modulus of elasticity (MOE), whereas the incorporation of expanded spelt did not result in a statistically significant deterioration of these properties.
3. The addition of expanded rice tended to increase the internal bond strength (IB), while expanded spelt reduced IB, particularly at contents exceeding 10%.
4. Increasing the proportion of expanded particles, irrespective of their type, resulted in increased thickness swelling (TS) and water absorption (WA). This adverse effect was more pronounced for expanded rice than for expanded spelt.
5. Among the investigated materials, expanded spelt exhibited more favourable performance, as it had a considerably smaller negative effect on the mechanical properties of lightweight particleboards.

REFERENCES

1. BARCZEWSKI M., SUÁREZ L., MIETLIŃSKI P., KLOZIŃSKI A., ORTEGA Z. (2024). Relationship Between the Shape of Giant Reed-Based Fillers and Thermal Properties of Polyethylene Composites: Structural Related Thermal Expansion and Diffusivity Studies. Waste and Biomass Valorization, 15:7033–7042. https://doi.org/10.1007/s12649-024-02626-w
2. BORUSZEWSKI P., BORYSIUK P., JANKOWSKA A., PAZIK J. (2022). Low-Density Particleboards Modified with Expanded and Unexpanded Fillers-Characteristics and Properties. Materials, 15(13), 4430. https://doi.org/10.3390/ma15134430
3. BORUSZEWSKI P., BORYSIUK P., MAMIŃSKI M., CZECHOWSKA J. (2016). Mat compression measurements during low-density particleboard manufacturing. BioResources, 11(3), 6909-6919. https://doi.org/10.15376/biores.11.3.6909-6919
4. CZECHOWSKA J., ZBIEĆ M., BORYSIUK P. (2010). Popcorn-modified particleboards. Part 1. Mechanical properties. In: 7th International Science Conference Chip and Chipless Woodworking Processes, Terchová, Slovakia, 219-223.
5. DOLEZELOVÁ M., SCHEINHERROVÁ L., KREJSOVÁ J., KEPPERT M., ČERNY R., VIMMROVÁ A. (2021). Investigation of gypsum composites with different lightweight fillers. Construction and Building Materials, 297, 123791. https://doi.org/10.1016/j.conbuildmat.2021.123791
6. DZIURKA D., MIRSKI R., DUKARSKA D., DERKOWSKI A. (2015). Possibility of using expanded polystyrene and rape straw to manufacture lightweight particleboards. Maderas. Ciencia y Tecnología, 17(3), 647-656. https://doi.org/10.4067/S0718-221X2015005000057
7. EL HAJAM M., SUN W.J., HAFEZ I., HOWELL C., TAJVIDI M. (2025). In situ growth of mycelium in a lignocellulosic scaffold enabled by cellulose nanofibrils for lightweight insulation. Composites Part A: Applied Science and Manufacturing, 199, 109223. https://doi.org/10.1016/j.compositesa.2025.109223

8. EN 16368 Lightweight Particleboards – Specifications
9. KARUA P., ARIFUZZAMAN M., ISLAM M.S. (2023). Effect of jute fiber reinforcement on the mechanical properties of expanded perlite particles-filled gypsum composites. Construction and Building Materials, 387, 131625. https://doi.org/10.1016/j.conbuildmat.2023.131625
10. KHARAZIPOUR A., BOHN C. (2007). Use of popcorn for timber and composite materials. United States Patent US8568895B2.
11. LENGYEL K., BARBU M.C., CAMPEAN M., BOGDAN B. (2018). Improving properties of particleboards with reduced density. BioResources, 13(1), 1289-1302. https://doi.org/10.15376/biores.13.1.1289-1302
12. LUO S., GAO L., GUO W. (2020). Effect of face layer manipulation on the density profile and properties of low-density particleboard. Wood Research, 65(1), 125-134. https://doi.org/10.37763/wr.1336-4561/65.1.125134
13. LUO S., GAO L., GUO W. (2020). Effect of expanded polystyrene content and press temperature on the properties of low-density wood particleboard. Maderas. Ciencia y Tecnología, 22(4), 549-558. https://doi.org/10.4067/S0718-221X2020005000413
14. MARTYNIAK D., PĘDZIK M., ŻUREK G., TOMCZAK K., GĄSIOROWSKI R., KOMOROWICZ M., JANISZEWSKA-LATTERINI D. (2025). Exploitation of Perennial Plant Biomass for Particleboards Designed for Insulation Applications. Materials, 18(2), 352. https://doi.org/10.3390/ma18020352
15. MONTEIRO S., MARTINS J., MAGALHÄES F.D., CARVALHO L. (2016). Low density wood-based particleboards bonded with foamable sour cassava starch: Preliminary studies. Polymers, 8(10), 354. https://doi.org/10.3390/polym8100354
16. MONTEIRO S., NUNES L., MARTINS J., MAGALHÄES F.D., CARVALHO L. (2020). Low-density cardoon (Cynara cardunculus L.) particleboards bound with potato starch-based adhesive. Polymers, 12(8), 1799. https://doi.org/10.3390/polym12081799
17. PEREZ-PACHECO E., RIOS-SOBERANIS C.R., MINA-HERNÁNDEZ J.H., MOO-HUCHIN V.M. (2024). Use of cellulose fiber from Jipijapa (Carludovicapalmata) as fillers in corn starch-based biocomposite film. Iranian Polymer Journal, 33, 157-168. https://doi.org/10.1007/s13726-023-01244-y
18. PN-EN 317:1999 Płyty wiórowe i płyty pilśniowe - Oznaczanie spęcznienia na grubość po moczeniu w wodzie
19. PN-EN 319:1999 Płyty wiórowe i płyty pilśniowe - Oznaczanie wytrzymałości na rozciąganie w kierunku prostopadłym do płaszczyzn płyty
20. PN-EN 323:1999 Płyty drewnopochodne - Oznaczanie gęstości
21. PN-EN 310:1994 Płyty drewnopochodne - Oznaczanie modułu sprężystości przy zginaniu i wytrzymałości na zginanie
22. REGMI S., BAJWA D., IGATHINATHANE C., NAHAR N. (2022). High fiber fraction DDGS - A functional filler for manufacturing low-density particleboards. Industrial Crops and Products, 181, 114793. https://doi.org/10.1016/j.indcrop.2022.114793
23. RÖLLIG P., TUDOR E.M., BARBU M.C., DIRESKE M. (2024). Effect of the particle geometry on lightweight particleboard from Paulownia using high-frequency pressing technology. Wood Material Science and Engineering, 19(3), 683-690. https://doi.org/10.1080/17480272.2023.2286625

24. SHUPIN L., LI G., WENJING G. (2020). Effect of expanded polystyrene content and press temperature on the properties of low-density wood particleboard. Maderas. Ciencia y tecnología, 22(4): 549-558, DOI: 10.4067/S0718-221X2020005000413
25. TAGHIYARI H.R., TAHERI A., OMRANI P. (2017). Correlation between acoustic and physical-mechanical properties of insulating composite boards made from sunflower stalk and wood chips. European Journal of Wood and Wood Products, 75, 409-418. https://doi.org/10.1007/s00107-016-1101-7
26. XU J., SUGAWARA R., WIDYORINI R., HUANG G., KAWAI S. (2004). Manufacture and properties of low-density binderless particleboard from kenaf core. Journal of Wood Science, 50(1), 62-67. https://doi.org/10.1007/s10086-003-0522-1

THE EFFECT OF STEAMING ON THE ACIDITY OF PINE WOOD

Michal Dudiak – Adrián Banski

Abstract

This study evaluates the impact of pressure steaming with saturated water steam on the moisture dynamics and acidity changes in the sapwood and heartwood of pine wood (Pinus sylvestris L.). Surface pH measurements were taken on dried, planed specimens using a pH-meter with a specialized SenTix Sur surface electrode. The results show that native heartwood is naturally more acidic (pH 4.7) than sapwood (pH 5.1) due to the accumulation of resin acids and phenolic compounds. Steaming induced progressive wood acidification in both zones, reaching final minima of 4.0 for heartwood and 4.1 for sapwood under the most intensive treatment (125 °C for 18 h). This decrease is chemically driven by the thermal autohydrolysis and deacetylation of hemicelluloses, which liberates free acetic acid. Thermodynamically, autoclave decompression also caused an immediate moisture loss of 7.7 to 11.7 through flash self-evaporation. Statistical analysis confirmed that both steaming temperature and exposure time are highly significant, additive factors influencing wood acidity. These findings highlight the need to process sapwood and heartwood individually in industrial applications to ensure optimal surface coating adhesion.

Keywords: *pine wood, sapwood, heartwood, acidity, saturated water steam.*

INTRODUCTION

Pine wood (*Pinus sylvestris* L.) represents a foundational raw material within the European woodworking sector. Its widespread industrial utilization is driven not only by its abundance across regional climatic zones but also by its distinct microstructural and chemical attributes (Fengel and Wegener, 2003). These inherent properties render it an exceptional substrate for advanced technological processing and surface treatment applications. Within the coating industry, pine serves as an essential model for investigating the complex interactions between natural wood anatomy and rigorous industrial specifications.

The macroscopic architecture of the pine matrix is defined by a sharp anatomical differentiation between the sapwood and heartwood zones (Fengel and Wegener, 2003; Rowell, 2012). While the highly permeable sapwood is ideal for deep protective impregnation, the heartwood region undergoes a natural modification through the accumulation of secondary metabolites (Hill, 2006; Ekeberg *et al.,* 2006). This elevated concentration of resins and hydrophobic extractives within the core forms a dense diffusion barrier, which substantially alters fluid sorption behavior and can compromise

Technical University in Zvolen, T. G. Masaryka 24, 960 01 Zvolen
e-mail: michal.dudiak@tuzvo.sk

the mechanical adhesion of industrial coating systems (Budakçı *et al.,* 2019; Bergström, 2003).

Beyond liquid permeability, the density and distinctive structural pattern of the pine matrix directly govern both the aesthetic value of the surface and its long-term optical permanence. Surface reflectance and color fastness are strictly dependent on the photochemical stability of the underlying lignin-carbohydrate complex. Consequently, maintaining the visual integrity of the wood surface relies on the chemical resistance of its macromolecular constituents particularly the capacity of lignin to withstand ultraviolet (UV) photo-degradation and subsequent oxidative reactions (George *et al.,* 2005; Tolvaj *et al.,* 2005).

To mitigate some of these natural variations and improve material performance, wood steaming is frequently employed. This controlled process exposes the raw material to saturated water steam within pressurized autoclaves. The primary objectives of this hydrothermal technology are to optimize rheological properties, eliminate internal growth stresses, and achieve uniform color homogeneity across the wood cross-section.

When subjected to operational temperatures ranging from 100°C to 140°C, a partial hydrolysis of the cell wall biopolymers is triggered. This process is initiated by the thermal degradation of hemicelluloses, which is accompanied by the release of water-soluble extractive substances. The overall kinetics of these chemical transformations are determined by the specific thermal mode and exposure duration, leading to the progressive decomposition of structural polysaccharides. Crucially, the autocatalytic effect of the released acetic and formic acids induces the further oxidation of carbohydrates and pectins; the subsequent dehydration of pentoses yields 2-furaldehyde (Fengel and Wegener, 2003; Sundqvist, 2006; Hill, 2006; Willems *et al.,* 2015; Vilkovský *et al.,* 2022; Dzurenda, 2024).

In parallel, structural transformations occur within the lignin matrix, characterized by the generation of free radicals and a simultaneous increase in the concentration of phenolic hydroxyl groups. This chemical restructuring leads to the synthesis of new chromophoric systems, which manifests macroscopically as a distinct darkening of the wood. This color shift directly correlates with broader modifications of the material's visual, physical, and mechanical attributes (Hon *et al.,* 2001; Fengel and Wegener, 2003; Sundqvist *et al.,* 2006; Výbohová *et al.,* 2018).

Concurrently, the concentration of hydrogen ions within the wood matrix quantified as the pH value serves as a critical indicator of its overall chemical reactivity. Wood acidity is directly proportional to the concentration of free and bound organic acids. These acidic components significantly influence not only the curing kinetics of applied adhesives and coating systems but also the natural resistance of the material against biotic degradation agents. In its native state, *Pinus sylvestris* L. exhibits a mildly acidic reaction, with the pH of its aqueous extracts typically falling between 4.0 and 5.0. Compared to many deciduous species, pine possesses a higher natural acidity, a characteristic directly attributed to the specific composition of its extractives and resin acids, such as abietic acid.

However, subjecting the wood to hydrothermal treatment with saturated steam induces deep chemical alterations that result in progressive tissue acidification. This drop in pH is primarily driven by deacetylation processes, during which free organic acids are cleaved and released from the hemicellulose chains. This phenomenon plays a significant role in both the sapwood and heartwood zones. Ultimately, the resulting variations in acid and extractive concentrations directly impact industrial processing parameters, imposing distinct limitations on the subsequent application of surface coatings and structural

adhesives (Kosíková *et al.,* 1999; Faix *et al.,* 2002; Fengel and Wegener, 2003; Trübswetter 2006; Irle 2012; Rowell 2012; Wang *et al.,* 2012; Geffert *et al.,* 2019.
The aim of the work is to determine the acidity of dried, steamed pine sapwood and heartwood for moisture w ≈ 10%, using a direct pH measurement method - SenTix Sur surface electrode.

MATERIALS AND METHODS

For the research, 25 pine trunks with a length of 6.3 m with a clearly visible sapwood and heartwood zone were selected from the Štiavnické vrchy locality (GPS. 48.4161247N, 18.8593111E, Central Slovakia region).
The center lumber with a width of 300–400 mm and a thickness of 50 mm was produced by cutting along the edge, which was subsequently divided into two asymmetric parts by longitudinal sawing. By transverse shortening of these parts, a 2 m long lumber was produced, which was randomly divided into 5 groups. The semi-finished products of the 1st group, in the number of 15 pieces, were not steamed. The other semi-finished products were steamed in mode I/t = 105 °C and pressure p = 0.12 MPa; and in mode II/t = 125 °C and pressure p = 0.23 MPa. Individual groups of steamed semi-finished products were taken from the pressure autoclave after τ = 6 h and τ = 18 h of steaming. The technological process was carried out in a pressure autoclave APDZ 240 (Himmasch AD, Chaskovo, Bulgaria) in the company Sundermann s.r.o. in Banská Štiavnica (Slovakia). The conditions for steaming pine core wood in a saturated water steam environment, including the time intervals for sampling individual groups of steamed semi-finished products, are shown in the diagram in Fig. 1.

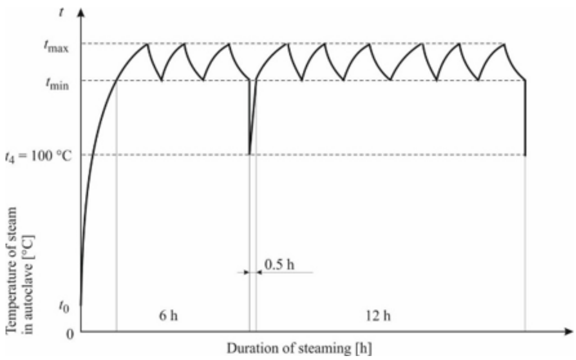

Figure 1. Diagram of the process of steaming pine wood.

Table 1. Technological conditions for steaming wood.

Steaming modes	t_{min}	t_{max}	t_4	Time of the technological process of steaming wood	
Mode I	102.5	107.5	100	$\tau_1 = 6$ h	$\tau_2 = 12\ (+0.5^a)$ h
Mode II	117.5	122.5	100		

Note: a After the specified period of wood treatment, exactly according to the specified diagram (course), 0.5 h must be added to the basic steaming time of pine wood. This time between individual treatment periods serves to reduce the pressure and for safe opening of the autoclave and manipulation when selecting one group of treated semi-finished products from the autoclave, closing and pressurizing the autoclave with saturated water steam.

The moisture content of the wood was determined before entering the technological process itself by randomly selecting 5 sapwood blanks and 5 blanks with a false heartwood, from which samples were sawn to determine the wood moisture content. The moisture content of the dried blanks was also determined, where 5 sapwood blanks and 5 blanks with a false heartwood were randomly selected from which samples were sawed to determine the wood moisture content. The moisture content of wet and dried wood was determined by the gravimetric method according to STN EN 13183-1 (2003).
Surface treatment of all dried blanks was carried out by milling on a JET JPT-410HH machine (STROJE Slovensko, Banská Bystrica, Slovak Republic).
Measurement of the acidity of dried native and steamed pine sapwood and heartwood was performed on a planed surface using a pH-meter pH7110 with a SenTix Sur surface electrode (Dudiak and Dzurenda 2020).
Measuring the acidity of beech wood consists in applying the surface electrode of the SenTix Sur pH-meter type: pH7110 to the surface of the wood. The acidity value was read after the pH value stabilized on the pH-meter display. At the point of measuring the pH of dry wood with a SenTix Sur surface electrode, first one drop of distilled water was dripped onto the surface of the wood using a dropper, and then the surface contact electrode was pressed against the surface of the wood in the place of the dropped drop, thereby creating contact between the electrode and the surface of the wood. The pH value was read after approx. 180 to 240 seconds of stabilization of the electrode on the pH-meter pH7110. The record of the measurement of the acidity of dry pine wood is shown in Fig. 2.

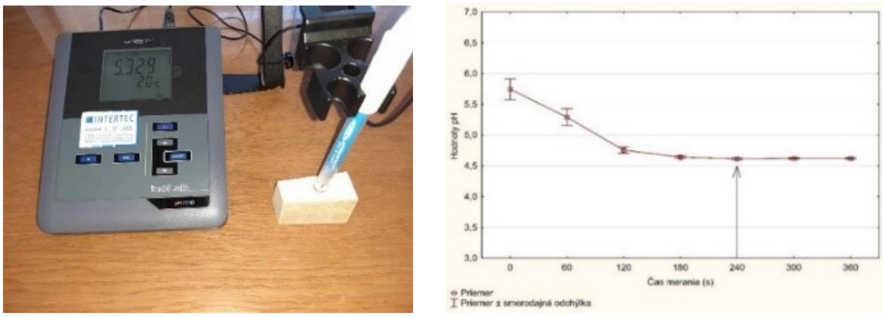

Figure. 2 Measurement of pH on the surface of pine wood after moistening it with a drop of distilled water.

RESULTS AND DISCUSSION

The moisture values of pine sapwood and heartwood, measured before the steaming process, after the steaming process in a pressure autoclave and after drying in a hot air dryer, are shown in Table 2.

Table 2. Changes in average wood moisture content during the steaming and drying cycles (mean ± SD).

Pine wood	Number of measurements (-)	Before steaming (%)	After steaming (%)	Decrease in wood moisture content after steaming (%)	After drying (%)	Decrease in wood moisture content after drying (%)
Native SW pine	60	63.9 ± 3.9	--	--	12.0 ± 0.4	81.2
Steamed SW pine (Mode I.)	30	--	58.3 ± 1.2*	8.7	12.1 ± 0.3*	79.2
Steamed SW pine (Mode II.)	30	--	56.9 ± 0.7*	10.9	12.0 ± 0.2*	78.9
Native HW pine	60	59.7 ± 3.7	--	--	11.9 ± 0.3	80.1
Steamed HW pine (Mode I.)	30	--	55.1 ± 0.8*	7.7	12.1 ± 0.2*	78.0
Steamed HW pine (Mode II.)	30	--	52.7 ± 0.8*	11.7	12.2 ± 0.1*	76.8

Based on the provided data, the native sapwood initially exhibited a higher moisture content (63.9±3.9%) than the heartwood (59.7±3.7%). The hydrothermal steaming process led to a verifiable reduction in pre-drying moisture content in both anatomical zones, with the magnitude of this reduction depending on the specific operational parameters:

Mode II induced a more pronounced post-steaming moisture drop than Mode I. Specifically, moisture levels fell by10.9% (down to 56.9%) in the sapwood and by 11.7% (down to 52.7%) in the heartwood. Following the final kiln-drying phase, moisture content achieved near-total homogenization across all specimen groups. Final moisture values stabilized within a narrow margin of 11.9% to 12.2%, corresponding to a total relative moisture reduction of 76.8% to 81.2% from the initial green state.

The acidity values of pine wood measured before the steaming process with saturated water steam and during the technological process measured in both modes and in time intervals of 6 and 18 h after are shown in Figure 3.

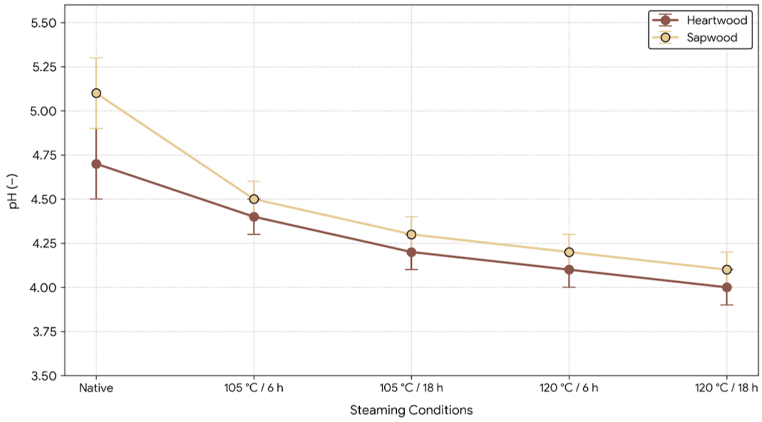

Figure 3. Influence of steaming conditions on pine wood pH.

Initially, the native wood displayed distinct baseline acidity levels between the heartwood and sapwood. The heartwood exhibited a lower average pH of 4.7, whereas the sapwood was less acidic at 5.1. The inherently higher acidity of the native heartwood is a natural consequence of heartwood formation, a process involving the mortality of parenchyma cells and the subsequent accumulation of secondary metabolites predominantly resin acids and phenolic compounds which naturally lower the pH. The slightly higher data variability observed in the control samples reflects the expected natural heterogeneity of unmodified wood biomass. Upon undergoing hydrothermal treatment, an immediate drop in pH was observed even under the mildest processing parameters (105°C for 6 h), falling to 4.4 in the heartwood and 4.5 in the sapwood. As the treatment was extended to 18 h and the temperature raised to 120°C, the pH continued to decline steadily, reaching its absolute minimum at the 120°C/18h combination (pH of 4.0 for heartwood and 4.1 for sapwood). Notably, while the sapwood maintained a marginally higher pH than the heartwood throughout all testing phases, the net pH reduction was more pronounced in the sapwood (ΔpH = 1.0) than in the heartwood (ΔpH = 0.7). This disparity indicates that the carbohydrate constituents of the sapwood, which is richer in accessible free hemicelluloses, undergo more intensive initial hydrolysis compared to the extractive-saturated heartwood. Following modification, the standard deviation stabilized at 0.1, confirming that the hydrothermal process uniformly affects the wood matrix and homogenizes its chemical profile. Physiochemically, this pH reduction during steaming is primarily driven by the thermal autohydrolysis of hemicelluloses. Exposing wood to elevated temperatures and moisture induces the deacetylation of polyoses (chiefly galactoglucomannans, the primary non-cellulosic polysaccharides in softwoods). This cleavage of acetyl groups releases free acetic acid into the moisture matrix, sharply increasing the concentration of oxonium ions (H_3O^+) and driving down the pH. This mechanism is inherently autocatalytic; the newly liberated acid accelerates the hydrolytic cleavage of remaining polysaccharide chains and furthers the degradation of the lignin-carbohydrate complex (Tjeerdsma *et al.,* 2005; Sundqvist *et al.,* 2006; Wang *et al.,* 2012; Bonifazi *et al.,* 2015; Timar *et al.,* 2016; Hofmann *et al.,* 2022).

Furthermore, this rising acidity is closely linked to total color changes (ΔE*). The acidic environment acts as a catalyst for the dehydration of pentoses and hexoses into furfural and 5-hydroxymethylfurfural. These volatile intermediates subsequently undergo condensation reactions with lignin and other structural components, generating dark chromophoric systems. To quantify the impact of the technological parameters (steaming temperature and duration) and their interaction on the resulting acidity of the two pine wood zones, a two-way analysis of variance (ANOVA) was performed. The statistical outputs confirm that the degradation mechanism is highly sensitive to both independent variables:

Effect of Temperature: Steaming temperature proved to be the most critical variable for both heartwood and sapwood ($p < 0.001$). Elevating the temperature from 105°C to 120°C forces a sharp increase in acidic components, demonstrating that the activation energy required for hemicellulose deacetylation is primarily governed by thermal intensity.

Effect of Time: The duration of steaming was also found to be highly significant ($p < 0.01$). Prolonging the exposure window facilitates the continuous generation of acetic acid, leading to a progressive accumulation of acidity in both anatomical zones. Interaction of Factors (Temperature/Time): The mutual interaction between temperature and time was statistically insignificant ($p > 0.05$). This finding is scientifically relevant as it shows that the timeline of pH reduction follows a parallel trajectory regardless of whether the processing temperature is set to 105°C or 120°C. The individual effects of these two factors are therefore additive rather than synergistic.

CONCLUSION

In this study, the effects of pressure steaming parameters (temperature and time) on pH changes in pine sapwood and heartwood (*Pinus sylvestris* L.) were evaluated. Based on experimental results and statistical analyses, the following main conclusions can be formulated:

- The steaming process causes an immediate decrease in the moisture content of the wood (by 7.7% to 11.7%) immediately after the pressure in the autoclave is released due to thermodynamic self-evaporation using the accumulated heat.
- Hydrothermal treatment causes a gradual acidification of the wood. Natural heartwood is naturally more acidic than sapwood due to the concentration of resin acids and accompanying substances. After steaming, the pH value in both zones decreased to final minima of 4.0 (heartwood) and 4.1 (sapwood). This decrease is chemically caused by thermal autohydrolysis and deacetylation of hemicelluloses (mainly galactogluco-mannans), which releases free acetic acid and increases the concentration of hydrogen ions H_3O^+.
- Two-factor analysis of variance (ANOVA) confirmed that both steaming temperature ($p < 0.001$) and exposure time ($p < 0.01$) are highly significant factors determining the increase in acidity, with their effect being additive, without synergistic interaction ($p > 0.05$). Since heartwood and sapwood show different chemical sensitivities, it is essential to approach both zones individually in industrial management to ensure optimal adhesion of subsequent coating systems and surface quality.

REFERENCES

1. Fengel, D.; Wegener, G. Wood: Chemistry, Ultrastructure, Reactions; Walter de Gruyter: Berlin, Germany, 2003; pp. 25–60.
2. Rowell, R.M. Handbook of Wood Chemistry and Wood Composites, 2nd ed.; CRC Press: Boca Raton, FL, USA, 2012; pp. 55–92.
3. Hill, C.A.S. Wood Modification: Chemical, Thermal and Other Processes; John Wiley & Sons: Chichester, UK, 2006; pp. 15–43.
4. Ekeberg, D.; Flæte, P.-O.; Eikenes, M.; Fongen, M.; Naess-Andresen, C.F. Qualitative and quantitative determination of extractives in heartwood of Scots pine (*Pinus sylvestris* L.) by gas chromatography. J. Chromatogr. A 2006, 1110, 120–127.
5. Budakçı, M.; Saygin, E.; Şenol, S. ffect of resin cleaning process on adhesion strength of water-based varnishes. BioResources 2019, 14(1), 1317-1332.
6. Bergström, B. Chemical and structural changes during heartwood formation in *Pinus sylvestris*. Wood Sci. Technol. 2003, 37, 221–233.
7. George, B.; Suttie, E.; Merlin, A.; Deglise, X. Photodegradation and photostabilisation of wood—The state of the art. Polym. Degrad. Stab. 2005, 88, 268–274.
8. Tolvaj, L.; Mitsui, K. Light source dependence of the photo-induced discoloration of wood. J. Wood Sci. 2005, 51, 468–473. 10.1007/s10086-004-0693-4
9. Sundqvist, B.; Karlsson, O.; and Westremark, U. Determination of formic-acid and acid concentrations formed during hydrothermal treatment of birch wood and its relation to color, strength and hardness. Wood Sci. Technol. 2006, 40, 549–561.
10. Hill, C.A.S. Wood Modification: Chemical, Thermal and Other Processes; John Wiley & Sons: Chichester, UK, 2006; pp. 1–239.
11. Willems, W.; Altgen, M.; Militz, H. Comparison of EMC and durability of heat treated wood from high versus low water vapour pressure reactor systems. Int. Wood Prod. J. 2015, 6, 12–18. https://doi.org/10.1179/2042645314Y.0000000083
12. Dzurenda, L.; Dudiak, M. Homogenization of the Color of Beech Sapwood and False Heartwood by the Steaming Process. Forests 2024, 15, 1009.
13. Vilkovský, P.; Vilkovská, T.; Klement, I.; Čunderlík, I. The Analysis Effect of Selected Factors on the Shear Strength of Woodbark at Different Wood Species. Forests 2022, 13, 637. https://doi.org/10.3390/f13050637
14. Hon, N.S.D.; Shiraishi, N. Wood and Cellulosic Chemistry; CRC Press: Boca Raton, FL, USA, 2001; p. 928, ISBN 9780824700249.
15. Výbohová, E., Geffertová, J., Geffert, A. Impact of steaming on the chemical composition of maple wood. BioRes. 2018, 13(3), 5862-5874.
16. Rowell, R.M. Handbook of Wood Chemistry and Wood Composites, 2nd ed.; CRC Press: Boca Raton, FL, USA, 2012; pp. 703.
17. Geffert, A.; Geffertová, J.; Dudiak, M. Direct method of measuring the pH value of wood. Forests 2019, 10, 852.
18. Trübswetter, P. Wood Modification by Steaming. Holztechnologie 2006, 47, 16–21.
19. Kosíková, B.; Čunderlík, I.; Kúdela, J.; Kačík, F. Chemical Changes in Wood During Steaming. Wood Res. 1999, 44, 35–42.
20. Irle, M. pH and Why You Need to Know it. Available online: http://www.wbpionline.com/features/ph-and-why-you-need-to-know-it/ (accessed on 20 August 2012).
21. Wang, W.; Cao, J.; Cui, F.; Wang, X. Effect of pH on Chemical Components and Mechanical Properties of Thermally ModifiedWood. Wood Fiber Sci. 2012, 44, 46–53.

22. Faix, O.; Labbe, H. Characterization of wood chemical changes in steaming and their effects on color and other properties*. Holzforschung, 2002, 56, 651–657.
23. Dudiak, M., Dzurenda, L. (2020). Acidita (pH) termicky a hydrotermicky upravovaného bukového dreva. In: Trieskové a beztrieskové obrábanie dreva 2020: vedecký časopis. Zvolen: Technická univerzita vo Zvolene, 2020, s. 37-40.
24. Timar, M.C.; Varodi, A.; Hacibektsoglu, M.; Campean, M. Color and FTIR analysis of chemical changes in beech wood (Fagus silvatica L.) after light steaming and heattreatment in two different environments. BioResources 2016, 11, 8325–8343.
25. Tjeerdsma, B.; Militz, H. Chemical changes in hydrothermal treated wood: FTIR analysis of combined hydrothermal and dry heat-treated wood. Eur. J. Wood Wood Prod. 2005, 63*, 102–111. https://doi.org/10.1007/s00107-004-0532-8
26. Wang, W.; Cao, J.; Cui, F.; Wang, X. Effect of pH on Chemical Components and Mechanical Properties of Thermally ModifiedWood. Wood Fiber Sci. 2012, 44, 46–53.
27. Sundqvist, B.; Karlsson, O.; and Westremark, U. Determination of formic-acid and acid concentrations formed during hydrothermal treatment of birch wood and its relation to color, strength and hardness. Wood Sci. Technol. 2006, 40, 549–561.
28. Bonifazi, G.; Calienno, L.; Capobianco, G.; Monaco, A. L.; Pelosi, C.; Picchio, R.; Serranti, S. 2015. Modeling color and chemical changes on normal and red heart beech wood by reflectance spectrophotometry, Fourier Transform Infrared spectroscopy and hyperspectral imaging. Polymer Degradation and Stability 2015, 113 10-21. http://dx.doi.org/10.1016/j.polymdegradstab.2015.01.001
29. Hofmann, T., Tolvaj, L., Visi-Rajczi, E. et al. Chemical changes of steamed timber during short-term photodegradation monitored by FTIR spectroscopy. Eur. J. Wood Prod. 2022, 80, 841–849 https://doi.org/10.1007/s00107-022-01814-

ACKONWLEDGEMENT

This paper was prepared within the grant project: VEGA 1/0423/25, and the KEGA 015TU Z4/2025 project Creation of support tools for further and update training of workers in the woodworking industry for the needs of Industry 4.0, as the result of work of the authors and the considerable assistance of the agencies.

25.80
Fühler
Anzeige
Logger

CHIP AND CHIPLESS WOODWORKING PROCESSES, 15(1): 55–60, 2026
Zvolen, Technical University in Zvolen, ISSN 1339-8350 (online)

HARDNESS OF STEAMED BEECH SAPWOOD AND FALSE HEARTWOOD DETERMINED BY LEEB HARDNESS TESTER ISH-SPHA

Ladislav Dzurenda – Michal Dudiak

Abstract

The paper presents the results of measuring the hardness of native and steamed beech sapwood and false heartwood by the dynamic method using Leeb hardness tester ISH-SPHA with a type D measuring probe.
The hardness of beech sapwood perpendicular to the fibers in the radial plane is HL = 319.8 ± 31.4 and in the tangential plane NL = 349.9 ± 36.1. The hardness values of false heartwood perpendicular to the fibers in the radial plane are HL = 328.4 ± 48.2 and in the tangential plane NL = 359.9 ± 42.3.
The hardness of steamed whitewood, beechwood in mode I. at a steaming temperature of t = 105 °C for τ = 18 hours is lower in the radial plane than in unsteamed beechwood by ΔHL = 8.5 and in the tangential plane by ΔHL = 6.6. In steamed beechwood in mode II. at a steaming temperature of t = 120 °C for τ = 9 hours in the radial plane it is lower than in unsteamed beechwood by ΔHL = 11.2 and in the tangential plane by ΔHL = 13.0.
Similar trends in hardness decrease are also observed in steamed beech wood with false heartwood. The hardness of steamed beech wood with false heartwood according to mode I. in the radial plane is HL = 316.5, which represents a decrease in comparison with unsteamed beech wood by ΔHL = 11.9 and in the tangential plane HL = 348.5 with a decrease by ΔHL = 11.4. In steamed beech wood with mode II. the hardness of the wood in the radial plane is HL = 311.8, which is a lower value in comparison with unsteamed beech wood by ΔHL = 16.6 and in the tangential plane HL = 339.1, which is a lower value by ΔHL = 20.8.

Keywords: *beech wood, sapwood, false heartwood, steaming, hardness, Leeb hardness tester ISH-SPHA.*

INTRODUCTION

The wood of the Beech species is classified as a heartless, mature wood species with the possible occurrence of a false heartwood. The color of beech wood in the mature sapwood zone is light whitish-gray, or white-pink Nečesaný (1959), Makovíny (2010), Dzurenda – Dudiak (2022).
A false heartwood is a growth defect in beech wood that forms during the growth of the tree in the mature wood zone. It occurs by the penetration of air into the mature wood zone through wounds on the trunk or branches Nečesaný (1958), Požgaj *et al*., (1997), Bauch

Technical University in Zvolen, T. G. Masaryka 24, 960 01 Zvolen
e-mail: dzurenda.ladislav@gmail.com

and Koch (2001) Molnar *et al.,* (2001), Račko and Čunderlík (2010), Trenčiansky *et al.,* (2017). Among other things, the color of the heartwood differs from the white-gray or pale brown color of beech wood by a range of shades of red-brown Gorczynski (1951), Požgaj *et al.,* (1997), Dzurenda – Dudiak (2022).

These color differences between heartwood and sapwood often necessitate the exclusion or partial limitation of certain sawmill assortments for the production of bent furniture, sports equipment, or construction and joinery products.

One of the alternatives to eliminate the aforementioned color differences between sapwood and heartwood is its heat treatment of the wood by steaming Dzurenda-Dudiak (2025).

The hardness of wood is a property that expresses the resistance of wood to the penetration of foreign bodies into its volume. Knowledge about wood hardness is used in the processes of mechanical splitting and woodworking, chip formation, selection of woodworking tools, as well as in the selection of wood species for the production of a particular product, e.g. from the aspect of abrasion resistance of the tread surface of the flooring. Wood hardness is measured by: static methods (Janka hardness test, Brinell HB hardness test), dynamic method (Leeb HL hardness test).

The aim of the work is to determine the hardness of steamed beech and false heartwood perpendicular to the fibers in the radial and tangential planes by a dynamic method using the Leeb hardness tester ISH-SPHA.

MATERIALS AND METHODS

In order to eliminate the differences between the color of the sapwood and the false heartwood, the blanks with dimensions of 32 x 50 x 800 mm made of wet beech sapwood and false heartwood were steamed in a pressure autoclave APDZ 240 at Sundermann s.r.o. Banská Štiavnica. The first group of blanks was steamed in mode I. - saturated water steam at a temperature of $t = 105 \pm 2.5$ °C for a period of $\tau = 18$ hours and the second group of blanks was steamed in mode II. - saturated water vapor at a temperature of $t = 120 \pm 2.5$ °C for a period of $\tau = 9$ hours.

After steaming, the semi-finished products were dried in hot air in a dryer according to the Dzurenda (2022) mode in order to preserve the wood color achieved by the technological steaming process. The load-bearing surfaces of the dried wood were machined on a horizontal plane milling machine FS 200.

The wood hardness was measured using a portable Leeb hardness tester ISH-SPHA (INSZIE Czech s.r.o., Brno, Czech Republic) with a type D measuring probe, Fig. 1.

Fig. 1. *Leeb portable hardness tester ISH-SPHA*

The measurement of the hardness of materials by the dynamic Leeb method is based on the principle of measuring the impact velocity vA and the rebound velocity vR after the impact of a carbide hammer with a ball of a certain diameter in a tube chamber on the surface of the measured body. The ratio of the rebound velocity vR to the impact velocity vA is a measure of the dynamic Leeb hardness of the test sample.

$$HL = \frac{v_R}{V_A} \, .1000 \qquad (1)$$

Where: v_A – impact velocity,
v_R – rebound velocity.

Changes in the hardness of steamed beech wood compared to unsteamed beech wood are expressed both in the form of the values of the differences in the measured values ΔHL:

$$\Delta HL = HL_{Bk} - HL_{Bk-P} \qquad (2)$$

Where: HL_{Bk} - hardness of unsteamed beech wood in a given direction,
$HL_{Bk\text{-}P}$ – hardness of steamed beech wood in a given direction.

RESULTS AND DISCUSSION

The results of measurements of beech wood from the sapwood zone and the false heartwood zone perpendicular to the fibers in the radial plane and tangential plane are given in Table 1 in the form of notation: average value and standard deviation.

Table 1. Hardness of native and steamed beech sapwood and false heartwood.

Beech wood	Hardness perpendicular to the fibers:	sapwood	false heartwood
Not steamed	radial plane	319.8 ± 31.4	328.4 ± 48.2
	tangential plane	349.9 ± 36.1	359.9 ± 42.3
Steamed in mode I. temperature t = 105 °C, time τ = 18 h	radial plane	311.3 ± 42.8	316.5 ± 44.1
	tangential plane	343.3 ± 46.8	348.5 ± 53.1
Steamed in mode II. temperature t = 120 °C, time τ = 9 h	radial plane	308.6 ± 33.8	311.8 ± 37.8
	tangential plane	336.9 ± 37.7	339.1 ± 45.5

The differences in the hardness of unsteamed beech wood between sapwood and heartwood in the radial and tangential planes result from the fact that the cell walls of sapwood are not lignified and the lumens are not filled with tulsa, as well as from the different density of beech wood throughout the trunk, which is presented in the work: Dudiak (2023).
The lower hardness of wood in the radial plane compared to the tangential plane is attributed to the different morphology of the pith rays from the librifor fibers and their distribution in the wood, Perelygin (1965).

Due to steaming, the hardness of steamed beech sapwood, as indicated by the average hardness values perpendicular to the fibers in the radial and tangential directions, decreases. The average hardness value of steamed beech whitewood in mode I at a temperature of t = 105 °C for τ = 18 hours is in the radial plane HL = 311.3, which represents a decrease of ΔHL = 8.5 compared to unsteamed beechwood, and in the tangential plane HL = 343.3 with a decrease of ΔHL = 6.6. In color-homogenized beechwood in mode II. at a temperature of t = 120 °C for τ = 9 hours, the Leeb hardness in the radial plane HL = 308.6, which represents a decrease of ΔHL = 11.2 compared to unsteamed beechwood, and in the tangential plane HL = 336.9 with a decrease of ΔHL = 13.0.
Similar trends in hardness decrease are also observed in steamed beech wood from false heartwood. The hardness of steamed beech wood from false heartwood according to regime I. in the radial plane is HL = 316.5, which represents a decrease of ΔHL = 11.9, and in the tangential plane HL = 348.5 with a decrease of ΔHL = 11.4. In beech wood with uniform color according to regime II., the hardness of the wood in the radial plane is HL = 311.8, which is a value lower by ΔHL = 16.6 compared to unsteamed beech wood, and in the tangential plane with a value of HL = 339.1, the value is lower by ΔHL = 20.8.
As the steaming temperature increases, the hardness of beech wood decreases. However, the rate of decrease in the hardness values of beech wood is not large. The differences between the hardness of beech wood before steaming and after steaming are smaller than the values of the standard deviations of the hardness of beech wood, based on which it can be stated that the hardness of color-homogenized steamed beech wood both perpendicular to the fibers in the radial and tangential planes is within the tolerance of the natural variability of the hardness of beech wood.

In the professional literature, wood hardness values are mainly reported by static methods (Jankova hardness test, Brinell hardness test). Measuring wood hardness using a portable ISH-SPHA hardness tester with a type D measuring probe is simple, practical and fast if the requirements for the quality of the processed wood are met, as stated in the work: Bembenek, Kowalski. Pawlik: Analysis of the influence of surface roughness of different types of wood on the results of their hardness measured by the Leeb method.

CONCLUSION

Based on the results of experimental research into the influence of technological steaming conditions on wood hardness, the values of wood hardness perpendicular to the fibers in the radial plane and tangential plane of sapwood and false heartwood were determined before and after steaming in mode I. and mode II. by the dynamic method with a Leeb hardness tester ISH-SPHA with a measuring probe type D,
The hardness of steamed whitewood beech wood in mode I at a steaming temperature of t = 105 °C for τ = 18 hours is in the radial plane at HL = 311.3, which represents a decrease of ΔHL = 8.5 compared to unsteamed beech wood and in the tangential plane HL = 343.3 compared to unsteamed beech by ΔHL = 6.6. In steamed beech wood in mode II. at a steaming temperature of t = 120 °C for τ = 9 hours, the hardness value in the radial plane is HL = 308.6, which represents a decrease of ΔHL = 11.2 and in the tangential plane HL = 336.9 with a decrease of ΔHL = 13.0.
Similar trends in hardness decrease are also observed in steamed beech wood from false heartwood. The hardness of steamed beech wood from false heartwood according to mode I. in the radial plane is HL = 316.5, which represents a decrease of ΔHL = 11.9, and in the

tangential plane HL = 348.5 with a decrease of ΔHL = 11.4. In beech wood with uniform color according to regime II., the hardness of the wood in the radial plane is HL = 311.8, which is a value lower by ΔHL = 16.6 compared to unsteamed beech wood, and in the tangential plane with a value of HL = 339.1, the value is lower by ΔHL = 20.8.
As the steaming temperature increases, the hardness of beech wood decreases. The decrease in beech wood hardness is not large. The differences between the values of beech wood hardness before and after steaming are smaller than the values of the standard deviations of the hardness of unsteamed beech wood with a sapwood and a false heartwood, based on which it can be stated that the hardness of color-homogenized steamed beech wood both perpendicular to the fibers with a radial and tangential plane is within the tolerance of the natural variability of beech wood hardness.

Ackonwledgement:
This experimental research was prepared within the grant project: APVV-21-0051 "*Research of false heartwood and sapwood of Fagus sylvatica L. wood in order to eliminate color differences by the process of thermal treatment with saturated water steam"*.

REFERENCES

Bauch, J., Koch, G. (2001): Biologische und chemische Untersuchungen über *Holzverfarbungen der Rotbuche (Fagus sylvatica [L.]) und Möglichkeiten vorbeugender Maßnahmen. Abschlussbericht, Bundesforschungsanstalt für Forst- und H*olzwirtschaft, Universität Hamburg.

Bembenek, M., Kowalski, L., Pawlik, J. (2021): Analysis of the influence of surface roughness of various types of wood on the results of their hardness measured by the Leeb method. *IOP Conf. Ser.: Mater. Sci. Eng.* 1199 012071, DOI 10.1088/1757-899X/1199/1/012071

Dudiak, M. (2023): Density of beech *(Fagus sylvatica* L.) wood through a cross-section of the trunk. Acta Facultatis Xylologiae Zvolen. 65(2): 5 – 11. DOI: 10.17423/afx.2023.65.2.01

Dzurenda, L. (2022): Mode for hot air drying of steamed beech blanks while keeping the colours acquired in the steaming process. In: Acta Facultatis Xylologiae Zvolen. 64(1),81-88, DOI: 10.17423/afx.202264.1.07

Dzurenda, L., Dudiak, M. (2022): Modifikácia farby dreva v procese parenia sýtou vodnou parou. Zvolen: Technická nuniverzity vo Zvolene, 120 s.

Dzurenda, L., Dudiak, M. (2025): Eliminácia rozdielov farby bukového dreva bele a nepravého jadra procesom parenia. Zvolen: Technická univerzity vo Zvolene, ISBN 978-80-228-3498-8. 117 s.

Gorczynski, T. (1951): Badania anatomicznoporównawcze nad drewnem buka zwyczajnogo (Fagus silwatica L.). Rocz.demdr.Polsk. Tow. Bot.7. 3-114.

Makovíny, I. (2010): Úžitkové vlastnosti a použitie rôznych druhov dreva. Zvolen: TU Zvolen, 104 s.

Nečesaný, V. (1959): Jádro buka, štruktúra, vznik a vývoj. Vydavateľstvo Slovenskej akadémie vied, Bratislava, 256 s.

Molnár, S., Németh, R., Fehér, S., Tolvaj, L., Papp, G., Varga, F. (2001) Technical and technological properties of Hungarian beech wood consider the red heart. Wood research, 46(1),21-30.

Perelygin, L., M., (1965): *Náuka o dreve*. Bratislava: SVTL, 388 s.

Požgaj, A., Chovanec, D., Kuriatko, S., Babiak, M., (1997): *Štruktúra a vlastnosti dreva.* I. vydanie. Bratislava: Príroda a.s., 1993. s. 485. ISBN 80-07-00600-1.

Račko, V., Čunderlík, I. (2010): Zrelé drevo ako limitujúci faktor vzniku nepravého jadra buka (Fagus sylvatica L.). In: Acta facultatis xylologiae Zvolen, 52 (1):15 – 24.

Trenčiansky, M., Lieskovský, M., Merganič, J., Šulek, R. (2017): *Analysis and evaluation of the impact of stand age on the occurrence and metamorphosis of red heartwood*. Forest-Biogeosciences and Forestry, 10(3):605-610, https://doi.org/10.3832/ifor2116-010

CHIP AND CHIPLESS WOODWORKING PROCESSES, 15(1): 61–66, 2026
Zvolen, Technical University in Zvolen, ISSN 1339-8350 (online)

ACTIVATION ENERGY VALUE OF THE COLOR UNIFICATION OF BEECH SAPWOOD AND FALSE HEARTWOOD IN THE STEAMING PROCESS

Ladislav Dzurenda – Michal Dudiak

Abstract

The paper presents the results of experimental research into the influence of technological steaming conditions on the unification of the color of beech sapwood and false heartwood. The activation energy of the given physicochemical process E_a*=57kJ.mol*$^{-1}$ *was determined using the Arrhenius equation.*
The given value represents the minimum amount of energy required to achieve the activated state of reactions occurring in wood during steaming. Under steaming conditions, these are primarily chemical reactions such as: extraction of low-molecular substances, partial hydrolytic degradation of polysaccharide and lignin components of wood. These processes lead to the formation of chromophoric structures, which are macroscopically manifested by a change in the color of the wood.
The determined value of the activation energy is a parameter of the Arrhenius equation, which in a modified form can be an alternative for predicting the influence of temperature on the steaming time in the process of unifying the color of beech sapwood and heartwood.

Keywords: *activation energy, steaming, beech wood, sapwood, false heartwood, Arrhenius equation.*

INTRODUCTION

The wood of the beech species is classified as a heartless, mature wood species with the possible occurrence of a false heartwood. The color of beech wood in the sapwood and mature sapwood zone is light white-gray, or white-pink. In the color space CIE L*a*b*, the color of dry mature beech wood and sapwood is given by the values on the lightness coordinate L* = 78.9 ± 2.4 and the chromatic coordinates: a* = 7.6 ± 1.7; b*= 18.9 ± 1.9 Babiak *et al.,* (2004), Meints *et al.* (20117), Dzurenda (2023).
A false heartwood is a growth defect in beech wood that is formed during the growth of a tree in the mature wood zone. It is created by the penetration of air into the mature wood zone through wounds on the trunk or branches Bauch and Koch (2001) Molnár *et al.* (2001), Račko and Čunderlík (2010), Trenčiansky *et al.,* (2017). The color of the false heartwood differs, among other things, from the white-gray or pale brown color of beech wood by a range of shades of red-brown. In the color space CIE L*a*b*, the color of the

Technical University in Zvolen, T. G. Masaryka 24, 960 01 Zvolen
e-mail: dzurenda.ladislav@gmail.com

false heartwood is described by the values at the individual coordinates of the CIE Lab color space: L* = 64.9 ± 4.9; a* = 12.9 ± 2.1; b* = 19.6 ± 1.9 Dzurenda (2023).
The color difference of the false heartwood from the sapwood and mature wood is the cause of rejection, respectively. limited use of sawmill assortments from the production of bent furniture, sports equipment, or construction and joinery products.
One of the alternatives to eliminate the aforementioned color differences between sapwood and false heartwood, while maintaining the original structural and mechanical properties, is its heat treatment by steaming Dzurenda and Dudiak (2025). Previous research into color changes in beech sapwood and false heartwood by steaming has shown that the color change of false heartwood at the same temperature is 2 to 6 times lower than the color change of sapwood. As the temperature increases, the differences in the aforementioned changes decrease Dzurenda and Dudiak (2024).
Investigating the causes of differences in color changes of beech sapwood and false heartwood in thermal processes requires answering several fundamental questions. One of them is determining the value of active energy, i.e. the minimum energy required for the initiation and course of chemical reactions resulting in the formation of new chromophores.

The aim of the work is to determine the value of: activation energy Ea of physicochemical processes occurring during the unification of the color of beech sapwood and false heartwood by the steaming process.

MATERIALS AND METHODS

Experimental research on the influence of temperature and steaming time on the color change of beech sapwood and heartwood was carried out in the company Sundermann s.r.o. Banská Štiavnica, which has an APDZ 240 pressure autoclave (Himmasch AD, Haskovo, Bulgaria). As part of the research on the color change of sapwood and heartwood, the color change of sapwood and heartwood was monitored at a steaming temperature of t_I = 95 ± 2.5°C with saturated moist air at atmospheric pressure and saturated water steam at temperatures t_{II} = 105 ± 2.5°C, t_{III} = 115 ± 2.5°C, t_{IV} = 120 ± 2.5°C in 3h intervals during 21 hours of steaming.
Samples of beech wood with false heartwood, both unsteamed and steamed, were dried in a hot-air dryer according to the Dzurenda (2022) mode in order to preserve the original color of the wood, or the color acquired by the technological process of steaming.
The bearing surfaces of the samples of dried unsteamed and steamed lumber were machined on a horizontal plane milling machine FS 200.
The color measurement was performed with a Color reader CR-10 Plus colorimeter (Konica Minolta, Japan) with a reflection spectrum in the range of 400 - 700 nm. The D65 light source was used and the diameter of the optical sensing hole was 8 mm.
The values of lightness L*, red color a*, yellow color b* on the coordinates of the CIE color space L*a*b* are given in the form of the average measured value $\bar{x}$ and the standard deviation s_x.

$$x = \bar{x} \pm s_x \tag{1}$$

Where: $\bar{x}$ – average value,
s_x – standard deviation.

RESULTS AND DISCUSSION

The color of mature beech wood and false heartwood wood before steaming and after steaming with saturated moist air at the end of the steaming mode or steaming with saturated water steam after achieving color unification at individual steaming temperatures is shown in Fig. 1. and the color values in the color space CIE L*a*b* coordinates in Table 1. Dzurenda and Dudiak (2025).

native | $t = 95°C$, $\tau = 21$ h | $t = 105°C$, $\tau = 18$ h | $t = 115°C$, $\tau = 15$ h | $t = 120°C$, $\tau = 9$ h

Figure 1. Color of beech sapwood and heartwood before and after steaming.

The results of experimental research aimed at analyzing the influence of temperature and duration of steaming on the unification of the color of beech sapwood and false heartwood show that until the temperature $t_I \approx 95$ °C for a period of $\tau = 21$ hours, the unification of the colors of sapwood and false heartwood does not occur. The values in the color space CIE L*a*b* coordinates of mature beech wood are: L* = 70.5 ± 2.1, a* = 13.2 ± 1.2, b* = 19.3 ± 1.5 and of false heartwood L* = 66.8 ± 2.7, a* = 13.4 ± 1.8, b* = 19.6 ± 1.3. At a steaming temperature $t_{II} \approx 105$ °C for a period of $\tau = 18$ h beech wood of a uniform pale brown color is obtained with values on the coordinates: L* = 63.4 ± 2.3, a* = 13.0 ± 1.4, b* = 19.1 ± 1.6, at a steaming temperature $t_{III} \approx 115$ °C for a period of $\tau = 15$ h it has a brown color with values on the coordinates: L* = 59.0 ± 2.1, a* = 12.9 ± 1.4, b* = 18.8 ± 1.7 and at a steaming temperature $t_{IV} \approx 120$ °C for a period of $\tau = 9$ h dark brown-gray color with values on the coordinates: L* = 57.5 ± 2.0, a* = 13.4 ± 1.2, b* = 18.8 ± 1.5.

One of the alternatives for determining the activation energy value of the physico-chemical process of wood steaming eliminating the differences in the color of sapwood and non-heartwood is the calculation using the Arrhenius equation (1) and experimentally measured values: temperatures and steaming times.

$$k = A\, e^{-\frac{E_a}{RT}} \tag{1}$$

Where: k - reaction rate constant; T - absolute temperature (K); Ea - is the activation energy; R=8.314 J/mol·K; A - is the frequency factor.

Assuming first-order kinetics, the rate constant k is inversely proportional to the characteristic reaction time τ:

$$\tau = \frac{1}{k} \tag{2}$$

By substituting relation (1) into equation (2), the Arrhenius equation takes the form:

$$\tau = \frac{1}{A \cdot e^{-E_a/RT}} = \frac{1}{A} \cdot e^{E_a/RT} \qquad (3)$$

respectively, after logarithmization, the form of the linear dependence:

$$\ln \tau = -\ln A + \frac{E_a}{R} \cdot \frac{1}{T} \qquad (4)$$

From the linear dependence lnτ = f(1/T), the activation temperature Ea/Ra and subsequently the activation energy Ea are first determined using the coordinates of two points of the technological process (e.g. from experimentally determined minimum and maximum temperatures and their corresponding lnτ values):

$$\frac{E_a}{R} = \frac{\Delta \ln \tau}{\Delta(1/T)} = \frac{ln_{\tau(min)} - ln_{\tau_{max)}}}{\frac{1}{T_{(min)}} - \frac{1}{T_{(max)}}} = \frac{\ln 18 - ln\, 9}{\frac{1}{378,15} - \frac{1}{393,15}} = \frac{2,890 - 2,197}{0,002644 - 0,002543} = \frac{0,693}{0,000101} = 6861\, K \qquad (5)$$

Activation energy Ea:

$$\frac{E_a}{R} = 6861\, K, \Rightarrow E_a = 6861 \cdot R = 6861 \cdot 8,314 = 57\,042 \frac{J}{mol} = 57 kJ/mol \qquad (6)$$

The given value represents a fundamental kinetic parameter, which in the sense of the Arrhenius equation expresses the dependence of the rate constant of chemical reactions on thermodynamic temperature. Within the physicochemical processes of unification of the colors of beech wood sapwood and false heartwood (in the temperature interval t = 105 – 120 °C), it quantifies the minimum energy barrier of elementary reactions taking place in the wood mass. During the steaming of beech wood, several types of physical processes and chemical reactions take place: extraction of low-molecular substances, hydrolytic degradation of hemicelluloses and amorphous cellulose, structural changes of lignin, which result in the formation of new chromophoric structures affecting the change in the color of wood.

Based on the magnitude of the activation energy, the unification of the colors of beech sapwood and false heartwood by steaming can be classified, from the aspect of chemical reactions, into the group of reactions with medium-high activation energy values (E_a = 40 – 80 $kJ \cdot mol^{-1}$).

From a technological point of view, knowledge of the activation energy value in the process of unifying the color of sapwood and false heartwood by steaming is a basic prerequisite for modeling the kinetics of processes occurring in wood. The modified Arrhenius equation allows not only modeling the dependence of steaming time on temperature, but also effectively controlling the steaming process in order to minimize operating costs and degradation changes in steamed wood.

CONCLUSION

Based on the results of experimental research into the influence of technological steaming conditions on the unification of the color of sapwood and false heartwood of beech wood in the temperature interval t = 105 – 120 °C, the activation energy of the ongoing physicochemical processes E_a = 57 kJ·mol^{-1} was determined using the Arrhenius equation.

It represents the minimum amount of energy required to achieve the activated state of the ongoing reactions in beech wood during steaming. In the conditions of steaming of beech wood, these are primarily chemical reactions: extraction of low-molecular substances, hydrolytic degradation of hemicelluloses and amorphous cellulose, structural changes in lignin, which result in the formation of new chromophoric structures resulting in a change in the color of the wood.

Knowledge of the activation energy value of a particular physicochemical process is a basic prerequisite for solving the Arrhenius equation. In this case, the modified Arrhenius equation allows modeling the influence of temperature on steaming time on the unification of the color of beech sapwood and false heartwood.

Ackonwledgement:
This experimental research was prepared within the grant project: APVV 21-0051 Research of false heartwood and sapwood of *Fagus sylvatica* L. wood in order to eliminate color differences by the process of thermal treatment with saturated water steam as the result of work of author and the considerable assistance of the APVV agency, the KEGA 015TU Z4/2025 project Creation of support tools for further and update training of workers in the woodworking industry for the needs of Industry 4.0.

REFERENCES

Babiak, M.,; Kubovský, I.,; Mamoňová, M., (2004): Color space of selected local woods. In: *Interaction of wood with various Forms of Energy*. Technická univerzita vo Zvolene. s. 113 – 117. ISBN 80-228-1429-6.

Bauch, J., Koch, G. (2001): Biologische und chemische Untersuchungen über Holzverfarbungen der Rotbuche (Fagus sylvatica [L.]) und Möglichkeiten vorbeugender Maßnahmen. Abschlussbericht, Bundesforschungsanstalt für Forst- und Holzwirtschaft, Universität Hamburg.

Dzurenda, L. (2022): Mode for hot air drying of steamed beech blanks while keeping the colours acquired in the steaming process. In: Acta Facultatis Xylologiae Zvolen. 64(1),81-88, DOI: 10.17423/afx.202264.1.07

Dzurenda, L. (2023): Natural Variability of the Color of Beech Wood in the Color Space CIE L*a*b*. In: Forests 14, 1103. doi.org. 10.3390/f14061103.

Dzurenda, L., Dudiak, M. (2024): Homogenization of the color of beech sapwood and false heartwood by the steaming process. In: Forests. - ISSN 1999-4907. - Vol. 15, issue 6 https://www.mdpi.com/1999-4907/15/6/1009.

Dzurenda, L., Dudiak, M. (2025): Eliminácia rozdielov farby bukového dreva bele a nepravého jadra procesom parenia. Zvolen: Technická univerzity vo Zvolene, ISBN 978-80-228-3498-8. 117 s.

Gorczynski, T. (1951): Badania anatomicznoporównawcze nad drewnem buka zwyczajnogo (Fagus silwatica L.). Rocz.demdr.Polsk. Tow. Bot.7. 3-114.

Makovíny, I. (2010): Úžitkové vlastnosti a použitie rôznych druhov dreva. Zvolen: TU Zvolen, 104 s.

Nečesaný, V. (1959): Jádro buka, štruktúra, vznik a vývoj. Vydavateľstvo Slovenskej akadémie vied, Bratislava, 256 s.

Meints, T., Teischinger, A., Stingl, R., and Hassmann, C. (2017). "Wood colour of central European wood species: CIELAB characterisation and colour intensification," European Journal of Wood and Products 75, 499-509. DOI 10.1007/s00107-016-1108-0

Molnár, S., Németh, R., Fehér, S., Tolvaj, L., Papp, G., Varga, F. (2001) Technical and technological properties of Hungarian beech wood consider the red heart. Wood research, 46(1),21-30.

Požgaj, A., Chovanec, D., Kuriatko, S., Babiak, M., (1997): *Štruktúra a vlastnosti dreva.* I. vydanie. Bratislava: Príroda a.s., 1993. s. 485. ISBN 80-07-00600-1.

Račko, V., Čunderlík, I. (2010): Zrelé drevo ako limitujúci faktor vzniku nepravého jadra buka (Fagus sylvatica L.). In: Acta facultatis xylologiae Zvolen, 52 (1):15 – 24.

Trenčiansky, M., Lieskovský, M., Merganič, J., Šulek, R. (2017): *Analysis and evaluation of the impact of stand age on the occurrence and metamorphosis of red heartwood*. Forest-Biogeosciences and Forestry, 10(3):605-610, https://doi.org/10.3832/ifor2116-010

CHIP AND CHIPLESS WOODWORKING PROCESSES, 15(1): 67–73, 2026
Zvolen, Technical University in Zvolen, ISSN 1339-8350 (online)

AIRBORNE PARTICULATE EMISSIONS FROM WOODCHIP HANDLING: IMPLICATIONS FOR WORKER SAFETY IN BIOMASS-BASED HEATING PLANTS

Miloš Gejdoš – Martin Lieskovský – Daniel Tomčík

Abstract

The handling and movement of wood chips in biomass-based urban heating plants generate considerable amounts of airborne particulate matter ($PM_{2,5}$ and PM_{10}), which may pose risks to both worker health and the surrounding environment. This study quantified particulate matter concentrations during chip-loading operations and compared them with non-loading conditions using real-time laser-based monitoring. The results indicate that $PM_{2,5}$ and PM_{10} concentrations increased approximately threefold during loading activities, reaching mean values of 24.03 µg/m³ and 38.75 µg/m³, respectively. Continuous monitoring conducted near the storage site revealed short-term exceedances of World Health Organization (WHO) guideline values for $PM_{2,5}$, suggesting potential acute exposure risks. Spatial analysis showed that distance from the source significantly influenced particulate levels, with the highest concentrations observed within 50 m of the woodchip pile and a marked decrease beyond 100 m. Overall, the findings emphasize the necessity of implementing effective dust mitigation strategies, optimizing handling procedures, and enforcing appropriate safety protocols to minimize exposure to fine particulate matter during biomass processing operations.

Key words: *wood chips, particulate matter, dust emissions, worker safety, biomass storage, exposure monitoring*

INTRODUCTION

The increasing demand for renewable energy has led to a rapid expansion of biomass-based heating systems, requiring large-scale storage of woody fuels to ensure a continuous supply (Sahoo et al., 2019). However, alongside these benefits, biomass storage introduces a range of environmental and occupational risks, particularly related to airborne particulate matter (PM) emissions (Kim et al., 2015).
Fine particles such as $PM_{2,5}$ and PM_{10} are of major concern due to their potential to adversely affect respiratory health. Elevated concentrations may occur in the vicinity of biomass storage and handling operations, posing risks not only to workers but also to nearby residents (Gejdoš and Lieskovský, 2024). In addition to health impacts, dust accumulation in biomass storage facilities can contribute to serious safety hazards, including self-heating, spontaneous combustion, and dust explosions (Zhou et al., 2022; Varela et al., 2023). These risks are amplified in poorly ventilated storage systems, where thermal processes can escalate into runaway reactions. Historical incident records further

Technical University in Zvolen, T. G. Masaryka 24, 960 01 Zvolen, National Forest Centre, Zvolen
e-mail: gejdos@tuzvo.sk

highlight the importance of effective monitoring and preventive measures (Müllerová, 2014).

Woodchip processing and handling are recognized sources of airborne wood dust (Jacobsen et al., 2021; Takougang et al., 2023). While occupational exposure has been widely documented, the proximity of storage sites to residential areas raises additional concerns regarding environmental exposure (Noll and Jirjis, 2012). Wood dust is classified as a known human carcinogen and has been associated with respiratory diseases, including asthma, chronic bronchitis, and allergic reactions (Siew et al., 2012; Pérez-Rios et al., 2009). Airborne particles generated during storage and handling may disperse beyond the immediate site, affecting the surrounding environment (Simpson et al., 2016).

To reduce these risks, various mitigation measures have been proposed, including covering biomass piles, maintaining optimal moisture conditions, and applying dust suppression technologies. Continuous monitoring of air quality is equally important, particularly in urban settings where human exposure may be significant (Chen et al., 2024; Lieskovský and Gejdoš, 2023). Recent studies emphasize the need for integrated assessments that combine occupational and environmental exposure to better evaluate overall health impacts (Chen et al., 2024; Chin et al., 2016).

Despite extensive research on wood dust exposure, studies that simultaneously evaluate workplace and ambient PM levels at urban biomass storage sites remain limited, especially in relation to international health guidelines. This gap is particularly relevant for centrally located heating plants.

In Slovakia, occupational exposure to wood dust is regulated by Government Act No. 356/2006 Coll., which classifies wood dust as a carcinogenic factor and sets technical exposure limits. Although compliance with these limits reduces health risks, it does not eliminate them entirely, underscoring the need for preventive measures.

The aim of this study is to assess particulate matter emissions associated with biomass storage in an urban heating plant and to evaluate potential exposure risks for both workers and nearby residents. The study combines (i) occupational exposure measurements conducted according to EN 689+AC and STN EN 482, and (ii) environmental monitoring of $PM_{2,5}$ and PM_{10} concentrations in the surrounding area. The results are evaluated in relation to the World Health Organization air quality guidelines (WHO, 2021) to determine potential exceedances and associated health implications.

MATERIAL AND METHODS

Study site

The study was conducted at a district heating plant in Hriňová, Slovakia, where woodchips are used as the primary fuel (Figure 1a). Such installations are typically located within urban areas and operate continuously, requiring frequent handling and replenishment of biomass, which can influence local air quality. The woodchip storage pile at the study site covered an area of approximately 30 × 60 m, with heights ranging from 5 to 15 m.

Measurement methodology

Instrumentation

Airborne particulate matter ($PM_{2,5}$ and PM_{10}) was measured using a portable laser-based monitor (Temtop M2000C), which provides real-time concentration data. For continuous monitoring, an AirNote device (Blues) was deployed to record particulate concentrations together with temperature and humidity. This combination enabled the assessment of both short-term fluctuations and long-term exposure patterns.

Measurement design

To evaluate the impact of biomass handling, $PM_{2,5}$ and PM_{10} concentrations were recorded during chip-loading operations and compared with non-loading periods. Occupational exposure measurements were conducted in accordance with EN 689+AC and STN EN 482, using 2-hour sampling intervals. In addition, continuous monitoring was carried out from 29 May to 23 June 2024 to capture temporal variability in particulate matter concentrations. The integration of short-term and long-term measurements provided a comprehensive assessment of air quality conditions. Measured values were compared with World Health Organization (WHO, 2021) air quality guideline values ($PM_{2,5}$: 15 µg/m^3; PM_{10}: 45 µg/m^3, 24-hour means) to provide context for potential health risks.

Spatial assessment

To evaluate the dispersion of particulate matter, measurements were conducted at the source and at distances of 50 m, 100 m, and 150 m from the woodchip pile (Figure 1b). Each location was monitored for at least 2 hours under stable weather conditions (wind speed < 1 m/s, no precipitation). Distances were measured using a Vertex Laser Geo rangefinder (Haglöf, Sweden). Measurements were taken at approximately 1.5 m above ground level and repeated to ensure accuracy.

Data analysis

All statistical analyses were performed using R software (R Core Team, 2024). Data processing was conducted using the dplyr package (Wickham et al., 2023). Differences between loading and non-loading periods were tested using Welch's t-test, while spatial variations were analysed using one-way ANOVA followed by post-hoc comparisons.

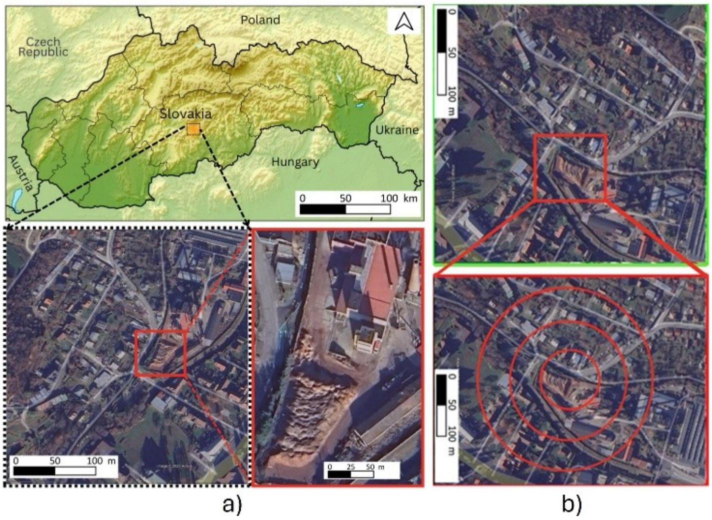

Fig. 1 (a) Study site in Hriňová (Slovakia) with woodchip storage; (b) measurement layout showing sampling distances (0, 50, 100, and 150 m) from the woodchip pile.

RESULTS

Occupational exposure

Chip-loading operations resulted in significantly higher particulate matter concentrations compared to non-loading conditions (Figure 2; Table 1).

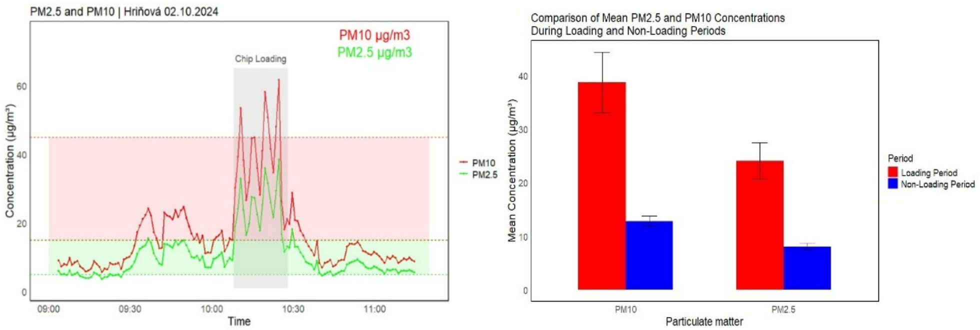

Fig. 2 Time series of $PM_{2,5}$ and PM_{10} concentrations during loading and non-loading periods (left) and mean concentrations with 95% confidence intervals (right).

Tab. 1 Comparison of PM concentrations during loading and non-loading periods.

Pollutant	Loading Period Ø(µg/m^3)	Non-Loading Period Ø(µg/m^3)	t-value	Degrees of Freedom (df)	Mean difference	95% CI	Cohen's d	p-value
$PM_{2,5}$	24.03	8.07	9.58	20.36	15.96	12.49-19.43	3.88	< 0.001
PM_{10}	38.75	12.80	9.51	20.32	25.95	20.26-31.63	3.88	< 0.001

Mean $PM_{2,5}$ increased from 8.07 to 24.03 µg/m^3, while PM_{10} rose from 12.80 to 38.75 µg/m^3. These differences were statistically significant ($p < 0.001$) for both pollutants, with large effect sizes (Cohen's d = 3.88).
During loading, $PM_{2,5}$ short-term means exceeded WHO 24-hour guideline values, whereas concentrations during non-loading periods remained within recommended limits.

Continuous monitoring

Continuous monitoring revealed substantial temporal variability in PM concentrations (Figure 3). Mean values remained relatively low ($PM_{2,5}$: 8.38 µg/m^3; PM_{10}: 8.75 µg/m^3), but short-term exceedances were observed, particularly for $PM_{2,5}$.
$PM_{2,5}$ exceeded the WHO guideline (15 µg/m^3, 24-hour mean) for 82.5 hours (14.2% of the monitoring period), with a maximum daily mean of 43.7 µg/m^3. In contrast, PM_{10} exceedances were rare (0.5 hours; max daily mean 70.9 µg/m^3).
Overall, three days exceeded the daily limit for $PM_{2,5}$ and one day for PM_{10}, indicating episodic exposure peaks despite acceptable average conditions.

Spatial distribution

PM concentrations decreased with increasing distance from the woodchip pile (Figure 3 – right part). The highest levels were recorded at 50 m (PM_{10}: 70.9 µg/m^3; $PM_{2,5}$: 43.7 µg/m^3), followed by a marked reduction at 100 m (PM_{10}: 33.4 µg/m^3; $PM_{2,5}$: 21.5 µg/m^3). At 150 m, concentrations remained similar to those at 100 m (PM_{10}: 35.6 µg/m^3; $PM_{2,5}$: 22.5 µg/m^3), indicating stabilization beyond 100 m. $PM_{2,5}$ concentrations exceeded WHO guideline values at all measured distances, while PM_{10} exceeded the limit only at 50 m.
Statistical analysis confirmed a significant effect of distance on both PM_{10} and $PM_{2,5}$ ($p < 0.001$). Post hoc comparisons showed no significant differences between 100 m and 150 m, indicating that the main reduction occurs between 50 m and 100 m (Table 2).

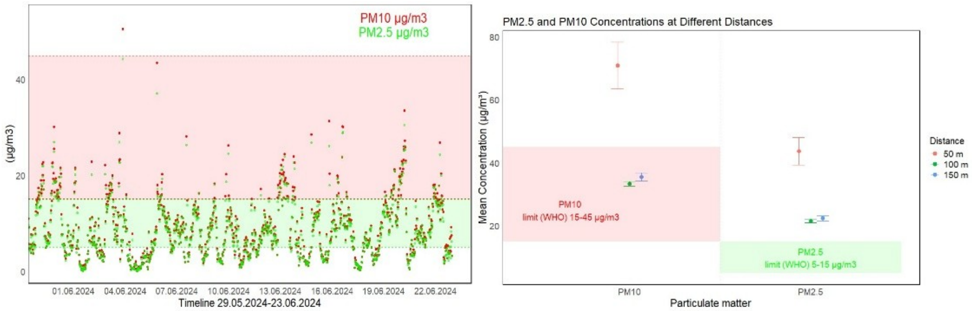

Fig. 3 (left) Hourly and daily $PM_{2,5}$ and PM_{10} concentrations with WHO guideline values; (right) mean concentrations at increasing distances from the woodchip pile.

Tab. 2 ANOVA and post hoc results for PM concentrations by distance.

Particulate matter	Comparison	Mean Difference (µg/m^3)	95% Confidence Interval	p-value
PM_{10}	150 m - 100 m	2.22	-5.27 to 9.70	0.766
	50 m - 100 m	37.51	30.07 to 44.96	< 0.001
	50 m - 150 m	35.30	27.87 to 42.72	< 0.001
$PM_{2,5}$	150 m - 100 m	0.91	-3.55 to 5.38	0.880
	50 m - 100 m	22.13	17.70 to 26.57	< 0.001
	50 m - 150 m	21.22	16.79 to 25.64	< 0.001

DISCUSSION AND CONCLUSION

This study demonstrates that biomass handling in urban heating plants significantly increases airborne particulate matter concentrations, particularly during chip-loading operations, where $PM_{2,5}$ and PM_{10} levels were approximately three times higher than during non-loading periods. Although average concentrations remained within guideline values, continuous monitoring revealed frequent short-term exceedances, especially for $PM_{2,5}$, indicating potential acute exposure risks. These findings highlight the importance of considering short-term variability in addition to long-term averages when assessing air quality impacts.
Particulate concentrations decreased with increasing distance from the source; however, elevated $PM_{2,5}$ levels persisted beyond 100 m, confirming the ability of fine particles to disperse and remain suspended in the surrounding environment.
From a practical perspective, the results emphasize the need for effective dust mitigation strategies, particularly during handling operations. Measures such as improved material

handling, dust suppression, and the use of personal protective equipment can significantly reduce exposure risks. Continuous air quality monitoring remains essential for ensuring safe operating conditions and protecting both workers and nearby populations. These results are particularly relevant for urban heating plants located in close proximity to residential areas. This is particularly relevant for urban heating plants located in close proximity to residential areas.

ACKNOWLEDGEMENTS

This study was funded by the European Commission under the LignoSilva project [Grant Agreement #101059552] through the Horizon Europe—Teaming for Excellence program. The work was further supported by a contract between the National Forest Centre and the Ministry of Ag-riculture and Rural Development of the Slovak Republic within the research framework NLC 2022–2026 Digiwood. The contribution was also supported by the Slovak Research and Development Agency through project APVV-22-0001. Additionally, this work was carried out with support from the Recovery and Resilience Plan of the Slovak Republic under project no. 09I05-03-V02-00001.

REFERENCES

1. Chen, X., Yan, H., Ma, L., Fang, Q., Zhang, C., Chen, G., Yin, C., 2024. Comprehensive experimental study of microbial respiration during self-heating in biomass storage piles. Fuel 362, 130746. https://doi.org/10.1016/j.fuel.2023.130746.
2. Chin, Y., Darvell, L.I., Lea-Langton, A., Williams, A., 2016. Ignition Risks of Biomass Dust on Hot Surfaces. Energy & Fuels 30. https://doi.org/10.1021/acs.energyfuels.5b02622.
3. Gejdoš, M., Lieskovský, M., 2024. Overview of Health and Safety Risks in the Process of Production and Storage of Forest Biomass for Energy Purposes—A Review. Energies 17, 1064. https://doi.org/10.3390/en17051064.
4. Government of the Slovak Republic. Government Directive Nr. 356/2006 Body of Laws: On Protecting the Health of Employees from Risks Related to Exposure to Carcinogenic and Mutagenic Factors at Work; Government of the Slovak Republic: Bratislava, Slovakia,2020.
5. Jacobsen, G., Schaumburg, I., Sigsgaard, T., Schlünssen, V., 2021. Wood Dust Exposure Levels and Respiratory Symptoms 6 Years Apart: An Observational Intervention Study Within the Danish Furniture Industry. Annals of Work Exposures and Health 65, 1029–1039. https://doi.org/10.1093/annweh/wxab034.
6. Kim, K.-H., Kabir, E., Kabir, S., 2015. A review on the human health impact of airborne particulate matter. Environment International 74, 136–143. https://doi.org/10.1016/j.envint.2014.10.005.
7. Lieskovský, M., Gejdoš, M., 2023. Monitoring of Respiratory Health Risks Caused by Biomass Storage in Urban-Type Heating Plants. Forests 14, 707. https://doi.org/10.3390/f14040707.
8. Müllerová, J., 2014. Health and Safety hazards of biomass storage. https://doi.org/10.5593/SGEM2014/B41/S17.034.

9. Noll, M., Jirjis, R., 2012. Microbial communities in large-scale wood piles and their effects on wood quality and the environment. Applied microbiology and biotechnology 95, 551–63. https://doi.org/10.1007/s00253-012-4164-3.
10. Pérez-Rios, M., Ruano-Ravina, A., Etminan, M., Takkouche, B., 2009. A meta-analysis on wood dust exposure and risk of asthma. Allergy 65, 467–73. https://doi.org/10.1111/j.1398-9995.2009.02166.x.
11. Sahoo, U.K., Singh, S.L., Gogoi, A., Kenye, A., Sahoo, S.S., 2019. Active and passive soil organic carbon pools as affected by different land use types in Mizoram, Northeast India. PLoS ONE 14, e0219969. https://doi.org/10.1371/journal.pone.0219969.
12. Siew, S., Kauppinen, T., Kyyrönen, P., Heikkilä, P., Pukkala, E., 2012. Occupational exposure to wood dust and formaldehyde and risk of nasal, nasopharyngeal, and lung cancer among Finnish men. Cancer Management and Research 4, 223–32. https://doi.org/10.2147/CMAR.S30684.
13. Simpson, A.T., Hemingway, M.A., Seymour, C., 2016. Dangerous (toxic) atmospheres in UK wood pellet and wood chip fuel storage. Journal of Occupational and Environmental Hygiene 13, 699–707. https://doi.org/10.1080/15459624.2016.1167279.
14. STN EN 482, 2021. Workplace exposure. Procedures for the determination of the concentration of chemical agents. Basic performance requirements.
15. STN EN 689+AC, 2019. Workplace exposure. Measurement of exposure by inhalation to chemical agents. Strategy for testing compliance with occupational exposure limit values.
16. Takougang, I., Bukam Guemnyen, G.W., Edzamba, M.F., Lekeumo Cheuyem, F.Z., Assomo Ndemba, P.B., Pefura, W.Y., 2023. Exposure to Wood dust and its Respiratory Health Effects Among Wood Workers in Yaoundé (Cameroon). https://doi.org/10.1101/2023.12.28.23300613.
17. Varela, A., Arbizu, J., Tascón, A., 2023. Application of Factorial Analysis to the Study of Vented Dust Explosions in Large Biomass Storage Silos. Fire 6, 226. https://doi.org/10.3390/fire6060226.
18. WHO global air quality guidelines, 2021. particulate matter (PM2.5 and PM10), ozone, nitrogen dioxide, sulfur dioxide and carbon monoxide [www Document], n.d. https://www.who.int/publications/i/item/9789240034228 (accessed 5.18.26).
19. Wickham H, François R, Henry L, Müller K, Vaughan D, 2023. dplyr: A Grammar of Data Manipulation. R package (version 1.1.4) [software]. https://CRAN.R-project.org/package=dplyr.
20. Zhou, X., Li, X., Cui, Z., Wu, L., Zhou, H., Lu, X., 2022. Combustible wood dust explosions and impacts on environments and health - A review. Environmental Research 216, 114658. https://doi.org/10.1016/j.envres.2022.114658.

CHIP AND CHIPLESS WOODWORKING PROCESSES, 15(1): 75–80, 2026
Zvolen, Technical University in Zvolen, ISSN 1339-8350 (online)

RELATIONSHIP BETWEEN CUTTING FORCES AND SURFACE ROUGHNESS IN EDGE MILLING OF PARTICLEBOARD

Luďka Hanincová – Jiří Procházka – Vít Novák – David Kyselka

Abstract

This study investigates the relationship between cutting force and surface roughness during CNC edge milling of particleboard. Experiments were carried out on a 5-axis CNC machining center using a single-edge tool at a constant spindle speed of 18,000 min^{-1}. Feed per tooth (f_z = 0.2, 0.3, 0.4, 0.5 mm) and milling strategy (climb and conventional) were varied as the main technological factors. The results showed that increasing feed per tooth led to higher cutting force F_c and increased surface roughness R_a for both milling strategies. Conventional milling produced consistently higher roughness values compared to climb milling. Statistical analysis confirmed significant effects of feed per tooth and milling strategy on F_c and R_a, while their interaction was significant only for cutting force. A strong positive trend was observed for climb milling, while a statistically significant relationship was confirmed for conventional milling. These findings indicate that cutting force can serve as an indirect indicator of surface quality. The results highlight the potential for using force-based monitoring in real-time process control and optimization in wood machining.

Key words: *particleboard, CNC milling, cutting force, surface roughness, feed per tooth, milling strategy*

INTRODUCTION

Particleboard is widely used in furniture manufacturing due to its favorable cost-to-performance ratio and suitability for mass production. In many applications, machined edges represent critical functional surfaces intended for edge banding, bonding, coating, or direct visual use. Therefore, edge quality significantly affects both the final product appearance and the efficiency of subsequent processing operations. Edge roughness and integrity are thus considered key quality indicators in wood-based panels (Demir et al., 2022; Garrido et al., 2024).

The quality of milled edges is influenced by several technological factors, including feed per tooth, spindle speed, tool geometry, and milling strategy. Among these, feed per tooth is consistently reported as a dominant factor affecting surface roughness, with increasing values generally leading to surface deterioration (İşleyen and Karamanoğlu, 2019; Sedlecký and Gašparík, 2017; Szwajka et al., 2023).

Cutting force represents an important process indicator, as it reflects the interaction between the cutting tool and the workpiece material and is closely related to chip formation,

Mendel University in Brno, Faculty of Forestry and Wood Technology, Department of Wood Science and Technology, Zemědělská 3, Brno, 613 00, Czech Republic
e-mail: ludka.hanincova@mendelu.cz

tool loading, and energy demand. Previous studies have shown that cutting forces increase with chip load and are often accompanied by changes in surface quality (Pałubicki, 2021; Li et al., 2023).

Recent research has also highlighted the potential of cutting force as a signal for indirect prediction of surface quality, particularly within sensor-based and data-driven monitoring approaches (Szwajka et al., 2023; Župerl and Čuš, 2019; Górski et al., 2022). However, studies directly addressing the relationship between cutting force and surface roughness during CNC edge milling of particleboard under defined cutting conditions remain limited.

Therefore, the aim of this study was to evaluate the relationship between cutting force F_c and surface roughness R_a during CNC edge milling of particleboard under different feed per tooth values and two milling strategies.

MATERIAL AND METHODS

Material

A commercially available particleboard (thickness 18 mm) was used as the workpiece material. Prior to machining, specimens were conditioned under standard laboratory conditions.

CNC milling conditions

Edge milling was performed on a 5-axis CNC machining center Morbidelli m100 at a constant spindle speed of 18,000 min^{-1} using a single-edge end mill (D = 16 mm). The investigated factor was feed per tooth (f_z = 0.2, 0.3, 0.4, 0.5 mm). Two milling strategies were applied: climb and conventional milling. All tests were conducted under identical conditions with a constant tool state.

Cutting force measurement

Cutting forces were measured using a Kistler 9257B dynamometer. The cutting force component Fc was evaluated from the stable cutting region, excluding tool entry and exit. Cutting force measurements were carried out in three repetitions for each combination of cutting conditions and milling strategy.

Surface quality evaluation

Surface quality was assessed using a Keyence VR-6000 optical 3D profilometer. Measurements were performed in representative regions in the central part of the machined edge (Figure 1). For each cutting condition, measurements were performed in 3 regions, with 9-line profiles evaluated per region. The roughness parameter R_a was used to characterize surface quality.

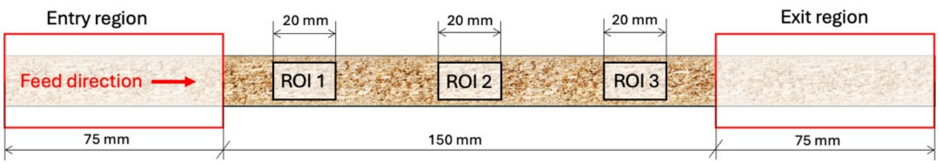

Figure 1: Selection of measurement areas on the milled edge.

Data analysis

Statistical evaluation included analysis of variance (ANOVA) to assess the effects of feed per tooth and milling strategy. The relationship between F_c and R_a was analyzed using correlation and linear regression models, evaluated separately for each milling strategy and for the complete dataset.

RESULTS

Effect of feed per tooth on cutting force

The mean cutting force F_c increased with feed per tooth under both milling strategies (Figure 2). In climb milling, F_c increased from 6.88 N at f_z = 0.2 mm to 8.30 N at f_z = 0.4 mm, followed by a slight decrease at f_z = 0.5 mm (7.92 N). In conventional milling, a more pronounced increase was observed, from 4.45 N at f_z = 0.2 mm to 8.69 N at f_z = 0.5 mm.

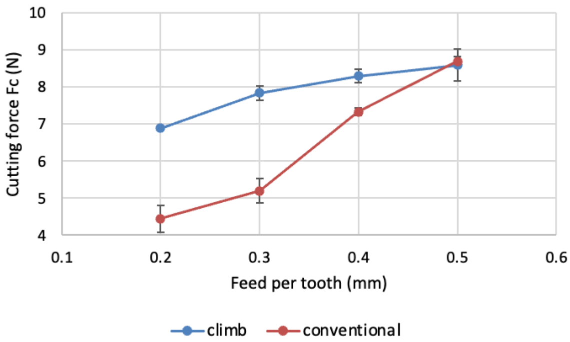

Figure 2: Effect of feed per tooth on cutting force under climb and conventional milling.

Two-way ANOVA confirmed that both milling strategy and feed per tooth significantly affected cutting force ($p < 0.001$). In addition, a significant interaction between both factors was found ($p < 0.001$), indicating that the influence of feed per tooth depended on the applied milling strategy.

Effect of feed per tooth on surface roughness

The roughness parameter R_a increased with increasing feed per tooth for both milling strategies (Figure 3). In climb milling, R_a increased from 29.23 µm to 49.34 µm, while in conventional milling the values increased from 37.11 µm to 51.99 µm.

For all tested cutting conditions, conventional milling produced higher roughness values than climb milling.

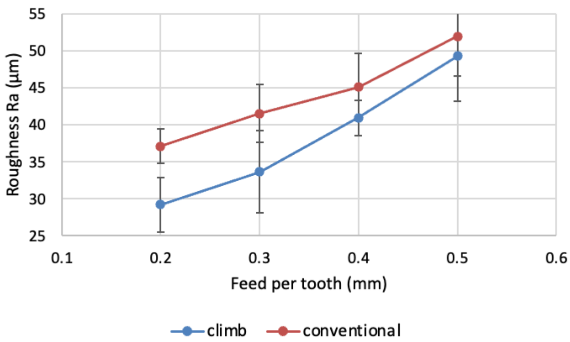

Figure 3: Effect of feed per tooth on surface roughness R_a.

Two-way ANOVA revealed that both milling strategy ($p = 0.0069$) and feed per tooth ($p < 0.001$) significantly affected R_a. However, the interaction between both factors was not significant ($p = 0.666$), indicating a similar roughness response to increasing feed per tooth under both milling strategies.

Relationship between cutting force and surface roughness

Linear regression analysis showed positive relationships between cutting force and roughness for both milling strategies (Figure 4).

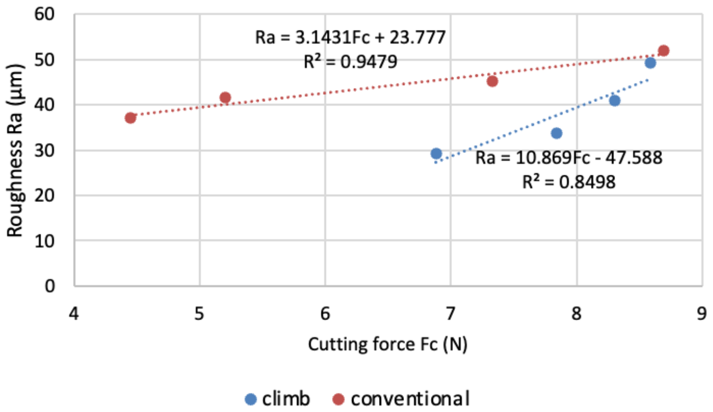

Figure 4: Relationship between cutting force and surface roughness with linear regression for both milling strategies.

For climb milling, a strong trend was observed ($R^2 = 0.850$), although the regression model did not reach statistical significance at the 95% confidence level ($p = 0.078$).

For conventional milling, an even stronger relationship was found ($R^2 = 0.948$), and the regression model was statistically significant ($p = 0.026$).

These results indicate that increasing cutting force was associated with increasing surface roughness, particularly under conventional milling conditions.

DISCUSSION

The results confirmed that feed per tooth is a dominant factor affecting both cutting force and surface quality during CNC edge milling of particleboard. Increasing fz led to higher Fc and Ra values under both milling strategies, which is consistent with established machining mechanisms. Higher feed per tooth increases uncut chip thickness and material removal per tooth engagement, resulting in higher resistance during chip formation and thus higher cutting force (Pałubicki, 2021; Thibaut et al., 2016).

The increase in surface roughness with increasing fz can be attributed to both geometrical and material-related effects. Higher chip thickness increases the theoretical scallop height and promotes less stable chip detachment. In particleboard, the heterogeneous structure further contributes to surface damage through particle pull-out, edge tearing, and irregular fracture. Similar trends have been reported for wood-based composites (İşleyen and Karamanoğlu, 2019; Demir et al., 2022; Zhu et al., 2022).

Conventional milling produced consistently higher roughness values than climb milling, indicating more favorable surface generation in climb milling. This difference is related to chip formation mechanisms: while climb milling starts with maximum chip thickness and promotes more stable cutting, conventional milling begins with near-zero chip thickness, which may increase rubbing, unstable fracture, and edge damage. These effects are particularly pronounced in heterogeneous materials such as particleboard and support the preference for climb milling in applications requiring high edge quality (Śmietańska et al., 2020; Bedelean et al., 2023).

Compared with cutting force, surface roughness exhibited higher variability, reflecting the influence of material heterogeneity. While F_c represents a stable process signal, R_a is additionally affected by local variations in particle distribution, density profile, and fracture behavior.

A key finding of this study is that a strong positive relationship was observed for both milling strategies, although statistical significance was confirmed only for conventional milling. The high coefficients of determination ($R^2 = 0.850$ for climb and $R^2 = 0.948$ for conventional milling) indicate that increasing cutting force is associated with increasing roughness. This suggests that cutting force can serve as an indirect indicator of surface quality, as both variables are governed by common process mechanisms such as chip thickness and material removal conditions (Raman et al., 2012; Demir et al., 2022; Szwajka et al., 2023). The lower statistical significance for climb milling is likely related to the limited number of experimental conditions.

From an industrial perspective, this relationship is particularly relevant, as cutting force can be monitored in real time, while surface roughness is typically evaluated offline. This highlights the potential for using force-based monitoring for process optimization and quality control in wood machining.

The study was limited to a single material, tool geometry, and cutting condition. Further research should verify the observed relationships under different materials, tool wear conditions, and broader parameter ranges.

CONCLUSION

Based on the experimental results obtained during CNC edge milling of particleboard, the following conclusions can be drawn:

1) Feed per tooth significantly affected both cutting force and surface roughness during CNC edge milling of particleboard.

2) Increasing feed per tooth increased F_c and worsened surface quality under both milling strategies.

3) Conventional milling produced significantly rougher surfaces than climb milling.

4) Strong positive relationships between F_c and R_a were found, particularly for conventional milling ($R^2 = 0.948$; $p = 0.026$).

5) The results suggest the potential of F_c as an indirect indicator of surface quality for future real-time monitoring of wood-based panel machining.

REFERENCES

Bedelean, B., Ispas, M., & Răcășan, S. (2023). Combining artificial neural network and response surface methodology to optimize the drilling operating parameters of MDF panels. Forests, 14(11), 2254. https://doi.org/10.3390/f14112254

Demir, A., Cakiroğlu, E. O., & Aydin, I. (2022). Effects of CNC processing parameters on surface quality of wood-based panels used in furniture industry. Drvna industrija, 73(4), 363–371. https://doi.org/10.5552/drvind.2022.2109

Garrido, N. M. B., Martins, J., Davim, J. P., & Carvalho, L. (2024). Investigation into the effects of machining parameters on the edge quality of particleboards-Modelling and Optimization.

Górski, J., Podziewski, P., & Borysiuk, P. (2022). The machinability of flat-pressed, single-layer wood-plastic particleboards while drilling—experimental study of the impact of the type of plastic used. Forests, 13(4), 584. https://doi.org/10.3390/f13040584

İşleyen, Ü. K., & Karamanoğlu, M. (2019). The influence of machining parameters on surface roughness of mdf in milling operation. Bioresources, 14(2), 3266–3277. https://doi.org/10.15376/biores.14.2.3266-3277

Li, R., Yao, Q., & Wang, X. (2023). Optimization of cutting power and power efficiency during particleboard helical milling. Materialwissenschaft und werkstofftechnik, 54(2), 158–167. https://doi.org/10.1002/mawe.202200136

Pałubicki, B. (2021). Cutting forces in peripheral up-milling of particleboard. Materials, 14(9), 2208. https://doi.org/10.3390/ma14092208

Pałubicki, B., Hlásková, L., Frömel-Frybort, S., & Rogoziński, T. (2021). Feed force and sawdust geometry in particleboard sawing. Materials, 14(4), 945. https://doi.org/10.3390/ma14040945

Raman, N. A., Sharif, S., & Izman, S. (2012). Mathematical modeling of cutting force in milling of medium density fibreboard using response surface method. Advanced materials research, 445, 51–55. https://doi.org/10.4028/www.scientific.net/amr.445.51

Sedlecký, M., & Gašparík, M. (2017). Power consumption during edge milling of medium-density fiberboard and edge-glued panel. Bioresources, 12(4), 7413–7426. https://doi.org/10.15376/biores.12.4.7413-7426

Śmietańska, K., Podziewski, P., Bator, M., & Górski, J. (2020). Automated monitoring of delamination factor during up (conventional) and down (climb) milling of melamine-faced MDF using image processing methods. European journal of wood and wood products, 78(3), 613–615. https://doi.org/10.1007/s00107-020-01518-9

Szwajka, K., Zielińska-Szwajka, J., & Trzepieciński, T. (2023). The use of a radial basis function neural network and fuzzy modelling in the assessment of surface roughness in the MDF milling process. Materials, 16(15), 5292. https://doi.org/10.3390/ma16155292

Thibaut, B., Denaud, L., Collet, R., Marchal, R., Beauchêne, J., Mothe, F., Méausoone, P.-J., Martin, P., Larricq, P., & Eyma, F. (2016). Wood machining with a focus on french research in the last 50 years. Annals of forest science, 73(1), 163–184. https://doi.org/10.1007/s13595-015-0460-2vv

Zhu, Z., Buck, D., Wang, J., Wu, Z., Xu, W., & Guo, X. (2022). Machinability of different wood-plastic composites during peripheral milling. Materials, 15(4), 1303. https://doi.org/10.3390/ma15041303

Županl, U., & Čuš, F. (2019). A cyber-physical system for surface roughness monitoring in end-milling. Strojniski Vestnik-Journal of Mechanical Engineering, 65(2), 67-78.

THE INFLUENCE OF CO_2 LASER ENGRAVING PARAMETERS ON COLOUR CHANGES OF WOOD SURFACE

Ivan Kubovský – Jozef Kúdela – Michal Andrejko

Abstract
This paper deals with the influence of CO_2 laser engraving process parameters on colour changes of selected wood surfaces. Experimental samples of spruce, beech and oak wood were exposed to laser radiation with a wavelength of 10.6 μm at different levels of laser power and raster density. The amount of energy applied to the surface was expressed as the total irradiation dose (H). Colour changes, expressed in the CIE $L^*a^*b^*$ colorimetric space, were recorded for all wood species even at low laser power and the lowest raster density. At the maximum values of the mentioned parameters (compared to the surfaces of untreated samples), the lightness value (L^*) decreased by more than 50% and the total colour difference (ΔE) increased by more than 40%. Heat-induced changes in the structures of chromophores, which are part of the main components of wood (lignin, hemicelluloses), are responsible for the colour changes of wood. The knowledge gained enables optimization of the laser process to achieve targeted treatment of wood surfaces without mechanical degradation of the material.

Key words: *CO_2 laser, wood, colour, engraving, laser power, raster density.*

INTRODUCTION

Laser processing and engraving of wood is a non-contact technology with high precision and flexibility. Currently, much attention is paid to the study of wood surfaces engraved with CO_2 lasers with the aim of modifying their structure and properties (Nath et al. 2020; Kúdela et al. 2021; Gurau et al. 2017; Jurek and Wagnerová 2021; Reinprecht and Vidholdová 2021; Guo et al. 2021; Li et al. 2021; Lungu et al. 2022). The energy concentrated in the laser beam delivered to a specific location on the engraved wood surface is converted into heat. As a result of the energy concentrated in the laser beam, thermal degradation of the surface structures of wood occurs in the heat-affected zone. High energy values cause sublimation of the surface layer of wood, accompanied by the formation of a charred, or molten layer (Kúdela et al. 2022; Kúdela et al. 2024). Chemical and structural changes also occur on the surface of the wood treated in this way, which is reflected in changes in its morphology, colour and wetting by liquids (Wust et al. 2005; Barcikowski et al. 2006; Kačík and Kubovský 2011; Kačíková et al. 2013; Kubovský et al. 2014; Li et al. 2018). The colour of the wood is a sensitive indicator of these temperature changes. The key role in the colour change is played by lignin, which is subject to thermal decomposition at lower temperatures than cellulose (Nguila et al. 2006; Kubovský et al. 2020). Understanding the relationship between laser parameters (laser power, laser head

Technical University in Zvolen, T. G. Masaryka 24, 960 01 Zvolen
e-mail: kubovsky@tuzvo.sk

feed speed) and the resulting colour is key for industrial applications where high aesthetic quality of engraved motifs is required.
The aim of the work was to comprehensively evaluate the influence of radiation produced by a CO_2 laser on colour changes in wood under various engraving parameters and to determine the functional dependence of colour quantities on the irradiation dose.

MATERIALS AND METHODS

Experimental material and engraving parameters

Test specimens with dimensions of 50 mm × 100 mm × 15 mm (width × length × thickness) were prepared from three wood species - spruce wood (*Picea abies* Karst.), beech wood (*Fagus sylvatica* L.) and oak wood (*Quercus robur* L.). The surfaces of the specimens were sanded with P180 grit sandpaper before engraving. The moisture content of the specimens was 12%. During engraving, the specimen surfaces were placed 17 mm below the focal point of the focusing lens of the CO_2 laser device CM-1309 (Shenzhen Reliable Laser Tech, China). The maximum laser power at the resonator output was 137.5 W. The laser head moved above the specimen surface in the direction of the fibers at a constant speed of 350 $mm \cdot s^{-1}$. The radiation intensity varied with the change in laser power and raster density (number of rasters per millimeter of width). Three sets of specimens were prepared. The first set was engraved at a laser power of 11 W, the second at a power of 16.5 W and the third set at a power of 22 W. A FieldMaxII-TOP power meter (Coherent, U.S.A.) with a sensor located in the plane of the sample surface was used to measure the laser power. The number of rasters per millimeter of width was 2, 5, 10, 20 and 30 mm^{-1}. This represented 5 combinations and each combination was represented by four bodies, plus four untreated (reference) samples. The radial surfaces of all bodies were uniformly irradiated over the entire length and width under the selected conditions (Fig. 1).

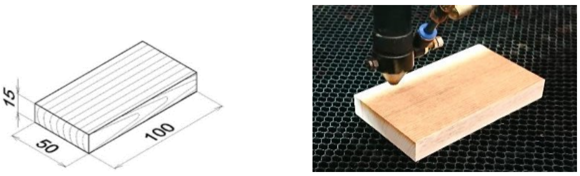

Fig. 1 Test specimen (left) and CO_2 laser engraving (right)

The influence of several parameters of the laser engraving device on the colour changes of the tested wood surface is represented in the experiments by a single variable – the total irradiation dose (*H*) determined according to equation (1).

$$H = \frac{P_e \cdot x \cdot n \cdot y}{A \cdot v} \qquad (1)$$

where P_e (W) is the effective power of the laser beam on the sample surface, x (mm) is the sample length, n (mm^{-1}) is the raster density, y (mm) is the width of the trace engraved by the laser beam after one path on the wood surface, v ($mm \cdot s^{-1}$) is the speed of the laser head movement and A (mm^2) is the area irradiated during one passage of the laser beam. The width of the trace was measured using a Leica EC3 camera (Leica Microsystems, Switzerland).

The irradiation dose per unit surface area of the samples (at the specified parameter values) calculated according to the above equation and is summarized in the Table 1.

Table 1 Parameters used in wood engraving with CO_2 laser

Laser power P_e (W)		11	16.5	22
		Irradiation dose H ($J \cdot cm^{-2}$)		
Raster density n (mm^{-1})	2	6.17	9.26	12.34
	5	15.42	23.14	30.86
	10	30.84	46.28	61.71
	20	61.68	92.57	123.43
	30	92.52	138.85	185.15

The laser parameters (power, feed rate, focal length and raster density) were selected based on experience from previous measurements (Kúdela et al. 2021) as well as on the results from the literature cited in the introduction of the paper.

Colour measurement

The colorimetric values L^*, a^* and b^* of the reference bodies and bodies after CO_2 laser engraving were measured with a spectrophotometer Spectro guide 45/0 gloss (BYK-GARDNER GmbH, Germany). The measurement was made at ten locations within one body. The colour differences ΔL^*, Δa^* and Δb^* under different irradiation conditions and the total colour difference ΔE were determined according to the following equations:

$$\Delta L^* = L_2 - L_1 \quad (2)$$

$$\Delta a^* = a_2 - a_1 \quad (3)$$

$$\Delta b^* = b_2 - b_1 \quad (4)$$

$$\Delta E = \sqrt{\Delta L^2 + \Delta a^2 + \Delta b^2} \quad (5)$$

where index "1" represents the colour coordinate value of the reference wood sample before radiation and index "2" represents the colour coordinate value of the wood sample after radiation with a CO_2 laser.

RESULTS AND DISCUSSIONS

Colour changes

The basic statistical characteristics (average value = $\bar{x}$, STD = s) of the colour values (L^*, a^*, b^*), obtained for spruce, beech and oak wood, over the whole raster density range and all three laser power levels are listed in Table 2, 3 and 4.

The most striking effect of laser engraving was a significant decrease in the lightness value (L^*) in the studied wood species. The resulting quality and shade of engraving were influenced by the type of wood and the setting of the laser parameters, quantitatively represented by the irradiation dose. Its increase resulted in a transition from slight yellowing/browning of the wood surface to carbonization with a significant decrease in lightness ($L^* < 30$).

Coniferous wood (spruce) showed a higher variability of colour changes, due to the alternation of spring and summer wood, which absorb laser energy differently. In beech wood, due to the homogeneous structure and more uniform absorption of the applied energy, the colour changes were smoother. Oak wood, due to its distinctive circular-pore structure with different densities of spring and summer wood, showed a surface with an inhomogeneous colour shade after engraving.

The properties of individual wood species also had an impact on the values in the chromaticity plane. The a^* value increased at low irradiation doses (the wood acquired a reddish hue). At high values, a sharp decrease was recorded (during carbonization $a^* \rightarrow 0$). The b^* coordinate showed a similar trend. The initial increase (increased yellow colour) was replaced by a sharp decrease with intensive formation of the carbon layer. The values of the total colour difference (ΔE) ranged in a wide range - from about 5 (at low energy) to > 40 (engraving at the highest laser power and the highest raster density).

Table 2 Colour values of L^*, a^* and b^* in engraved spruce wood surfaces with a CO_2 laser

Colour Values	Basic Statistical Character	Power 11 W					
		Raster density (mm^{-1})					
		Reference	2	5	10	20	30
L^*	$\bar{x}$	84.93	78.14	68.03	65.93	54.99	48.48
	s	0.98	0.96	1.04	1.82	2.43	1.48
a^*	$\bar{x}$	3.23	4.79	8.19	8.23	9.84	10.19
	s	0.39	0.34	0.31	0.61	0.51	0.45
b^*	$\bar{x}$	19.53	25.02	32.37	33.54	32.00	30.45
	s	0.99	0.61	0.83	0.91	1.64	0.63
		Power 16.5 W					
		Raster density (mm^{-1})					
		Reference	2	5	10	20	30
L^*	$\bar{x}$	84.93	77.22	66.40	59.99	49.57	44.00
	s	0.98	1.45	1.17	3.72	2.55	2.06
a^*	$\bar{x}$	3.23	4.86	8.29	9.25	10.33	9.31
	s	0.39	0.31	0.22	0.76	0.45	0.52
b^*	$\bar{x}$	19.53	24.84	31.43	33.24	30.83	27.18
	s	0.99	0.37	0.41	0.98	1.43	1.60
		Power 22 W					
		Raster density (mm^{-1})					
		Reference	2	5	10	20	30
L^*	$\bar{x}$	84.93	74.84	62.52	59.09	46.54	41.27
	s	0.98	0.66	3.79	3.38	2.32	2.15
a^*	$\bar{x}$	3.23	5.33	8.78	9.29	9.98	9.45
	s	0.39	0.37	0.45	0.35	0.56	0.29
b^*	$\bar{x}$	19.53	25.53	31.46	33.22	29.66	26.84
	s	0.99	0.61	1.05	0.98	1.52	0.97

Table 3 Colour values of L^*, a^* and b^* in engraved beech wood surfaces with a CO_2 laser

Colour Values	Basic Statistical Character	Power 11 W					
		Raster density (mm^{-1})					
		Reference	2	5	10	20	30
L^*	$\bar{x}$	75.58	65.78	48.80	44.29	35.44	33.07
	s	1.51	1.49	1.39	1.29	1.45	1.60
a^*	$\bar{x}$	6.77	7.18	7.85	6.91	6.29	6.53
	s	0.47	0.44	0.29	0.44	0.40	0.60
b^*	$\bar{x}$	17.52	19.40	20.15	18.87	17.14	16.88
	s	0.86	0.63	0.92	0.91	0.87	1.23
		Power 16.5 W					
		Raster density (mm^{-1})					
		Reference	2	5	10	20	30
L^*	$\bar{x}$	75.58	62.44	45.17	40.13	31.99	28.02
	s	1.51	0.49	1.73	0.93	1.27	0.73
a^*	$\bar{x}$	6.77	7.28	8.80	5.85	6.12	5.38
	s	0.47	0.24	0.55	0.51	0.35	0.36
b^*	$\bar{x}$	17.52	19.50	20.39	16.73	15.72	14.02
	s	0.86	0.41	0.97	0.90	0.73	0.86
		Power 22 W					
		Raster density (mm^{-1})					
		Reference	2	5	10	20	30
L^*	$\bar{x}$	75.58	60.08	42.50	41.16	31.31	24.28
	s	1.51	0.92	0.57	2.56	1.66	1.62
a^*	$\bar{x}$	6.77	6.64	8.07	7.24	6.14	4.66
	s	0.47	0.24	0.25	0.53	0.65	0.50
b^*	$\bar{x}$	17.52	18.65	19.36	19.17	15.62	10.94
	s	0.86	0.44	0.27	1.40	1.63	1.02

Table 4 Colour values of L^*, a^* and b^* in engraved oak wood surfaces with a CO_2 laser

Colour Values	Basic Statistical Character	Reference	2	5	10	20	30
		Power 11 W – Raster Density (mm^{-1})					
L^*	$\bar{x}$	67.97	57.10	46.88	39.35	31.43	26.65
	s	2.06	1.51	3.27	3.20	2.53	1.95
a^*	$\bar{x}$	6.61	7.13	7.31	6.34	5.75	5.00
	s	0.29	0.29	0.59	0.89	0.56	0.90
b^*	$\bar{x}$	19.96	20.92	19.46	17.45	13.14	10.29
	s	0.63	0.35	1.55	2.03	1.86	2.14
		Power 16.5 W – Raster density (mm^{-1})					
		Reference	2	5	10	20	30
L^*	$\bar{x}$	67.97	52.79	43.17	36.74	29.52	23.90
	s	2.06	1.52	3.31	2.02	2.25	2.37
a^*	$\bar{x}$	6.61	6.71	6.77	6.12	5.62	4.50
	s	0.29	0.49	0.85	0.84	0.62	1.22
b^*	$\bar{x}$	19.96	19.41	17.90	16.25	11.57	8.40
	s	0.63	0.98	1.46	1.13	1.55	2.17
		Power 22 W – Raster density (mm^{-1})					
		Reference	2	5	10	20	30
L^*	$\bar{x}$	67.97	52.57	36.92	35.91	27.00	21.85
	s	2.06	2.16	2.23	2.90	1.86	1.41
a^*	$\bar{x}$	6.61	6.95	6.43	6.43	4.93	4.43
	s	0.29	0.39	0.61	0.68	0.54	0.51
b^*	$\bar{x}$	19.96	19.83	16.55	16.39	10.36	7.41
	s	0.63	0.73	1.12	1.80	1.12	0.99

Figure 2 shows the surface of beech, oak and spruce wood before and after CO_2 laser engraving.

Fig . 2 View of the surfaces of laser-engraved samples

The functional dependences of the colour values of spruce, beech and oak wood on the total irradiation dose were described by the same type of equation (Table 5).

Table 5 Functional dependences of colour quantities on irradiation dose

Wood	L^*	a^*	b^*
Spruce wood	$y = -11.39.5\ln(x) + 101.9$ $R^2 = 0.972$	$y = -0.0002x^2 + 0.0045x + 7.5$ $R^2 = 0.824$	$y = -0.0002x^2 - 0.0049x + 32.8$ $R^2 = 0.811$
Beech wood	$y = -11.78\ln(x) + 85.79$ $R^2 = 0.957$	$y = 7.746e^{-0.002x}$ $R^2 = 0.609$	$y = -0.0001x^2 - 0.0235x + 19.8$ $R^2 = 0.902$
Oak wood	$y = -10.5\ln(x) + 76.2$ $R^2 = 0.978$	$y = 7.141e^{-0.003x}$ $R^2 = 0.919$	$y = -0.0003x^2 - 0.1335x + 21.2$ $R^2 = 0.963$

The results from Table 5 indicate the validity of the dependencies for several types of wood. Despite the differences in structures and original colours, these dependences were close, which is also evident from the high values of the coefficient of determination. The only exception was the coordinate a^* in spruce, which required a different type of equation than beech and oak.

Based on the measured values, functional dependences L^*, a^*, b^* on the irradiation dose were created for three types of wood (Tab. 5). Appropriate setting of laser parameters is crucial for obtaining targeted colour changes in wood. The derived equations and the established correlations between colour changes and total irradiation dose will allow for targeted modification of colour and other surface properties of wood.

CONCLUSIONS

CO_2 laser engraving is a complex physical-chemical process, in which targeted thermal degradation of the surface structures of wood occurs. The influence of all CO_2 laser parameters on the modification of the surface properties of wood can be replaced by a single quantity - the total irradiation dose. The brightness of the wood surface and the colour shade depend on the irradiation dose and the type of wood. Research has shown that changes in the colour of wood after CO_2 laser engraving are exactly quantifiable using the CIE $L^*a^*b^*$ system, while the resulting visual effect can be predicted. The possibility of precise adjustment of laser parameters allows the creation of graphic elements on the surface of wood with high aesthetic value and excellent contrast.

The main conclusions can be summarized in three points:

1. By choosing the irradiation dose, it is possible to precisely control the shade from light brown to deep black.
2. Increasing the irradiation dose will cause a permanent decrease in lightness (L^*), which will affect the increase in the total colour difference (ΔE).
3. The derived relationships between colour changes and the total irradiation dose will allow for targeted changes in the colour of the wood surface.

ACKNOWLEDGEMENTS

This work was supported by the Slovak Research and Development Agency under the Contract No. APVV-20-0159, and by the VEGA Agency of the Ministry of Education, Research, Development and Youth of the Slovak Republic and the Slovak Academy of Sciences, Grant No. 1/0179/25.

REFERENCES

1. Barcikowski, S., Koch, G., Odermatt, J. (2006). Characterisation and modification of the heat affected zone during laser material processing of wood and wood composites. Holz Roh. Werkst. 64, 94–103.
2. Wust, H., Haller, P., Wiedemann, G. (2005). Experimental Study of the Effect of a Laser Beam on the Morphology ofWood Surfaces. In Proceedings of the Second European Conference on Wood Modification, Göttingen, Germany, 6–7 October 2005.
3. Kubovský, I., Kačík, F. (2014). Colour and Chemical Changes of the LimeWood Surface Due to CO2 Laser Thermal Modification. Appl. Surf. Sci. 321, 261–267.

4. Li, R., He, C., Xu, W., Wang, X.A. (2022). Prediction of Surface Roughness of CO2 Laser Modified Poplar Wood Via Response Surface Methodology. Maderas. Ciencia y Tecnología 24, 1–12.
5. Kúdela, J., Kubovský, I., Andrejko, M. (2022). Influence of irradiation parameters on structure and properties of oak wood surface engraved with a CO2 laser. Materials 15, 8384.
6. Kúdela, J., Kubovský, I., Andrejko, M. (2024). Discolouration and Chemical Changes of BeechWood After CO2 Laser Engraving. Forests 15, 2211.
7. Guo, Q., Wu, Z., Zhang, C., Yang, C., Ma, Y., Xu, F., Cao, Z. (2021). Study on a New Clean Machining Method Instead of Sanding Technology forWood. Alex. Eng. J. 60, 2369–2380.
8. Gurau, L., Petru, A., Varodi, A., Timar, M.C. (2017). The Influence of CO2 Laser Beam Power Output and Scanning Speed on Surface Roughness and Colour Changes of Beech (Fagus sylvatica). BioResources 12, 7395–7412.
9. Kačík, F., Kubovský, I. (2011). Chemical Changes of Beech Wood Due to CO2 Laser Irradiation. J. Photochem. Photobiol. A, 222, 105–110.
10. Kačíková, D., Kačík, F., Čabalová, I., Ďurkovič, J. (2013). Effects of thermal treatmenton chemical, mechanical and colour traits in Norway spruce wood. Bioresources Technology, 144, 669–674.
11. Li, R., Xu, W., Wang, X., Wang, C. (2018). Modeling and Predicting of the Color Changes of Wood Surface During CO2 Laser Modification. J. Clean. Prod. 183, 818–823.
12. Nath, S., Waugh, D.G., Ormondroyd, G.A., Spear, M.J., Pitman, A.J., Sahoo, S., Mason, P. (2020). CO2 Laser Interactions with Wood Tissues During Single Pulse Laser-incision. Opt. Laser Technol. 126, 106069.
13. Jurek, M., Wagnerová, R. (2021). Laser Beam Calibration forWood Surface Colour Treatment. Eur. J. Wood Wood Prod., 79, 1097–1107.
14. Reinprecht, L., Vidholdová, Z. (2021). The Impact of a CO2 Laser on the Adhesion and Mold Resistance of a Synthetic Polymer Layer on a Wood Surface. Forests, 12, 242.
15. Lungu, A., Timar, M.C., Beldean, E.C., Georgescu, S.V., Cosereanu, C. (2022). Adding Value to Maple (Acer pseudoplatanus) Wood Furniture Surfaces by Different Methods of Transposing Motifs from Textile Heritage. Coatings, 12, 1393.
16. Kúdela, J., Andrejko, M., Mišíková, O. (2021). Wood Surface Morphology Alteration Induced by Engraving with CO2 Laser Under Different Raster Density Values. Acta Fac. Xylologiae Zvolen, 63, 35–47.
17. Kubovský, I., Kačíková, D., Kačík, F. (2020). Structural Changes of Oak Wood Main Components Caused by Thermal Modification. Polymers, 12, 485.
18. Nguila Inari, G., Pétrissans, M., Gerardin, P. (2006). Chemical reactivity of heat-treated wood. Wood Sci. Technol., 41, 157.

CHIP AND CHIPLESS WOODWORKING PROCESSES, 15(1): 89–94, 2026
Zvolen, Technical University in Zvolen, ISSN 1339-8350 (online)

WORKING TIME UTILIZATION IN UPHOLSTERED FURNITURE MANUFACTORING

Dorota Michalak – Barbara Prałat – Krzysztof Wiaderek – Tomasz Rogoziński

Abstract

The study aimed to evaluate working time utilisation at selected workstations in an upholstered furniture manufacturing company with a low level of mechanisation. Continuous time studies were conducted at structural frame assembly, foam-and-wadding application, and upholstery workstations. The working time utilisation index (Kr) was used to determine the share of net working time devoted to direct production activities. The obtained Kr values ranged from 0.70 to 0.83, indicating that auxiliary activities accounted for 17–30% of net working time. The lowest utilisation was recorded for structural frame assembly (Kr = 0.70), followed by foam-and-wadding application (Kr = 0.72), while upholstery achieved the highest value (Kr = 0.83). The main sources of time losses were component collection, material shortages, internal transport, and workplace organisation. The results indicate that improving material preparation, workplace layout, internal logistics, and work standardisation could significantly increase production efficiency. Organisational improvements should therefore precede investments in additional labour or selective automation.

Key words: *Working time utilization; upholstered furniture; labour productivity; production efficiency; work organization.*

INTRODUCTION

Furniture manufacturers currently face increasing operating costs and a growing shortage of skilled workers. These conditions limit the effectiveness of traditional production-management practices and increase the need for process optimization, rational resource allocation, and carefully targeted modernization. Although Poland remains one of the world's leading furniture exporters, its continued competitiveness cannot be based solely on relatively low labor costs. Companies must increasingly improve productivity through better work organization, standardization, digital production management, and selective automation (Grzegorzewska & Stasiak-Betlejewska., 2020; Grzegorzewska & Sedliačiková, 2021; Łukiewska & Brelik, 2021).

This challenge is particularly important in upholstered furniture manufacturing, where numerous operations continue to depend on manual labor. The assembly of structural frames, application of foam and wadding, sewing, upholstering, and final finishing require considerable embólie involvement. The level of automation in these areas remains

Poznań University of Life Sciences, ul. Wojska Polskiego 38/42, 60-627 Poznań, Poland
e-mail: dorota.michalak@up.poznan.pl

substantially lower than that associated with Industry 4.0. Consequently, the performance of an upholstered furniture plant is strongly influenced by the organization of human work, availability of materials, internal transport, workplace layout, and coordination between production departments (Červený et al., 2022a; Brunello et al., 2025).

Numerous methods have been proposed to improve production efficiency, including Lean Manufacturing, digital production monitoring, ergonomic workplace design, and simulation-based optimization. Among these approaches, Lean Manufacturing provides practical tools for identifying and reducing activities that consume resources without directly increasing the value of the product. In a case study conducted in the furniture industry, the implementation of standardization, Visual Management, Kaizen, and 5S improved employee working-time efficiency and accelerated the production process. Such findings indicate that organizational changes should be considered before a company increases employment or invests in complex machinery (Pawłyszyn et al., 2024; Buchmeister & Vujica Herzog, 2024).

Reliable production data are necessary for both Lean improvement and computer simulation. One measure that can support the identification of inefficient production areas is the working time utilization index Kr (Strumiński, 1984). The indicator expresses the proportion of net working time devoted to the principal operation. Its application makes it possible to determine whether low workstation performance is associated with the pace of direct work or with supporting activities such as component collection, internal transport, workplace organization, and correction of production shortages (Buchmeister & Vujica Herzog, 2024). The evaluation of production efficiency using time-based indicators is well established in the wood-processing industry, particularly in highly automated manufacturing systems. Previous studies have focused on the performance of automated production lines such as the TechnoPORTA system implemented at PORTA KMI Poland (Kwidziński et al., 2022; Michalak et al., 2024). These studies demonstrated that detailed analyses of time-related performance indicators can effectively identify production bottlenecks and support process optimization in automated manufacturing environments.

However, comparable studies remain scarce in the upholstered furniture sector, where production relies predominantly on manual operations rather than automated technological lines. The high variability of manual work, dependence on operator skills, and frequent occurrence of auxiliary activities make the assessment of working time utilisation considerably more challenging. Consequently, quantitative evaluations of working time utilisation at individual upholstery workstations are still limited, despite their potential value for identifying organisational inefficiencies and supporting decisions regarding process improvement and selective automation.

Therefore, this study aimed to determine the working time utilisation index Kr for selected workstations in an upholstered furniture company. It focused on operations characterised by a particularly low level of mechanisation, including frame assembly, foam and wadding application, and upholstery

MATERIAL AND METHODS

The study was conducted at a Polish company specialising in upholstered furniture manufacturing. The analysis focused on three workstations with a low degree of mechanisation: the structural frame assembly workstation, the workstation where completed frames were covered with foam and wadding and the upholstery workstation.

At the time of the study, the company did not use an integrated Enterprise Resource Planning (ERP) system for production planning and control. Production orders and the allocation of tasks to individual workstations were managed using paper-based documentation. Consequently, information concerning production orders and their progress was not recorded digitally at the workstation level.

Working time was recorded through continuous observation using a direct time study with a digital stopwatch. The analysis concerned net working time, which means that statutory breaks were excluded. Each measurement was conducted for three employees with comparable experience and professional competencies. The individual measurements were subsequently averaged to reduce the influence of differences in employees' working pace.

The activities recorded at each workstation were divided into direct and auxiliary operations (Buchmeister & Vujica Herzog, 2024). Direct operations contributed immediately to the completion of the analysed production stage. Auxiliary operations included component collection, workplace preparation, internal transport, replenishment of missing parts, and other activities necessary to continue production but not directly contributing to the completion of the principal operation (Buchmeister & Vujica Herzog, 2024). Due to the very short duration and frequent alternation of individual supporting tasks (e.g., reaching for tools or materials), auxiliary activities were recorded collectively rather than classified into separate categories.

The working time utilisation index was calculated using equation (1):

$$Kr = tw/T,$$

where kr is the working time utilisation index, tw is the execution time, and t is the total working time during the shift.

RESULTS

The calculated working time utilisation index kr varied between the analysed workstations, ranging from 0.70 to 0.83 (Figure 1). This indicates that 70–83% of net working time was devoted to direct production activities, while the remaining 17–30% was occupied by auxiliary activities. These included workplace organisation, material handling, component collection, internal transport, and other supporting operations necessary to maintain production continuity but not directly contributing to product completion. Due to the very short duration and frequent alternation of these activities, they were analysed collectively rather than classified into separate categories.

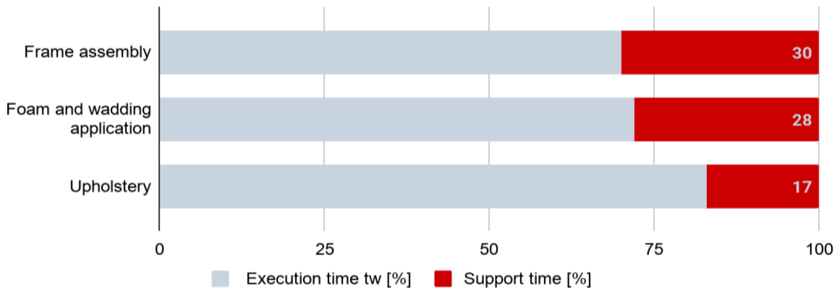

Figure 1. Total working time structure at the analyzed workstations.

The structural frame assembly workstation achieved the lowest working time utilisation index kr = 0.70, which means that auxiliary activities accounted for 30% of working time.

At the foam-and-wadding application workstation, the average processing time for one module was approximately 8 min. The working time utilization index reached kr = 0.72.

The highest working time utilization index was recorded at the upholstery workstation kr = 0.83. Upholstering one complete corner sofa required approximately 60 min, with direct production activities accounting for 83% of net working time. The remaining 17% consisted of auxiliary activities accompanying the upholstery process.

For an 8-hour workday, devoting 30%, 28%, and 17% of that time to support tasks amounts to 2.4 hours, 2.2 hours, and 1.4 hours, respectively.

DISCUSSION

The results indicate that working time utilisation in upholstered furniture production is strongly affected by organisational and logistical factors. This is consistent with previous studies showing that non-value-adding activities, such as material handling, unnecessary movement, waiting, and workplace organisation, can substantially reduce production efficiency (Buchmeister & Vujica Herzog, 2024; Pawłyszyn et al., 2024). Therefore, improvement efforts should focus primarily on better material preparation, internal logistics, and work organisation rather than solely on increasing the pace of direct manual operations.

The identified potential for improvement is consistent with Lean Manufacturing principles. Standardisation, 5S, Visual Management, and Kaizen may help reduce unnecessary activities and improve production flow (Pawłyszyn et al., 2024; Buchmeister & Vujica Herzog, 2024). Improved material supply and the use of complete production kits may additionally limit interruptions caused by missing components (Sütçü et al., 2011), while barcodes or QR codes could support material identification and production control (Červený et al., 2022a, 2022b).

Internal transport and workplace layout should also be considered important areas for improvement. Previous studies have shown that layout redesign and simulation can support more efficient material flow and allow alternative production configurations to be evaluated before implementation (Sütçü et al., 2011; Bambura et al., 2020). Discrete-event simulation may therefore complement time-study results by assessing alternative buffer locations, transport routes, and workstation arrangements (Bambura et al., 2020; Büchi et al., 2020).

The findings also suggest that organisational improvements should precede extensive automation. In highly manual furniture production, selective mechanisation may be justified for repetitive and labour-intensive operations, but investment decisions should consider production volume, product variety, labour requirements, and expected time savings (Buchmeister & Vujica Herzog, 2024; Brunello et al., 2025; Büchi et al., 2020; Červený et al., 2022a). Ergonomic improvements should accompany these changes, as they may reduce physical workload and production waste (Guimarães et al., 2015).

A limitation of the present study is the relatively small number of employees and analysed production operations. In addition, auxiliary activities were recorded collectively because of their short duration and frequent alternation. Further research should therefore include more employees, production cycles, product variants, and a more detailed classification of auxiliary activities.

CONCLUSION

The working time utilization indices Kr were 0.70 for structural frame assembly, 0.72 for foam and wadding application, and 0.83 for upholstery, indicating that 17–30% of working time was spent on auxiliary activities, which represents a key area for improvement.

The structural frame assembly workstation had the lowest efficiency (Kr = 0.70), with about 30% of time (about 2.4 h per shift) spent on auxiliary tasks. This was mainly due to missing or incorrect components, suggesting a need for better production documentation and coordination. An ERP system integrating orders with component lists could reduce these issues.

At the foam and wadding application workstation (Kr = 0.72), 28% of time was auxiliary, mainly due to internal transport and workplace organization. Improvements should focus on optimizing material flow and buffer storage layout, followed by further measurements to assess effects.

The upholstery workstation achieved the highest efficiency (Kr = 0.83). Further gains may be achieved through better order coordination and digital support for preparing component sets.

Overall, the results show that auxiliary activities significantly reduce efficiency across all workstations. Implementing digital production planning (e.g., ERP systems) and improving material flow organization could reduce these losses, although their impact requires further verification.

Future work should focus on redesigning material flows, applying Lean Manufacturing tools, and validating improvements through repeated studies or simulations, as well as extending analysis to other manual processes such as upholstery and sewing.

REFERENCES

Bambura, R., Sujová, E., & Čierna, H. (2020). Utilization of computer simulation for optimization of furniture production system. *BioResources, 15*(3), 6752–6765. https://doi.org/10.15376/biores.15.3.6752-6765

Brunello, A., Fabris, G., Gasparetto, A., Montanari, A., Saccomanno, N., & Scalera, L. (2025). A survey on recent trends in robotics and artificial intelligence in the furniture industry. *Robotics and Computer-Integrated Manufacturing, 93*, 102920. https://doi.org/10.1016/j.rcim.2024.102920

Buchmeister, B., & Vujica Herzog, N. (2024). Advancements in data analysis for the work-sampling method. *Algorithms, 17*(5), 183. https://doi.org/10.3390/a17050183

Büchi, G., Cugno, M., & Castagnoli, R. (2020). Smart factory performance and Industry 4.0. *Technological Forecasting and Social Change, 150*, 119790. https://doi.org/10.1016/j.techfore.2019.119790

Červený, L., Sloup, R., Červená, T., Riedl, M., & Palátová, P. (2022a). Industry 4.0 as an opportunity and challenge for the furniture industry—A case study. *Sustainability, 14*(20), 13325. https://doi.org/10.3390/su142013325

Červený, L., Sloup, R., & Červená, T. (2022b). The potential of smart factories and innovative Industry 4.0 technologies—A case study of different-sized companies in the furniture industry in Central Europe. *Forests, 13*(12), 2171. https://doi.org/10.3390/f13122171

Grzegorzewska, E., Sedliačiková, M., Drábek, J., & Behún, M. (2020). Evaluating the international competitiveness of Polish furniture manufacturing industry in comparison to the selected EU countries. *Acta Facultatis Xylologiae Zvolen, 62*(2), 149–164. https://doi.org/10.17423/afx.2020.62.2.14

Grzegorzewska, E., & Sedliačiková, M. (2021). Labour productivity in the sustainable development of wood-based industry: A case for the European Union countries. *BioResources, 16*(2), 3643–3661. https://doi.org/10.15376/biores.16.2.3643-3661

Guimarães, L. B. de M., Anzanello, M. J., Ribeiro, J. L. D., & Saurin, T. A. (2015). Participatory ergonomics intervention for improving human and production outcomes of a Brazilian furniture company. *International Journal of Industrial Ergonomics, 49*, 97–107. https://doi.org/10.1016/j.ergon.2015.02.002

Kwidziński, Z., Hanincová, L., Tyma, E., Bednarz, J., Sankiewicz, Ł., Knitowski, B., Pędzik, M., Procházka, J., & Rogoziński, T. (2022). The efficiency of edge banding module in a mass customized line for wooden doors production. Applied Sciences, 12(24), 12510. https://doi.org/10.3390/app122412510

Łukiewska, K., & Brelik, A. (2021). A model for measuring the international competitiveness of furniture industry in the European Union countries. *European Research Studies Journal, 24*(Special Issue 3), 334–350. https://doi.org/10.35808/ersj/2432

Michalak, D., Kwidziński, Z., Sankiewicz, Ł., Knitowski, B., Bednarz, J., Drewczyński, M., Rogoziński, T., & Pędzik, M. (2024). The impact of door leaf parameters on the efficiency of the automated technological line. *Acta Facultatis Xylologiae Zvolen, 66*(2), 115–124. https://doi.org/10.17423/afx.2024.66.2.10

Pawłyszyn, I., Kołodziej, A., & Krawczyk, K. (2024). Impact of Lean solutions implementation on employee efficiency—A case study of a furniture company. *Organizacja i Zarządzanie, 90*, 1–26. https://doi.org/10.21008/j.0239-9415.2024.090.01

Strumiński, J., Dolny, S., & Cegiel, E. (1984). Technologiczne projektowanie zakładów mechanicznej obróbki drewna. Część I: Zagadnienia ogólnoprojektowe i technologiczne. Poznań: Wydawnictwo Akademii Rolniczej w Poznaniu.

Sütçü, A., Tanrıtanır, E., Durmuşoğlu, B., & Koruca, H. I. (2011). An integrated methodology for layout design and work organisation in a furniture manufacturing plant. *The South African Journal of Industrial Engineering, 22*(1). https://doi.org/10.7166/22-1-42

CHIP AND CHIPLESS WOODWORKING PROCESSES, 15(1): 95–102, 2026
Zvolen, Technical University in Zvolen, ISSN 1339-8350 (online)

EFFECTIVENESS OF WOOD DUST EXTRACTION SYSTEM OF HAND HELD BELT SANDER

Alena Očkajová[1] – Martin Kučerka[1] – Miroslav Dado[2]

Abstract
The paper evaluates the effectiveness of the integrated extraction system of a hand-held belt sander during the sanding of beech wood. The mass concentrations of the inhalable and respirable fractions of wood dust in the operator's breathing zone were compared during sanding without the dust collection box and with the dust collection box. The experiment was carried out using three sanding belt grits, P40, P120 and P240. For the inhalable fraction, the use of the box achieved an exposure reduction of approximately 78,5 ÷ 85,8 %, while for the respirable fraction it was 65,8 ÷ 74,9 %. In addition, the material removal rate and the amount of dust captured in the box were evaluated and the dust capture efficiency was calculated from these values, reaching 74,3 % for P240, 58,5 % for P120 and 38,7 % for P40. The results confirm the significant protective effect of the dust collection box, but at the same time indicate that, during coarser sanding, the absolute amount of removed material increases and the dust capture efficiency decreases.

Key words: *wood dust; belt sander; dust collection box; beech wood; inhalable fraction; respirable fraction*

INTRODUCTION

Wood dust generated during wood machining represents a significant risk factor in the working environment. Its effects are associated with health risks for workers, possible damage to fine and precise equipment, and with fire and explosion hazards in operation (Balog and Tureková 2005; Beljaková et al. 2009).

Dust is generally defined as a set of solid particles with a diameter below 100 µm which can remain suspended in workplace air for a long time, sediment only with difficulty, settle not only on horizontal surfaces but also on inclined structures and, the smaller the particle, the greater the angle required for it to slide down (Očkajová et al. 2023), during any subsequent resuspension these dust particles become a source of secondary dustiness. From the point of view of its effect on the human body, it is important to distinguish mainly the inhalable fraction, i.e. particles entering the body through the nose and mouth, and the respirable fraction, which penetrates deeper parts of the respiratory system (STN EN 481 1998; WHO 1999).

The health risks of wood dust are described mainly in relation to respiratory diseases, allergic manifestations, irritation of mucous membranes and the carcinogenic effect of dust from hardwood species (Buchancová et al. 2003; Baran and Teul 2007; Tian et al. 2007; Marková and Očkajová 2018; Očkajová et al. 2020; Čavlović et al. 2023).

[1]Matej Bel University, Tajovského 40, 974 01 Banská Bystrica
[2]Technical University in Zvolen, T. G. Masaryka 24, 960 01 Zvolen
e-mail: alena.ockajova@umb.sk; martin.kucerka@umb.sk; dado@tuzvo.sk

Wood dust, especially from hardwood species (in our vegetation zone this concerns beech and oak), has been classified among category 1 carcinogens (which means a proven carcinogen for humans, for which technical guideline values are specified in legislation), similarly to tropical wood species (Mračková 2001; Horvat et al. 2007). In workers in joinery and wood-processing operations, diseases such as pneumoconiosis (dusting of the lungs), i.e. the effect of the respirable fraction of wood dust) did not occur, but cancers of the paranasal sinuses did occur, and therefore in this case it is necessary to take into account not only the respirable fraction but the entire inhalable fraction, i.e. particles captured in the area of the upper respiratory tract (WHO, 1999; STN EN 481 1998).

Wood sanding is one of the finishing operations in which a very thin layer is removed from the surface of the material and a high proportion of fine dust particles is generated (Očkajová 2002). Dust formation is influenced by the wood species, wood moisture content, thermal treatment, sanding direction in relation to the grain direction, technical parameters of the sander, condition of the sanding belt, as well as the grit size of the abrasive (Očkajová et al. 2016; Očkajová et al. 2019). With finer grits, a higher proportion of smaller particles can be expected, whereas coarser grits increase the mass removal of material and the formation of larger particles (Očkajová et al. 2010). At present, hand-held electric tools, including sanders, are widely used in wood processing and produce a high proportion of dust particles. Previous research on the sanding of beech wood showed that the proportion of particles with a size of up to 0,08 mm can exceed 90 % of all captured dust (Očkajová and Banski 2013; Očkajová et al. 2014; Očkajová et al. 2018).

The basic technical measures for limiting dust dispersion during hand-held sanding include extraction directly at the point of origin and the use of a dust collection bag or box. However, practice shows that their effectiveness may depend on the grit size of the abrasive, the type of wood being machined, and the filling or clogging of the collection space (Mikušová 2019).

The dust capture efficiency of hand-held sanders therefore cannot be evaluated only according to the visible amount of dust captured in the dust collection box. It is important to assess the extent to which the collection system reduces the actual dust concentration in the operator's breathing zone. The practical use of these devices may be affected by the filling of the box, the permeability of the filter material, the sealing between the sander and the collection element, as well as the regularity of cleaning and maintenance. Laboratory verification of the effectiveness of the dust collection box thus provides a basis for a more objective assessment of the risk during hand-held sanding of wood (STN EN 50632-1; Mikušová 2019).

The aim of the paper is to assess the extraction effectiveness of the dust collection box, which is part of a hand-held belt sander, during the sanding of beech wood using three abrasive grits, P40, P120 and P240. The evaluation was carried out in two ways: by measuring the inhalable and respirable fractions in the operator's breathing zone during sanding without the box and with the dust collection box, and by comparing the material removal rate with the amount of dust captured in the box (Kučerka et al. 2022; Kučerka et al. 2023).

MATERIAL AND METHODOLOGY

The economically important wood species European beech (Fagus sylvatica L.) was used for the experiment. Test specimens were prepared with dimensions of 500 mm × 250 mm × 50 mm (length × width × thickness) and subsequently conditioned to a moisture content of

12 ± 1 %. Sanding was carried out along the grain using a Bosch PBS 75A hand-held belt sander.

Sanding belts 533 mm in length with corundum abrasive on a fabric backing, bonded with synthetic resin (Klingspor, model LS 309 XH), with grit sizes P40, P120 and P240, were used. The idle speed of the sanding belt was 350 $m \cdot min^{-1}$. After sanding each test specimen, the sanding belt was replaced with a new one.

Experimental measurements were carried out in a room meeting the requirements of the STN EN 50632-1 standard. The sampling of wood dust was based on the methodology according to Lamperová (2020) and Dado et al. (2020), while the general requirements for procedures for measuring chemical substances in workplace air were respected (STN EN 482: 2000; STN EN 689: 2000).

The mass concentration of wood dust was measured using a TSI DustTrak DRX 8533 aerosol monitor. An SKC IOM sampler located in the operator's breathing zone was connected to the monitor by a hose. The duration of one measurement was 180 s, which corresponded to the time required to sand the test specimen.

The effectiveness of reducing exposure to wood dust was expressed by comparing the mass concentration of dust during sanding without the dust collection box and with the dust collection box. The value R indicates the percentage reduction in dust concentration in the operator's breathing zone after using the dust collection box:

$$\mathbf{R = [(C_1 - C_2) / C_1] \times 100\ [\%]}$$

where C_1 is the mass concentration of dust during sanding without the dust collection box and C_2 is the mass concentration of dust during sanding with the dust collection box.

As a supplementary indicator, the dust capture efficiency in the box E was calculated as the ratio of the mass of dust captured in the box (m_k) and the total material removal rate over the time of one measurement. Since one measurement lasted 180 s, the time of 3 min was included in the calculation:

$$\mathbf{E = m_k / (Q_m \times t) \times 100\ [\%] = m_k / (Q_m \times 3\ min) \times 100\ [\%]}$$

RESULTS AND DISCUSSION

Fig. 1 provides an overall view of the concentrations of the inhalable and respirable fractions of beech dust during sanding without the dust collection box and with the dust collection box. For both fractions, substantially lower dust concentrations in the operator's breathing zone were achieved after using the box. A statistically significant difference between measurements without the box and with the box was confirmed for all comparisons ($p < 0{,}001$).

For the inhalable fraction, the concentrations with the dust collection box were approximately similar for all three grits. Without the use of the dust collection box, however, the concentration of the inhalable fraction at grit P240 was almost twice as high as that at grits P120 and P40. A probable explanation is the higher number of active abrasive grains in the finer abrasive, which simultaneously remove material and generate a greater proportion of fine dust (Očkajová, 2002).

A similar trend was also observed for the respirable fraction without the use of the dust collection box. The lowest formation of the respirable fraction was observed at grit P40, where larger abrasive grains penetrated deeper into the material and produced larger particles. With the finer grit P240, on the other hand, the proportion of particles capable of penetrating into deeper parts of the respiratory system increased.

When the dust collection box was used, the proportion of the respirable fraction in the inhalable fraction was approximately 74,5 % for P240, 58,4 % for P120 and 38,3 % for P40. This indicates that the finer abrasive P240 produced almost twice the proportion of fine particles compared with the coarser grit P40.

The reduction in exposure to the inhalable fraction when using the dust collection box ranged from 78,5 % (P40) to 85,8 % (P240). For the respirable fraction, the reduction reached 65,8 % for P240, 68,9 % for P120 and 74,9 % for P40 (Čavlović et al. 2022).

The concentrations obtained when using the dust collection box under laboratory conditions meet the requirements set by the standard, namely the maximum permissible exposure limits for solid aerosols with a predominantly irritating effect (Government Regulation of the Slovak Republic No. 355/2006), where the value for oak and beech is 2 ($mg \cdot m^{-3}$) and the classification is class 1A - proven carcinogen for humans; as well as the maximum permissible exposure limits (NPEL) for gases, vapours and aerosols with carcinogenic or mutagenic effects in occupational air (Government Regulation of the Slovak Republic No. 121/2024), where for hardwood dust (oak, beech), the inhalable fraction is 2 ($mg \cdot m^{-3}$) and the classification is class 1A.

This finding, however, cannot be transferred without reservation to operational conditions, because real workplaces may be affected by secondary dustiness, insufficient maintenance, cleaning and the condition of the collection system.

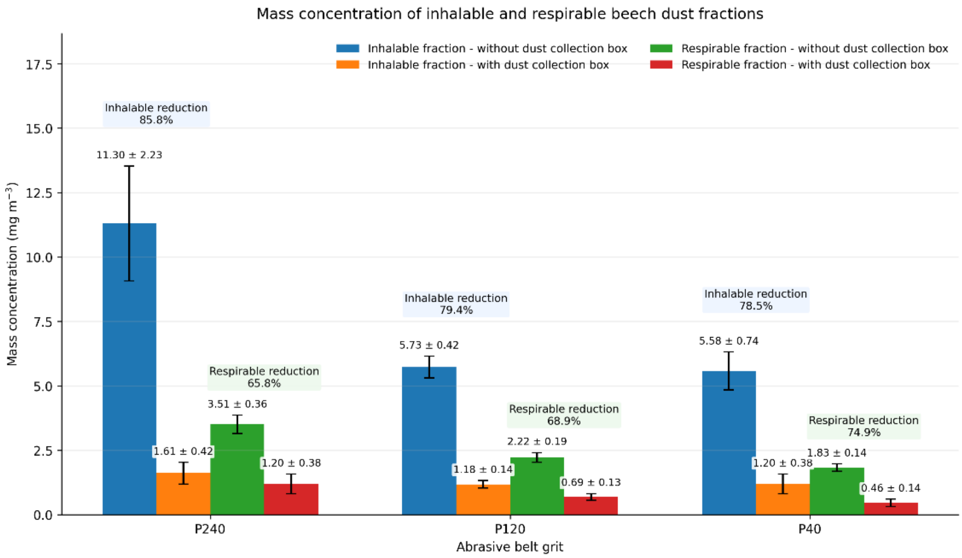

Fig. 1. Mass concentration of the inhalable and respirable fractions of beech dust during sanding without the dust collection box and with the dust collection box. Error bars represent SD. Reduction efficiency values are shown above each grit group.

Fig. 2 presents the material removal rate, the amount of dust captured in the box and the calculated dust capture efficiency. The material removal rate increased from 3,96 ± 0,41 $g \cdot min^{-1}$ for P240 through 6,63 ± 0,28 $g \cdot min^{-1}$ for P120 to 14,54 ± 0,39 $g \cdot min^{-1}$ for P40. At the same time, the absolute amount of dust captured in the box also increased, from 8,83 ± 1,40 g for P240 to 11,64 ± 0,97 g for P120 and 16,90 ± 1,73 g for P40.

The dust capture efficiency calculated from the ratio between captured dust and total material removal reached 74,3 % for P240, 58,5 % for P120 and 38,7 % for P40. The result shows that, during coarser sanding, a larger amount of dust is generated and captured in the box in absolute terms, but the relative capture efficiency decreases.

A possible explanation is the different granulometry of the generated dust. Larger particles generated at P40 may fill the box space differently, reduce its permeability more quickly or cause local clogging of the collection system. Although finer particles at P240 enter the operator's breathing zone more easily, when the box is used, they are captured more effectively in relative terms.

At the same time, with hand-held sanders it is problematic that the dust collection box usually does not have a reliable filling indication system. The extraction efficiency therefore also depends on the user, on the regularity of cleaning the box and on the type of wood being machined. When sanding softwood, the mechanism of filling the collection space may differ from that when sanding hardwood (Očkajová et al. 2018).

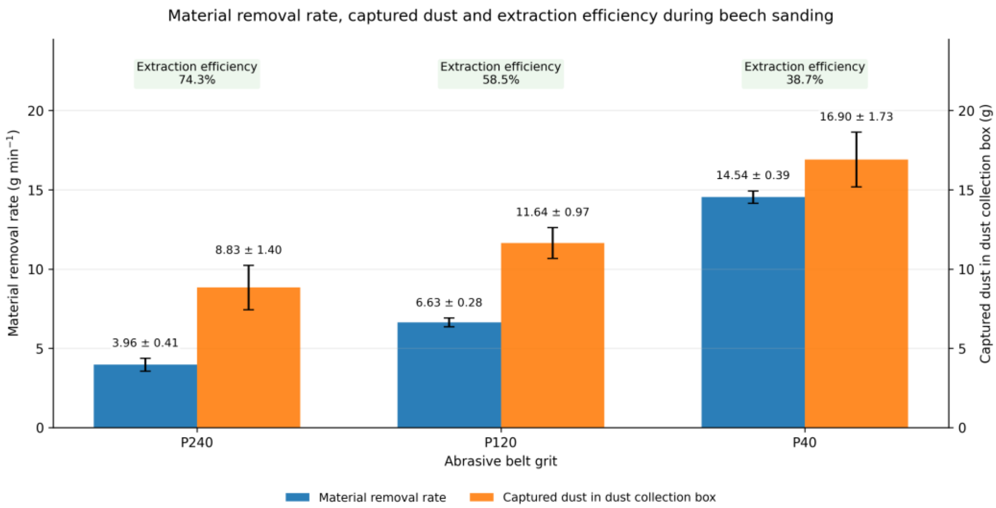

Fig. 2. Combined evaluation of material removal rate captured dust and extraction efficiency during beech sanding. The left y-axis shows the material removal rate ($g{\cdot}min^{-1}$), while the right y-axis shows the mass of dust captured in the dust collection box (g). Error bars represent SD. Extraction efficiency values are shown above each grit group.

CONCLUSION

The experiment confirmed that:

- the dust collection box of the hand-held belt sander significantly reduces the concentration of the inhalable and respirable fractions of beech dust in the operator's breathing zone,
- the highest reduction of the inhalable fraction was achieved at P240, while the highest reduction of the respirable fraction was recorded at P40,
- the supplementary evaluation of the dust captured in the box, compared with the material removal rate, showed the opposite trend: at P40, the greatest amount of dust was generated and captured in absolute terms, but the relative capture efficiency was the lowest,

- the grit size of the abrasive significantly affects the formation of the inhalable and respirable fractions and thus also the way of extraction using the dust collection box.

For practice, this implies the need for regular inspection and cleaning of the dust collection box, especially depending on sanding with lower grit sizes, the sanding direction relative to the wood fibres, the type of wood being sanded and longer work periods. Although integrated extraction represents an effective technical measure, it should not be understood as the only protection for the worker. In real operations, it is also necessary to take into account overall ventilation, secondary dustiness, workplace maintenance and the use of suitable personal protective equipment.

LITERATURE

BALOG, K. and TUREKOVÁ, I., 2005. Požiarnotechnické charakteristiky drevných prachov. In: Chemické spracovanie dreva. Zvolen: Technická univerzita vo Zvolene, 2005, s. 45-46.

BARAN, S. and TEUL, I., 2007. Wood dust: an occupational hazard which increases the risk of respiratory disease. *Journal of Physiology and Pharmacology: An Official Journal of the Polish Physiological Society*. 2007. Vol. 58, no. 5, p. 43–50.

BELJAKOVÁ, A., OČKAJOVÁ, A. and JOBBÁGY, J., 2009. Zisťovanie minimálnej teploty vznietenia bukového prachu v závislosti na modeli brúsenia. *Acta Universitatis Matthiae Belii*. 2009. Vol. No. 9, p. 36–43.

BUCHANCOVÁ, J. a kol., 2003. *Pracovné lekárstvo a toxikológia*. Bratislava: Osveta. ISBN 80-8063-113-1.

ČAVLOVIĆ, Anka O., BEŠLIĆ, I., PERVAN, S., BARLOVIĆ, N., MIKŠIK, M., KLARIĆ, M. and PREKRAT, S., 2022. Occupational exposure to inhalable and respirable wood dust of pedunculate oak (Quercus robur L.) in a furniture factory. *BioResources*. 2022. Vol. 17, no. 4, p. 5831–5847. DOI 10.15376/biores.17.4.5831-5847.

ČAVLOVIĆ, Anka O., BEŠLIĆ, I., PERVAN, S. and PREKRAT, S., 2023. Characteristics of thermally modified hardwood dust in determining workers' occupational exposure. *BioResources*. 2023. Vol. 18, no. 2, p. 3923–3937. DOI 10.15376/biores.18.2.3923-3937.

DADO, M., LAMPEROVÁ, A., KOTEK, L. and HNILICA, R., 2020. An Evaluation of On-Tool System for Sanding Dust Collection: Pilot Study. *Management Systems in Production Engineering*. 2020. Vol. 28, no. 3, p. 184–188. DOI 10.2478/mspe-2020-0027.

HORVAT, D., KOS, A., ZEČIĆ, Ž., JAZBEC, A., ŠUŠNJAR, M. and OČKAJOVÁ, A., 2007. Tree cutters' exposure to oakwood dust - A case study from Croatia. *Die Bodenkultur Journal of Land Management Food and Environment*. 2007. Vol. 58, no. 1, p. 59–65.

KUČERKA, M., OČKAJOVÁ, A., KMINIAK, R., PĘDZIK, M. and ROGOZIŃSKI, T., 2022. The Effect of the Granulometric Composition of Beech Chips from a CNC Machining Center on the Environmental Separation Technique. *Acta Facultatis Xylologiae Zvolen*. 2022. Vol. 6, no. 4(1), p. 89–97. DOI 10.17423/afx.2022.64.1.08.

KUČERKA, M., OČKAJOVÁ, A., KMINIAK, R., ROGOZIŃSKI, T., SYDOR, M., PĘDZIK, M., LO GIUDICE, V. and TODARO, L., 2023. Design and comparison of a suitable dust separation technique during the machining process in a CNC machining center. *Annals of Warsaw University of Life Sciences – SGGW*. 2023. Vol. 122, p. 99–107. DOI 10.5604/01.3001.0053.8673.

LAMPEROVÁ, A., 2020. Meranie a hodnotenie efektivity systému pre odsávanie prachu pri brúsení dreva. Diplomová práca. Technická univerzita vo Zvolene.

MARKOVÁ, I. and OČKAJOVÁ, A., 2018. *Hodnotenie rizika drevných prachov v pracovnom a životnom prostredí*. Online. 1. vyd. Belianum. Vydavateľstvo Univerzity Mateja Bela v Banskej Bystrici. ISBN 978-80-557-1391-5. Available from: 10.24040/2018.9788055713915.

MIKUŠOVÁ, L., OČKAJOVÁ, A., DADO, M., KUČERA, M. and DANIHELOVÁ, Z., 2019. Thermal treatment's effect on dust emission during sanding of meranti wood. *BioResources*. 2019. Vol. 14, no. 3, p. 5316–5326. DOI 10.15376/biores.14.3.5316-5326.

MRAČKOVÁ, E., 2001. Negatívne charakteristiky drevného prachu prejavujúce sa v pracovnom prostredí. In: *Trendy lesníckej, drevárskej a environmentálnej techniky a jej aplikácie vo výrobnom procese*. Zvolen: TU vo Zvolene. 2001. p. 33–38.

Nariadenie vlády Slovenskej republiky č. 355/2006 Z. z. o ochrane zamestnancov pred rizikami súvisiacimi s expozíciou chemickým faktorom pri práci.

Nariadenie vlády Slovenskej republiky č. 121/2024 Z. z. o ochrane zdravia zamestnancov pred rizikami súvisiacimi s expozíciou karcinogénnym faktorom, mutagénnym faktorom alebo reprodukčne toxickým faktorom pri práci.

OČKAJOVÁ, A., 2002. *Analýza faktorov v procese plošného brúsenia dreva*. 1. Zvolen: Technická univerzita vo Zvolene. ISBN 978-80-228-1185-8.

OČKAJOVÁ, A., BELJAKOVÁ, A. and SIKLIENKA, M., 2010. Morphology of Dust Particles from the Sanding Process of the Chosen Tree Species. *Wood Research*. 2010. Vol. 55, no. 2, p. 89–98.

OČKAJOVÁ, A. and BANSKI, A., 2013. Granulometria drevného brúsneho prachu z úzko-pásovej brúsky. *Acta Facultatis Xylologiae*. 2013. Vol. 55, no. 1, p. 85–89.

OČKAJOVÁ, A., STEBILA, J., RYBAKOWSKI, M., ROGOZINSKI, T., KRIŠŤÁK, Ľ. and LUPTÁKOVÁ, J., 2014. The Granularity of Dust Particles when Sanding Wood and Wood-Based Materials. *Advanced Materials Research*. 2014. Vol. 1001, p. 432–437. DOI 10.4028/www.scientific.net/AMR.1001.432.

OČKAJOVÁ, A., KUČERKA, M., KRIŠŤÁK, Ľ., RUŽIAK, I. and GAFF, M., 2016. Efficiency of Sanding Belts for Beech and Oak Sanding. *BioResources*. 2016. Vol. 11, no. 2, p. 5242–5254. DOI 10.15376/biores.11.2.5242-5254.

OČKAJOVÁ, A., KUČERKA, M., KRIŠŤÁK, Ľ. and IGAZ, R., 2018. Granulometric Analysis of Sanding Dust from Selected Wood Species. *BioResources*. 2018. Vol. 13, no. 4, p. 7481–7495. DOI 10.15376/biores.13.4.7481-7495.

OČKAJOVÁ, A., BARCÍK, Š., KUČERKA, M., KOLEDA, P., KORČOK, M. and VYHNÁLIKOVÁ, Z., 2019. Wood Dust Granular Analysis in the Sanding Process of Thermally Modified Wood versus its Density. *BioResources*. 2019. Vol. 14, no. 4, p. 8559–8572. DOI 10.15376/biores.14.4.8559-8572.

OČKAJOVÁ, A., KUČERKA, M., KMINIAK, R., KRIŠŤÁK, Ľ., IGAZ, R. and RÉH, R., 2020. Occupational Exposure to Dust Produced when Milling Thermally Modified Wood. *International Journal of Environmental Research and Public Health*. 2020. Vol. 17, no. 5, p. 1478. DOI 10.3390/ijerph17051478.

OČKAJOVÁ, A., BANSKI, A. and ROGOZIŃSKI, T., 2023. Tilt Angle of Wood Dust. *Annals of WULS, Forestry and Wood Technology*. 2023. Vol. 121, p. 37–42. DOI 10.5604/01.3001.0053.8589.

STN EN 481:1998. Ovzdušie na pracovisku. Určenie veľkosti frakcií na meranie častíc rozptýlených vo vzduchu.

STN EN 482: 2000. Ochrana ovzdušia. Pracovné ovzdušie. Všeobecné požiadavky na postupy merania chemických látok.

STN EN 689: 2000. Ovzdušie na pracovisku. Pokyny na hodnotenie inhalačnej expozície chemickým látkam na porovnanie s limitnými hodnotami a stratégia merania.

STN EN 50632-1. Electric motor operated tools. Dust measurement procedure. Part 1: General requirements.

TIAN, Z. F., INTHAVONG, K. and TU, J. Y., 2007. Deposition of Inhaled Wood Dust in the Nasal Cavity. *Inhalation Toxicology*. 2007. Vol. 19, no. 14, p. 1155–1165. DOI 10.1080/08958370701665525.

WHO. 1999. Hazard prevention and control in the work environment: Airborne dust. Geneva: World Health Organization, WHO/SDE/OEH/99.14.

Acknowledgments: This work was supported by the grant agency KEGA No. 004UMB-4/2024 and KEGA No. 015UMB-4/2025.

EFFECT OF FEED SPEED ON IMMEDIATE SPRING BACK IN DENSIFIED WOOD SURFACE

Varun Sharma – Daniel Chuchala

Abstract

From prehistoric times, wood served as humanity's primary resource for survival and innovation. Wood valued for its renewability and cost effectiveness, has found widespread application not just in construction but also on furniture production and beyond. Nevertheless, the mechanical strength and dimensional stability of many wood species remain moderate to insufficient, limiting its suitability for demanding engineering structure and high-performance usage. There are several methods to densify the wood to improve its mechanical properties and hardness, but it comes with undesirable challenge like spring back. In this study beech wood (Fagus sylvatica L.) is densified with the help roller burnishing tool attached to lathe machine. Densification process was carried out on lathe with two feed per revolution values $f_1 = 0.57$ mm and $f_2 = 1.14$ mm. The applied densification depth was $a_p = 1$ mm and the constant rolling speed of 103.3 m/min. The compression ratio and the spring back rates were investigated. When evaluated, the highest compression ratio among all the samples obtained when the wood densified at lower feed per revolution (f_1) and the lowest compression ratio was observed at higher value of feed per revolution (f_2). Although, statistical analysis showed that there is no significant effect of feed per revolution on compression ratio. It is also observed that feed per revolution has no impact on spring back property of wood.

Key words: *beech wood, spring back, compression ratio, feed per revolution, densification, rotary movement*

INTRODUCTION

Wood, as a renewable and versatile biomaterial has long been prized for its aesthetic appeal and mechanical properties in construction, furniture and engineering applications(Ormarsson & Sandberg, 2007). Due to high demand for traditional wood species prized for their superior mechanical properties, these resources face severe overexploitation. This preferential harvesting leaves abundant low-grade species underutilized, despite their potential availability. However, its natural limitations such as low surface hardness, poor wear resistance and dimensional instability under moisture often restrict its use in high performance scenarios. The density of wood is determined by the cell wall thickness and lumen size and it can be enhanced by minimising the void volume within the cell structure(Laine et al., 2016a). Densification markedly enhance the compressive strength of both hardwood and softwood across all orientations(Mania et al., 2024). Given that wood densification enhances its mechanical properties and hardness,

Gdansk University of Technology, Narutowicza 11/12, 80-233 Gdansk, Poland
e-mail: varun.sharma@pg.edu.pl, ORCID id: 0009-0004-1717-6931
e-mail: danchuch@pg.edu.pl, ORCID id: 0000-0001-6368-6810

numerous efforts have focused on developing effective processing methods(Cabral et al., 2022).

In this study the densification process is performed on cylindrical wood with the help of burnishing process. The compression ratio and the spring back behaviour will be assessed as a key indicator of successful densification in cylindrical wood samples. This evaluation will lay the foundation for subsequent studies aimed at mitigated spring back effects.

Material and methods

Five defects free beech wood (*Fagus sylvatica* L.) beams, each 1.52 m in length, were selected as the source material. From each beam four specimens measuring 0.305 m in length were taken out, yielding a total of 20 specimens (Fig 1). The initial moisture content of these specimens ranged from MC = 6±.5 %. Specimens were then machined into cylindrical shape using a conventional lathe machine tool. Turning parameters included a cutting speed of v_c = 150 m/min and a feed per revolution of f = 0.5 mm. Subsequently, the cylindrical surfaces were sanded with 80-grit size sandpaper to eliminate the cutter marks and achieve a smooth finish. Densification was carried out on conventional lathe machine tool (Fig 2) at the Gdansk University of Technology, Poland. Process parameters were a rolling speed of v_r = 103.3 m/min, densification depth of a_p = 1 mm and two values of feed per revolution f_1 = 0.57 mm and f_2 = 1.14 mm. This resulted in two sets of 10 densified specimens each, corresponding to the respective feed per revolution.

Figure 1. Test specimens before and after machined into cylindrical shape.

Figure 2. Densification of wood with the help of spinning roller.

Calculation of compression ratios and spring back after 24 hrs:

To calculate the compression ratio, just before the densification the initial diameter from cylindrical specimens were taken from 4 different points with the help of vernier calliper with ±0.01 mm precision, and the average of measure diameters was taken. For densification process the densification depth was aimed at 1 mm for all the specimens. After densification, the average diameter of the samples was measured again. To access whether these objectives could be met, the theoretical CR_{Theao} and the experimental compression ratio CR_{ex} were calculated adequately based on the Equation 1 and 2. The amount of spring back after 24hrs (SB_{24}) was calculated using equation 3. The statistical analysis of the data obtained was done with the help of ANOVA.

$$CR_{Theo} = \frac{(D_i) - (D_i - 2)}{(D_i - 2)} \times 100 \qquad (1)$$

where, CR_{Theo} is compression ratio theoretical and D_i is initial diameter.

$$CR_{ex} = \frac{(D_i - D_f)}{D_f} \times 100 \qquad (2)$$

where, CR_{ex} is compression ratio experimental, D_i is initial diameter and D_f is diameter after densification.

$$SB_{24} = \frac{(D_{24} - D_f)}{D_{24}} \times 100 \qquad (3)$$

where, SB_{24} is spring back after 24 hrs, D_{24} is diameter after 24 hrs and D_f is diameter after densification

RESULT AND DISCUSSION

The theoretical compression ratio, experimental compression ratio and spring back percentage was measured at the end of the experiments are given in Table1.

Table 1. Feed speed, rolling speed, Theoretical & experimental compression ratio % and spring back % obtained according to the process parameters.

Sample	Feed per revolution (mm)	Rolling speed (m/min)	Theoretical compression ratio (%)	Experimental compression ratio (%)	Spring back (%)
A1	0.57	103.3	4.31	1.93	0.04
A2	0.57	103.3	4.37	1.48	0.12
A3	1.14	103.3	4.32	1.60	0.08
A4	1.14	103.3	4.31	1.38	0.27
B1	0.57	103.3	4.33	2.10	0.18
B2	0.57	103.3	4.34	1.80	0.24
B3	1.14	103.3	4.31	1.35	0.19
B4	1.14	103.3	4.36	2.00	0.25
C1	0.57	103.3	4.30	1.93	0.07
C2	0.57	103.3	4.33	1.64	0.13
C3	1.14	103.3	4.33	1.52	0.11
C4	1.14	103.3	4.30	1.77	0.18
D1	0.57	103.3	4.40	0.48	0.13
D2	0.57	103.3	4.33	1.84	0.06
D3	1.14	103.3	4.30	1.84	0.02
D4	1.14	103.3	4.31	1.35	0.13
E1	0.57	103.3	4.31	1.65	0.07
E2	0.57	103.3	4.33	2.01	0.01
E3	1.14	103.3	4.31	1.47	0.17
E4	1.14	103.3	4.30	1.78	0.07

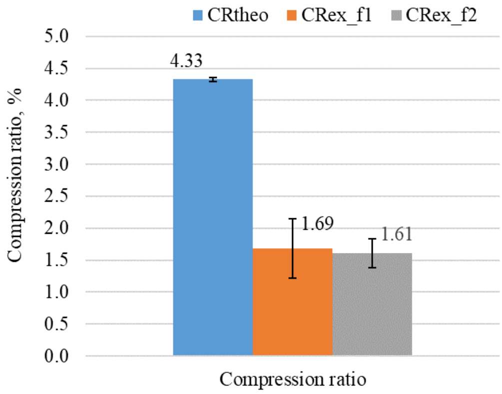

Figure 3: Theoretical and experimental compression ratios for two analysed feeds per revolution with standard errors values

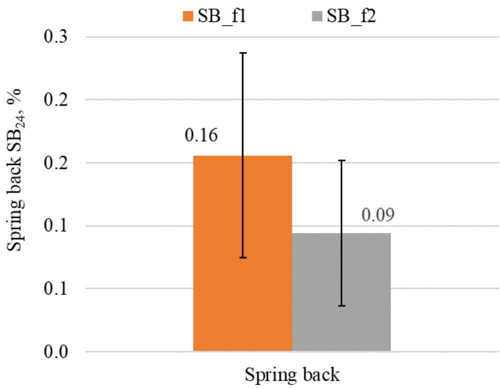

Figure 4: Spring back after 24 hrs for two analysed feed per revolution

As it can be seen from the figures 3 and 4, wood tries to regain its original shape after densification. The spring back effect is the phenomenon that occurs following densification, where material partially recovered its original shape due to the release of stored elastic effects (Laine et al., 2016; Tenorio et al., 2021). The tendency of wood to regain its shape it depends on the characteristic of wood species (Kaya & Sofuoğlu, 2023). Analysis of variance (ANOVA) was done to compare the Experiment compression ratio and Spring back for both the feed speeds given in table 2 and table 3 respectively.

Table 2. ANOVA for Experimental compression ratio percentage

Source	**DF**	**Adj SS**	**Adj MS**	**F-Value**	**P-Value**
Feed per revolution	1	0.1123	0.1123	0.87	0.364
Error	18	2.3304	0.1295		
Total	19	2.4427			

ANOVA result demonstrated no significant influence of feed speed on compression ratio (P=0.364 > 0.05) compression ratio remained between the two-feed speed, suggesting processing speed in this range has negligible effect on densification efficiency during wood densification process with 95% confidence level.

Table 3. ANOVA for Spring back percentage

Source	DF	Adj SS	Adj MS	F-Value	P-Value
Feed per revolution	1	0.008305	0.008305	1.49	0.238
Error	18	0.100218	0.005568		
Total	19	0.108523			

ANOVA revealed no significant effect of feed speed on spring back with 95% confidence level (P=0.238 > 0.05). Spring back values were statistically comparable between the two-feed speed, implying that variation in processing speed withing this range do not alter recovery elastically post burnishing.
Although from the obtained data it is seen that the highest compression ratio among all the samples obtained when the wood densified at with lower feed speed and the lowest compression ratio was observed at higher value of feed speed.

CONCLUSION

The obtained result can be summarised as follow:

- The wood material behavior remained relatively stable under the selected feed speed conditions.
- There is no significant effect of feed speed on the compression ration percentage.
- There is no significant effect of feed speed on the spring back.
- When evaluated in general it is found that highest compression ratio among all the samples obtained when the wood is densified at 0.57 mm of feed per revolution speed. Whereas, the lowest compression ratio was observed at 1.14 mm feed per revolution speed.
- Other parameters such as temperature, moisture content, wood grain orientation, density, or compression pressure may have a greater influence on spring back and compression behavior than feed speed alone.
- It is also possible that the selected feed speed range and densification depth was too narrow to create noticeable structural changes in the wood.

REFERENCES

Cabral JP, Kafle B, Subhani M, Reiner J & Ashraf M. (2022). Densification of timber: a review on the process, material properties, and application. In Journal of Wood Science (Vol. 68). Springer Japan. https://doi.org/10.1186/s10086-022-02028-3

Kaya Z & Sofuoğlu SD (2023). Use of Spinning Roller in Cylindrical Densification; Spring back in Black Poplar, Larch and Cedar of Lebanon after Densification. Bilge

International Journal of Science and Technology Research, *7*(2), 117–127. https://doi.org/10.30516/bilgesci.1278745

Laine K, Segerholm K, Wålinder M, Rautkari L & Hughes, M. (2016a). Wood densification and thermal modification: hardness, set-recovery and micromorphology. Wood Science and Technology, *50*(5), 883–894. https://doi.org/10.1007/s00226-016-0835-z

Mania P, Kupfernagel C & Curling S (2024). Densification of Delignified Wood: Influence of Chemical Composition on Wood Density, Compressive Strength, and Hardness of Eurasian Aspen and Scots Pine. Forests, *15*(6). https://doi.org/10.3390/f15060892

Ormarsson S & Sandberg D. (2007). Numerical simulation of hot-pressed veneer products: Moulding, spring-back and distortion. Wood Material Science and Engineering, *2*(3–4), 130–137. https://doi.org/10.1080/17480270801945355

Tenorio C, Moya R & Navarro-Mora A (2021). Flooring characteristics of thermo-mechanical densified wood from three hardwood tropical species in costa rica. Maderas: Ciencia y Tecnologia, *23*, 1–12. https://doi.org/10.4067/S0718-221X2021000100416

CHIP AND CHIPLESS WOODWORKING PROCESSES, 15(1): 109–120, 2026
Zvolen, Technical University in Zvolen, ISSN 1339-8350 (online)

METHODOLOGY FOR QUANTIFYING EDGE DELAMINATION IN CNC MILLING OF PLYWOOD

Veronika Šugárová – Lukáš Adamčík – Richard Kminiak

Abstract

This study focuses on the verification of a methodology for quantifying edge delamination in CNC milled plywood. The experimental analysis was carried out on birch plywood (Betula pendula Roth) using a 5-axis CNC machining centre under controlled conditions. Milling was performed at a constant cutting direction perpendicular to the grain (90°), while feed speeds of 5, 7.5, and 10 m·min⁻¹ were applied. Other machining parameters were kept constant. Delamination was evaluated using a Keyence VHX-7000 digital microscope. On each milled groove, ten areas of 10 × 5 mm were analysed. Within each scanned area, the fibre tear-out was identified. The reference plane was then defined manually based on visual assessment by adjusting its position to exclude surface irregularities related to the natural plywood structure while retaining only defects caused by mechanical damage. The delaminated area was subsequently quantified as the area below this reference plane. The study describes the measurement procedure and its application under defined machining conditions. The results provide a basis for assessing edge delamination in plywood using an area-based approach and enable comparison of delamination extent at different feed speeds.

Key words: *CNC milling, plywood, edge delamination, fibre tear-out, area-based measurement, surface integrity*

INTRODUCTION

Plywood is a widely used engineered wood material valued for its high mechanical properties, such as high strength, stiffness, and dimensional stability (Réh a GUOTH 2016). These characteristics make it suitable for a broad range of applications, particularly in construction and furniture manufacturing (Trzepieciński et al. 2025; Adamčík et al. 2025; Peignon et al. 2023). Milling is one of the most common machining processes used in woodworking, based on material removal by a rotating cutting tool (Gaff et al. 2016). The quality of the machined surface in plywood is influenced by a combination of factors, including tool geometry, feed speed, cutting edge sharpness, tool wear, and material properties such as density (Demir et al. 2022; Çakıroğlu et al. 2022). Improperly selected machining parameters often result in defects such as fibre tear-out, surface fuzziness or burning (Sejdiu et al. 2024). In plywood, this damage frequently manifests as the breaking and tearing of the upper veneer or the pull-out of inner layers (de Castro Saiki a Gomes 2024; Moustaphaoui et al. 2019; Çakıroğlu et al. 2022). These defects can be so severe that they cannot be eliminated by subsequent finishing operations such as sanding (Adamčík et

Technical University in Zvolen, T. G. Masaryka 24, 960 01 Zvolen
e-mail: xsugarova@is.tuzvo.sk

al. 2025). Edge delamination, defined as the separation of veneer layers, represents one of the most critical defects, as it significantly reduces product quality and cannot usually be removed by subsequent finishing processes (Śmietańska et al. 2020). Due to anisotropy of wood, where the orientation of the fibers relative to the cutting direction significantly alters the mechanisms of disintegration and cutting forces (Dvoracek et al. 2022), the cross-laminated configuration of plywood causes constant changes in the interaction between the tool and the fibers, leading to variable cutting mechanics and inconsistent damage formation (Dvoracek et al. 2022; Pichler et al. 2018). Moreover, there is currently no unified and systematic methodology for quantifying edge delamination in plywood under defined machining conditions (Szwajka a Trzepieciński 2016; Adamčík et al. 2025). Delamination in wood-based materials and composites is commonly evaluated using the delamination factor (F_d), defined as the ratio between the maximum damage diameter and the nominal hole diameter after drilling. This approach, widely applied in drilling studies (Patel a Chaudhary 2022; Trzepieciński et al. 2025). Other methods incorporate areal parameters (Śmietańska et al. 2020; Szwajka a Trzepieciński 2016; Tsao a Hocheng 2007). The present methodology uses areal delamination factor (A_{del}), enabling a comprehensive description of delamination. A further difference lies in the identification of damaged regions. Image-based approaches typically rely on contrast thresholding, which is suitable for homogeneous materials with distinct layer contrast. For plywood, characterized by heterogeneous structure, this may lead to misinterpretation of natural features. In this study, a reference plane is used to distinguish machining-induced damage. It is generated automatically and defined through controlled visual assessment. Additionally, multiple measurement areas along the machined edge are evaluated, providing a representative assessment of damage distribution.

Therefore, the aim of this study is to verify a methodology for quantifying edge delamination in CNC milling of plywood based on an area-based approach using digital microscopy.

MATERIALS AND METHODS

Preparation of samples

The study utilized only birch plywood (*Betula pendula Roth*), commercial grade BB/BB, with a thickness of 18 mm and panel dimensions of 1 525 mm × 1 525 mm (Demos Trade, Žilina, Slovakia). The material consisted of 15 layers. Before machining, the panels were resized using a sliding table saw into specimens measuring 380 mm × 380 mm, with a total of six boards prepared. All specimens were visually checked, and areas containing visible defects, such as knots, surface cracks, or local delamination, were excluded to avoid influencing the milling process. In addition, twenty smaller samples (50 mm × 50 mm) were produced for density measurement.

Milling of the samples

The machining experiments were carried out on a 5-axis CNC machining centre SCM Tech Z5 (SCM Group, Rimini, Italy). The workpieces were fixed using four vacuum clamping pods (120 × 120 mm) to ensure stable positioning and reduce vibration during cutting. The spacing of the pods was selected to provide sufficient rigidity while allowing machining of grooves with a length of 120 mm. A solid carbide (HWM) negative spiral cutter (IGM 192 HWM Z2 D10 × 32 L80 S8) was used. Grooves were machined using a slot milling strategy with step-down passes, where the total depth was divided into three successive passes. For each board, grooves with a length of 120 mm were produced in three cutting directions relative to the grain of the surface veneer: 0° (parallel), 45° (diagonal), and 90° (perpendicular). For subsequent evaluation, only the central 100 mm section of each groove was analysed, while 10 mm from each end was excluded to eliminate the influence of tool entry and exit. Feed speeds of 5, 7.5, and 10 m·min^{-1} were applied, while the spindle speed was set to 18,000 rpm.

Density measurement

The density of the plywood was determined according to STN EN 323 (1993) using an IMAL IB600 testing machine (IMAL S.r.l., San Damaso, Italy). The equipment enables automated testing of physical and mechanical properties of wood-based panels in compliance with European standards. Twenty specimens (50 × 50 mm) were used. Each sample was weighed with an accuracy of 0.01 g, and its dimensions were measured to 0.1 mm. Thickness was measured at the centre of the specimen, while width and length were recorded at mid-span positions.

Surface roughness measurement

Surface topography consists of irregularities at different spatial wavelengths, with roughness representing the short-wavelength component (Khazaeian 2006). Measurements were carried out using a Keyence VHX-7000 digital microscope (Keyence Corporation, Osaka, Japan), which also served for microscopic imaging. The evaluated measuring length was 100 mm, with a 200× lens magnification. Each machined surface was analysed using two scans (40 × 18 mm). In every scan, 16 profile lines were evaluated, 8 taken perpendicular and 8 parallel to the feed direction, giving a total of 32 profiles per scanned surface. Roughness was evaluated according to ISO 21920 (2021), using an L-filter with λc = 2.5 mm and an S-filter with λs = 8 µm. The parameter *R*a (arithmetical mean height) and *R*z was chosen due to its common use in literature. The *W*a parameter was used to quantify surface waviness, using an L-filter (λc = 2.5 mm) and an F-filter (λf = 8 mm).

Microscopic analysis of plywood edge delamination

Edge delamination was evaluated on CNC-milled birch plywood (*Betula pendula* Roth) using a Keyence VHX-7000 digital microscope (Keyence Corporation, Osaka, Japan). For each milled groove, ten measurement areas of 10 × 5 mm were defined along the upper machined edge. The quantification of delamination was based on the delaminated area (A_{del}). The parameter A_{del} was obtained from surface analysis based on a manually defined reference plane. This plane was established through controlled visual assessment by iteratively adjusting its position to suppress height variations associated with the intrinsic plywood structure, while preserving geometrical features corresponding to machining-induced damage. The delaminated region was subsequently quantified as the surface area below the defined reference plane. All measurements were performed using the integrated analysis tools of the Keyence VHX software.

RESULTS AND DISCUSSION

Density measurement

The average density of the tested beech plywood was 700.44 kg·m^{-3}, with a standard deviation of 14.59 kg·m^{-3}. The low variability in density observed among the specimens indicates that differences in surface quality are likely to be predominantly associated with the applied machining parameters rather than material heterogeneity. Therefore, density can be considered a controlled material characteristic that did not significantly affect the comparison of individual milling conditions.

Property	Mean ± SD	Min – Max
Density ($kg \cdot m^{-3}$)	700.44 ± 14.59	674.22 – 725.54

Tab. 1 Descriptive statistics of the density of beech plywood specimens (n = 20)

Surface roughness measurement

This part of the paper focuses on the statistical analysis of the measured data to assess the impact of the monitored factors on surface quality. The subject of the investigation was quantitative statistical characteristics represented by surface texture parameters: *R*a, *R*z, *R*p, *R*v, and *W*a. The main objective was to use two-way analysis of variance (ANOVA) to test the null hypothesis of equality of means and to determine whether the feed speed (at levels 5, 7.5, and 10 $m \cdot min^{-1}$) and the orientation of the veneers has a statistically significant effect on these variables. Prior to the analysis, the assumptions of normality and homogeneity of variances were verified using the Shapiro–Wilk and Levene tests, respectively. Although Levene's test indicated unequal variances among groups, ANOVA was considered appropriate due to its robustness against violations of variance homogeneity.

As might be seen in Tab 2, increasing the feed speed from 5 to 10 $m \cdot min^{-1}$ resulted in higher values of all evaluated parameters, indicating a deterioration in surface quality. When comparing grain directions, the transverse veneer generally exhibited higher roughness values than the longitudinal veneer. The largest differences were observed at the highest feed speed of 10 $m \cdot min^{-1}$, where the *R*a value reached 35.44 µm for the transverse grain direction compared with 26.15 µm for the longitudinal grain direction. Similar trends were found for the *R*z, *R*p, and *R*v parameters. The waviness parameter *W*a also increased with increasing feed speed. The highest values were recorded at 10 $m \cdot min^{-1}$, reaching 13.56 µm for the longitudinal grain direction and 11.00 µm for the transverse grain direction.

Grain direction	**Feed speed ($m \cdot min^{-1}$)**	***R*a (µm)**	***R*z (µm)**	***R*p (µm)**	***R*v (µm)**	***W*a (µm)**
Longitudinal	5	13,13 (± 5,02)	65,60 (± 26,36)	24,04 (± 10,28)	41,54 (± 18,88)	6,50 (± 2,68)
Longitudinal	7,5	20,23 (± 9,41)	94,56 (± 38,96)	42,21 (± 18,99)	52,42 (± 23,28)	9,67 (± 4,94)
Longitudinal	10	26,15 (± 15,14)	127,21 (± 96,19)	95,67 (± 94,38)	57,04 (± 43,62)	13,56 (± 8,77)
Transverse	5	14,85 (± 5,09)	91,67 (± 36,04)	29,73 (± 8,62)	61,85 (± 30,00)	5,46 (± 1,95)
Transverse	7,5	26,65 (± 8,77)	126,54 (± 44,28)	51,52 (± 15,32)	75,02 (± 31,89)	7,50 (± 2,65)
Transverse	10	35,44 (± 12,13)	186,17 (± 74,50)	69,46 (± 24,09)	116,63 (± 58,55)	11,00 (± 3,99)

Tab. 2 Mean values (± SD) of surface roughness (*R*a, *R*z, *R*p, *R*v) and waviness (*W*a) parameters for different grain directions and feed speeds

Statistical significance was evaluated at a 5% significance level ($\alpha = 0.05$). According to Tab. 3, feed speed was identified as the dominant factor influencing surface quality, significantly affecting all roughness and waviness parameters ($p < 0.05$). Grain direction significantly influenced *R*z, *R*v, and *W*a, while no significant effect was found for *R*a and *R*p. Significant interactions between feed speed and grain direction were observed for *R*a, *R*p, and *R*v, suggesting that the effect of feed speed varied depending on the veneer grain orientation.

	***R*a p-level**	***R*z p-level**	***R*p p-level**	***R*v p-level**	***W*a p-level**
feed speed	0.000	0.000	0.000	0.000	0.000
grain direction	0.074	0.000	0.444	0.000	0.002
feed speed*grain direction	0.004	0.933	0.005	0.000	0.137

Tab. 3 p-levels from two-factor analysis of variance (ANOVA)

The 3D surface topography (Fig. 1) revealed a regular pattern of machining marks generated by the milling cutter movement. The surface is characterized by clearly visible feed marks corresponding to the kinematic trajectory of the cutting edges. Similar patterns were described by Brenci and Gurău (2024), who attributed their formation to the cycloidal motion of the cutting edge during profile milling. The visibility and amplitude of these machining marks increased with feed speed, which is consistent with the observed increase in the roughness and waviness parameters. Findings of other authors support that the observed surface topography was influenced not only by the kinematic motion of the cutter but also by fibre deformation, local fibre pull-out occurring during the milling process and by the anatomical structure as well (Adamčík et al. 2025; Kopecký et al. 2019).

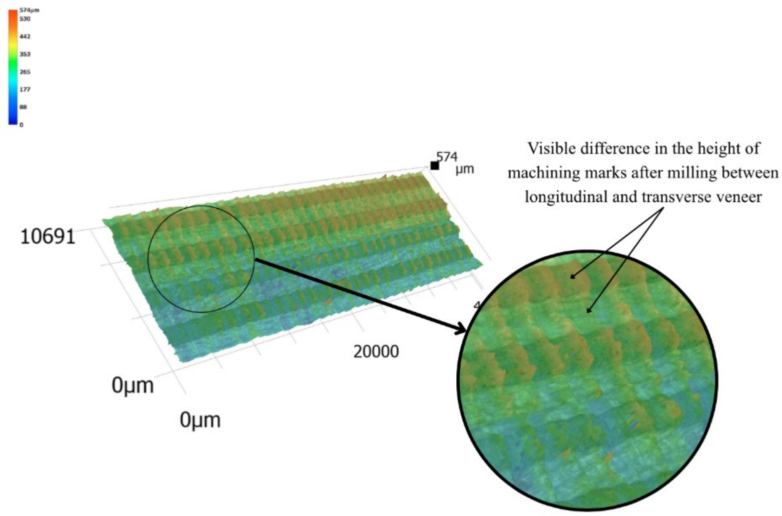

Fig. 1 3D surface topography after milling

The average values of roughness parameters *R*a, *R*z, *R*p, *R*v and waviness parameter *W*a for longitudinal and transverse veneer orientations are shown in Fig. 2. In all evaluated parameters, surface irregularities increased with increasing feed speed from 5 m·min^{-1} to 10 m·min⁻¹, indicating a deterioration of surface quality at higher feed rates. Two-way ANOVA revealed that feed speed significantly affected all evaluated parameters (*R*a, *R*z, *R*p, *R*v and *W*a; $p < 0.05$). This confirms that feed speed was the dominant factor influencing the quality of the milled plywood surface. Similar findings were reported by Adamčík et al. (2025), Pinkowski et al. (2024) and Demir et al. (2022), who observed increasing roughness with increasing feed speed due to higher feed per tooth and chip thickness. The increase in feed speed results in a larger volume of material removed by each cutting edge engagement. Consequently, cutting forces increase and the cutting process becomes less stable, leading to greater fibre deformation, fibre pull-out and surface fuzziness. Kuljich et al. (2013) reported that deeper fibre pull-out is associated with increased surface roughness and waviness. These defects were found to be strongly related to cutting forces, particularly to the parallel component of the cutting force. Increased cutting forces result in greater fibre deformation, leading to higher surface roughness and lower surface quality, which was previously reported by more authors (Korkmaz et al. 2024; Curti et al. 2021).

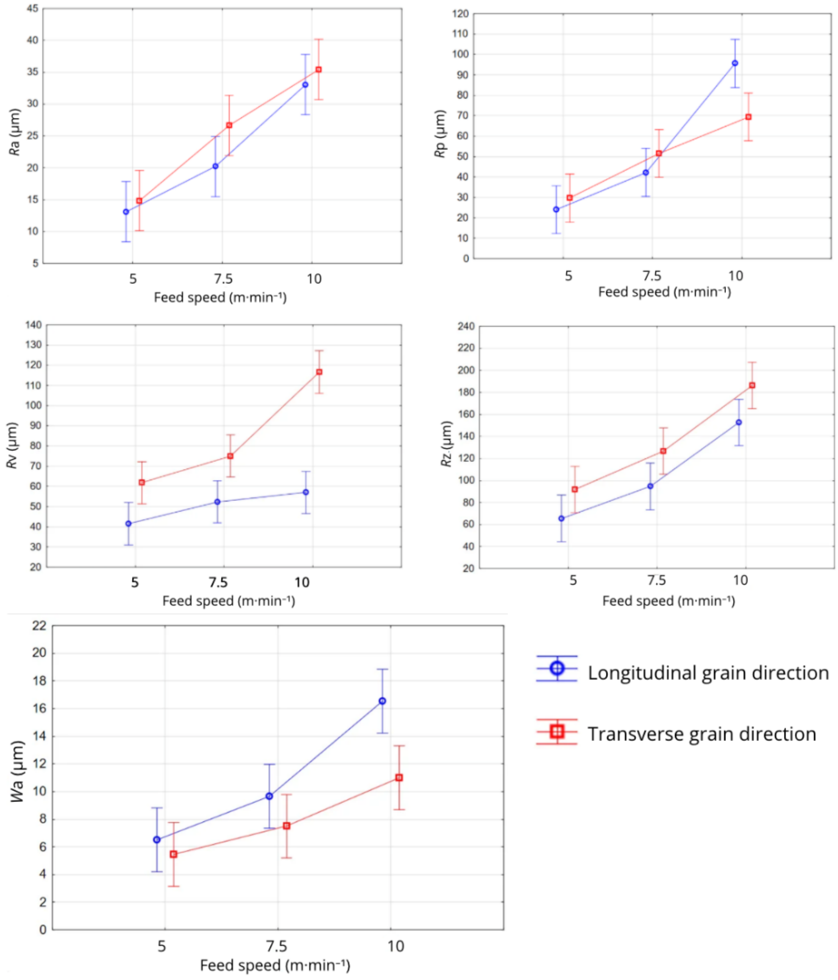

Fig. 2 Changes in *R*a, *R*z, *R*p, *R*v, and *W*a with feed speed and grain direction (longitudinal or transverse veneers) - 95% confidence intervals for population means

Microscopic analysis of plywood edge delamination

The 3D surface topography presented in Fig. 3 reveals that the milling process affected the integrity of the upper veneer. Several localized depressions can be observed along the edge region, corresponding to areas where wood fibres were torn out from the surface. The presence of deep indentations caused by fibre pull-out and protruding fibres remaining attached to the veneer surface are observed too. These defects indicate that the cutting process generated stresses exceeding the local strength of the wood structure, resulting in fibre fracture and detachment.

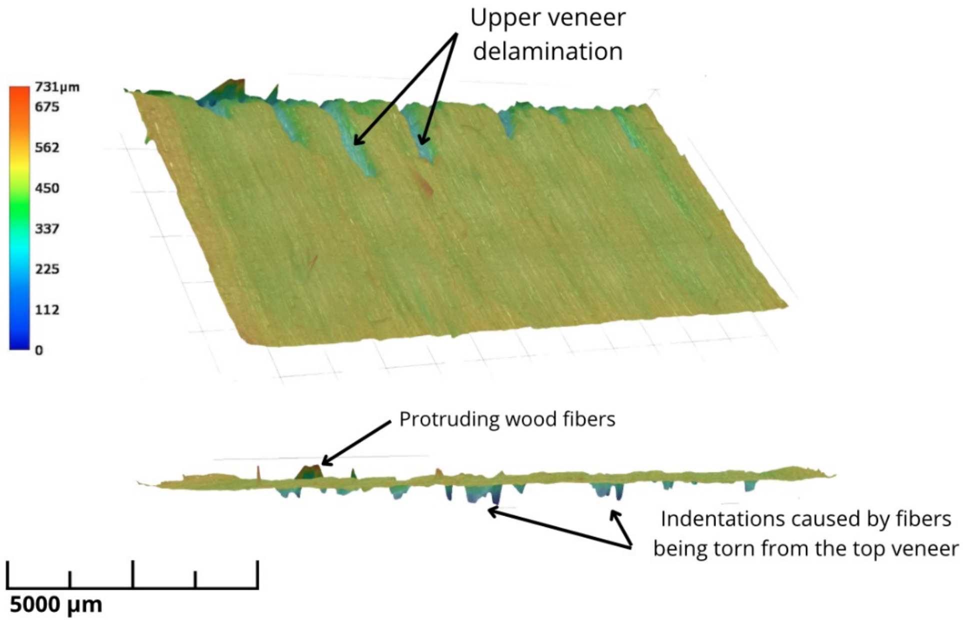

Fig. 3 3D surface topography of the milled plywood edge showing upper veneer delamination, protruding wood fibres, and indentations caused by fibre pull-out.

The observed defects are consistent with the findings of Prokeš (1982), who reported that fibre pull-out is strongly influenced by grain orientation and becomes more pronounced during machining across the grain. Similarly, more authors found that transverse cutting increases cutting forces and promotes crack formation beneath the machined surface (Porankiewicz a Goli 2013; Eyma et al. 2004). According to Kuljich et al. (2013), the depth of torn fibres is significantly correlated with cutting forces, particularly with their parallel component. Increased cutting forces lead to greater fibre deformation and deterioration of surface quality (Korkmaz et al. 2024; Dharmalingam et al. 2022), resulting in higher roughness and waviness values. The damage observed in the upper veneer can be classified as delamination, i.e., local separation and removal of veneer fragments caused by unsuitable machining conditions (Tsao a Hocheng 2007). Previous studies have shown that delamination increases with increasing feed speed and feed per tooth due to the higher cutting forces and chip thickness generated during machining (Adamčík et al. 2025; Dharmalingam et al. 2022; Szwajka a Trzepieciński 2016).

Delamination factor

The quality of the milled plywood edge was further evaluated using the delamination factor (A_{del}), which quantifies the extent of damage occurring in the upper veneer layer. The delamination factor was calculated as the ratio of the delaminated area (S_{del}) to the evaluated edge length (L_p = 10 mm).

$$A_{del} = \frac{S_{del}}{L_p}$$

where:
A_{del} - delamination factor (mm),
S_{del} - delaminated area (mm^2)
L_p - evaluated length of the test specimen (mm).

Higher values of A_{del} indicate a greater degree of fibre pull-out and veneer damage caused by the milling process. The delamination factor provides an effective indicator for assessing the suitability of selected cutting parameters and their influence on the integrity of the upper veneer.

Grain direction	Feed speed (m·min⁻¹)	n	Mean (A_{del})	SD	Min	Max
45°	5.0	30	0.146	0.062	0.056	0.251
45°	7.5	30	0.113	0.067	0.012	0.265
45°	10.0	30	0.081	0.069	0.003	0.314
90°	5.0	30	0.288	0.170	0.038	0.756
90°	7.5	30	0.294	0.192	0.043	0.857
90°	10.0	30	0.450	0.337	0.007	1.307

Tab. 4 Descriptive statistics of the delamination factor A_{del} depending on grain orientation of the upper veneer and feed speed

The delamination factor (A_{del}) shown in Tab. 4 showed a clear dependence on the grain orientation of the upper veneer. At all feed speeds, higher delamination values were observed for the 90° grain orientation than for the 45° orientation. At a feed speed of 5 m·min^{-1}, the mean A_{del} increased from 0.146 at 45° to 0.288 at 90°. This difference became even more pronounced at 10 m·min^{-1}, where the mean delamination factor reached 0.081 at 45° and 0.450 at 90°. Thus, the 90° orientation produced approximately 2.0 times higher delamination at 5 m·min^{-1} and more than 5.5 times higher delamination at 10 m·min^{-1}. This confirms that the upper veneer is much more susceptible to fibre pull-out when the cutting edge acts approximately perpendicular to the fibre direction. In this cutting configuration, the tool does not separate fibres cleanly but tends to lift, crack and tear them from the veneer surface. Similar behaviour was described by Adamčík et al. (2025) and Kuljich et al. (2013), who observed that transverse veneers are more prone to chipping and delamination during plywood edge milling. Microscopic analysis of Adamčík et al. (2025) showed that cutting forces may exceed the local strength of the veneer, leading to crack formation and complete fibre removal, in some cases down to the adhesive layer. Such damage is critical because it cannot be fully removed by subsequent sanding without excessive material removal.

For the 90° orientation, the delamination factor increased from 0.288 at 5 m·min^{-1} to 0.450 at 10 m·min^{-1}. This trend is consistent with the general machining theory and with previous studies reporting that delamination increases with increasing feed speed and feed per tooth (Trzepieciński et al. 2025; Szwajka a Trzepieciński 2016; Tsao a Hocheng 2007). Higher feed speed increases the amount of material removed by each cutting edge, resulting in higher chip thickness, increased cutting forces and less stable cutting conditions (Dvoracek et al. 2022; Eyma et al. 2004).

A different trend was observed for the 45° grain orientation, where the mean A_{del} decreased from 0.146 at 5 m·min^{-1} to 0.081 at 10 m·min^{-1}. In the 45° orientation, the cutting edge interacts with the fibres under an oblique angle, which may reduce the tendency for crack propagation directly along the veneer edge. Instead of being lifted perpendicularly from the surface, the fibres may be cut or sheared more gradually. While increasing feed speed clearly increased delamination at 90°, this trend was not observed at 45°, where delamination remained considerably lower. Therefore, the effect of feed speed should not be interpreted independently, but in interaction with the orientation of the upper veneer fibres. From a practical point of view, the most critical machining condition was the combination of 90° grain orientation and 10 m·min^{-1} feed speed, which produced the highest mean delamination factor and the highest variability.

CONCLUSIONS

The study verified an optical methodology for quantifying edge delamination in CNC-milled birch plywood using 3D surface analysis. The method enabled the evaluation of upper veneer damage based on delaminated area and maximum fibre tear-out depth. Feed speed significantly affected all evaluated roughness and waviness parameters. Increasing the feed speed from 5 to 10 m·min^{-1} led to a deterioration of surface quality, expressed by higher *R*a, *R*z, *R*p, *R*v, and *W*a values. Grain direction also played an important role, with transverse veneers generally showing higher surface irregularities than longitudinal veneers. The delamination factor (A_{del}) confirmed that the 90° grain orientation was more susceptible to upper veneer damage than the 45° orientation. The highest delamination was observed at 90° and 10 m·min^{-1}, while the lowest values were recorded for the 45° orientation. These results indicate that feed speed should not be evaluated independently, but in interaction with the grain orientation of the upper veneer. The proposed methodology provides a practical and repeatable tool for assessing edge delamination in plywood and may be used for optimizing CNC milling parameters to improve surface quality and reduce veneer damage.

REFERENCES

ADAMČÍK, Lukáš, Veronika ŠUGÁROVÁ, Richard KMINIAK, Jarmila SCHMIDTOVÁ, Adrián BANSKI a Peter GALAJDA, 2025. Optimization of technological parameters of CNC milling of plywood depending on surface roughness. *European Journal of Wood and Wood Products* [online]. 2025, zv. 83. Dostupné na: doi:10.1007/s00107-025-02272-6

BRENCI, Luminița-Maria a Lidia GURĂU, 2024. A Stratified Characterization of Surface Quality of Beech Processed by Profile Milling. *Applied Sciences* [online]. 2024, zv. 14, č. 1, s. 129. ISSN 2076-3417. Dostupné na: doi:10.3390/app14010129

ÇAKIROĞLU, Evren Osman, Aydın DEMIR, İsmail AYDIN a Ümit BÜYÜKSARI, 2022. Prediction of optimum CNC cutting conditions using artificial neural network models for the best wood surface quality, low energy consumption, and time savings. *BioResources* [online]. 2022, zv. 17, č. 2, s. 2501–2524. ISSN 19302126, 19302126. Dostupné na: doi:10.15376/biores.17.2.2501-2524

CURTI, R., B. MARCON a L. DENAUD, 2021. *Generalized cutting force model for peripheral milling of wood, based on the effect of density, uncut chip cross section, grain orientation and tool helix angle | European Journal of Wood and Wood Products* [online] [cit. 23.3.2025]. Dostupné na: https://link.springer.com/article/10.1007/s00107-021-01667-5

DE CASTRO SAIKI, Lucas Eiji a Guilherme Ferreira GOMES, 2024. Understanding and mitigating delamination in composite materials: A comprehensive review. *Mechanics of Advanced Materials and Structures* [online]. 2024, zv. 31, č. 30, s. 13147–13167. ISSN 1537-6494. Dostupné na: doi:10.1080/15376494.2024.2333490

DEMIR, Aydin, Evren Osman CAKIROGLU a Ismail AYDIN, 2022. Effects of CNC Processing Parameters on Surface Quality of Wood-Based Panels Used in Furniture Industry. *Drvna industrija* [online]. 2022, zv. 73, č. 4, s. 363–371. ISSN 18471153, 00126772. Dostupné na: doi:10.5552/drvind.2022.2109

DHARMALINGAM, Sangeetha, Om KUMAR a Felix SWAMIDOSS, 2022. Optimization of Drilling parameters for reduced Delamination Factor in non-functionalized and amine-functionalized Luffa/Epoxy Composites. *Journal of Polymer Research* [online]. 2022, zv. 29. Dostupné na: doi:10.1007/s10965-022-03197-x

DVORACEK, Ondrej, Daniel LECHOWICZ, Franz HAAS a Stephan FRYBORT, 2022. Cutting force analysis of oak for the development of a cutting force model. *Wood Material Science & Engineering* [online]. 2022, zv. 17, č. 6, s. 771–782. ISSN 1748-0272. Dostupné na: doi:10.1080/17480272.2021.1955296

EYMA, Florent, Pierre-Jean MÉAUSOONE a Patrick MARTIN, 2004. Strains and cutting forces involved in the solid wood rotating cutting process. *Journal of Materials Processing Technology - J MATER PROCESS TECHNOL* [online]. 2004, zv. 148, s. 220–225. Dostupné na: doi:10.1016/S0924-0136(03)00880-X

GAFF, Milan, Monika SARVAŠOVÁ-KVIETKOVÁ, Miroslav GAŠPARÍK a Martin SLÁVIK, 2016. DEPENDENCE OF ROUGHNESS CHANGE AND CRACK FORMATION ON PARAMETERS OF WOOD SURFACE EMBOSSING. *WOOD RESEARCH*. 2016, zv. 61.

KHAZAEIAN, A., 2006. 3D Characterization of wood surface quality: measurement strategy, influence of species and machining parameters. *Ph.D. Dissertation (in French)*. 2006.

KOPECKÝ, Zdeněk, Luďka HLÁSKOVÁ, Aleš SOLAŘ a Petr NESÁZAL, 2019. CUTTING FORCES IN QUASI-ORTHOGONAL CNC MILLING. *WOOD RESEARCH*. 2019, zv. 64.

KORKMAZ, M., M. BUDAKÇI a I. KILINÇ, 2024. *Assessment of surface roughness in milling of wood with different material temperature and cutting parameters :: BioResources* [online] [cit. 22.6.2026]. Dostupné na: https://bioresources.cnr.ncsu.edu/

KULJICH, Svetka, Roger E. HERNÁNDEZ, Angela M. LLAVÉ a Ahmed KOUBAA, 2013. Effects of Cutting Direction, Rake Angle, and Depth of Cut on Cutting Forces and Surface Quality during Machining of Balsam Fir. *Wood and Fiber Science*. 2013, s. 195–205. ISSN 0735-6161.

MOUSTAPHAOUI, Anouar El, Abdelkarim CHOUAF, Khadija KIMAKH a M'hamed CHERGUI, 2019. CHARACTERIZATION OF CEIBA PLYWOOD DELAMINATION IN MODE I USING AN ENERGETIC CRITERION. *WOOD RESEARCH*. 2019, zv. 64.

PATEL, Punit a Vijay CHAUDHARY, 2022. Delamination evaluation in drilling of composite materials – A review. *Materials Today: Proceedings* [online]. 2022, zv. 56, 3rd International Conference on Contemporary Advances in Mechanical Engineering, s. 2690–2695. ISSN 2214-7853. Dostupné na: doi:10.1016/j.matpr.2021.09.267

PEIGNON, A., J. SERRA, L. GÉLARD, A. CANTAREL, F. EYMA a B. CASTANIÉ, 2023. Mode I delamination R-curve in poplar laminated veneer lumber. *Theoretical and Applied Fracture Mechanics* [online]. 2023, zv. 126, s. 103982. ISSN 0167-8442. Dostupné na: doi:10.1016/j.tafmec.2023.103982

PICHLER, Philip, Martin LEITNER, Florian GRÜN a Christoph GUSTER, 2018. Evaluation of wood material models for the numerical assessment of cutting forces in chipping processes. *Wood Science and Technology* [online]. 2018, zv. 52. Dostupné na: doi:10.1007/s00226-017-0962-1

PINKOWSKI, G., M. PIERNIK, M. WOŁPIUK a A. KRAUSS, 2024. Effect of chip thickness and tool wear on surface roughness and cutting power during up-milling wood of different density | Request PDF. *ResearchGate* [online]. 2024 [cit. 22.3.2025]. Dostupné na: doi:10.15376/biores.19.4.9234-9248

PORANKIEWICZ, Bolesław a Giacomo GOLI, 2013. Cutting forces by Oak and Douglas fir machining. *Maderas. Ciencia y tecnología* [online]. 2013, zv. 16. Dostupné na: doi:10.4067/S0718-221X2014005000016

PROKEŠ, S, 1982. *Machining of wood and new wood materials. (Obrábění dřeva a nových hmot ze dřeva)*. 3. Praha: SNTL.

RÉH, R. a MARTIN GUOTH, 2016. Thermoplastic plywood and it's drawback when moderately heated. *Wood Research* [online]. [cit. 20.4.2026]. Dostupné na: https://www.woodresearch.sk/cms/thermoplastic-plywood-and-its-drawback-when-moderately-heated/

SEJDIU, Rrahim, Hysni OSMANI, Cevdet SOGUTLU, Kaltrina SEJDIU a Kaltrine JAKUPI, 2024. THE INFLUENCE OF MACHINING PARAMETERS ON THE SURFACE ROUGHNESS QUALITY OF BEECH WOOD (FAGUS SYLVATICA L. - A COMPREHENSIVE STUDY). 2024, zv. 19.

ŚMIETAŃSKA, Katarzyna, Piotr PODZIEWSKI, Marcin BATOR a Jarosław GÓRSKI, 2020. Automated monitoring of delamination factor during up (conventional) and down (climb) milling of melamine-faced MDF using image processing methods. *European*

Journal of Wood and Wood Products [online]. 2020, zv. 78, č. 3, s. 613–615. ISSN 1436-736X. Dostupné na: doi:10.1007/s00107-020-01518-9

SZWAJKA, Krzysztof a Tomasz TRZEPIECIŃSKI, 2016. Effect of tool material on tool wear and delamination during machining of particleboard. *Journal of Wood Science* [online]. 2016, zv. 62, č. 4, s. 305–315. ISSN 1611-4663. Dostupné na: doi:10.1007/s10086-016-1555-6

TRZEPIECIŃSKI, Tomasz, Krzysztof SZWAJKA, Joanna ZIELIŃSKA-SZWAJKA a Marek SZEWCZYK, 2025. Current Trends in Monitoring and Analysis of Tool Wear and Delamination in Wood-Based Panels Drilling. *Machines* [online]. 2025, zv. 13, č. 3, s. 249. ISSN 2075-1702. Dostupné na: doi:10.3390/machines13030249

TSAO, C. C. a H. HOCHENG, 2007. Effect of tool wear on delamination in drilling composite materials. *International Journal of Mechanical Sciences* [online]. 2007, zv. 49, č. 8, s. 983–988. ISSN 0020-7403. Dostupné na: doi:10.1016/j.ijmecsci.2007.01.001

ACKNOWLEDGMENT

This experimental research was prepared within the grant project: IPA 11/2026 Proposed Methodology for Evaluating the Degree of Delamination After CNC Milling of Plywood

ANALYSIS OF THE EFFECT OF DRYING CONDITIONS AND HYGROTHERMAL TREATMENT ON THE PROCESSING OF BEECH BLANKS CONTAINING REACTION WOOD

Tatiana Vilkovská – Ivan Klement – Peter Vilkovský

Abstract

Beech (Fagus sylvatica L.) is the dominant hardwood species in Slovakia, but its industrial utilization is limited by the frequent occurrence of tension wood, which negatively affects dimensional stability during drying. This study investigates the effect of drying conditions and hygrothermal treatment on the processing quality of beech sawn timber under industrial conditions. Beech lumber containing tension and normal wood was subjected to two drying modes: pressure steaming followed by kiln drying, and kiln drying without the steaming process. Steaming reduced the initial variability in moisture content; however, no significant differences in final moisture content were observed after drying. In contrast, statistically significant differences were confirmed in longitudinal deformation. Boards containing tension wood exhibited greater warp intensity in both drying modes, while steaming intensified stress release and increased combined deformation. The results demonstrate that tension wood content significantly affects dimensional stability, whereas moisture differences play a minor role. Technological optimization is essential to improve the processing efficiency of beech timber.

Keywords: *longitudinal warping. tension wood, beech, hygrothermal treatment, beech blanks*

INTRODUCTION

Beech is wood with high frequency of defects such as red heartwood, reaction wood (tension wood), dote and so forth. Currently, due to the development of wood technology, it is necessary to respect the major limiting factors in manufacturing such as energy sources and sources of wood raw material (Vidholdová *et al.* 2026). Considering the high proportion of beech wood, the way of its use is nowadays the subject of quality. The quality of beech wood is determined based on structure and properties of wood, frequency of defects in this material. Tension wood is thought of as an important wood defect because it causes negative alterations in solid wood quality and limits industrial utilization of wood. Findings confirmed 14 – 21 % ratio of tension wood in beech logs (Kúdela and Čunderlík 2012). Timber with content of tension wood has high longitudinal warping which affect their quality significantly. Drying shrinkage is a common phenomenon during the processing and utilization of wood induced by moisture loss. Drying stress is the main cause of wood deformation and cracking. The shrinkage differential between tangential and radial direction, moisture content gradient of wood and quality of wood as ell are reasons

Technical University in Zvolen, T. G. Masaryka 24, 960 01 Zvolen
e-mail: xhurakova@is.tuzvo.sk

induced the generation of drying stresses during drying process (Fu *et al.* 2023). The development of drying stresses is closely related to the coupled processes of heat and mass transfer and to the rheological behaviour of wood below the fibre saturation point, where differential shrinkage between surface and middle layers leads to tensile and compressive stress reversals. These mechanisms are particularly critical in the presence of reaction wood, where structural heterogeneity amplifies longitudinal deformation and increases the susceptibility to checking and warping (Yin, Liu 2021; Brischke, Alfredsen 2020). It is believed that the hygrothermal recovery of tension wood is responsible for the unique contraction observed in the gelatinous layer along the wood's longitudinal axis (Sujan *et al.* 2016). As also shown by authors Kúdela and Čunderlík (2012), along with Yamamoto *et al.* (2005) investigated the influence of reaction wood on material properties authors concluded that the increased cellulose content in reaction wood, coupled with weaker bonding between the G-layer and S_2 layer, leads to greater swelling of the other layers. This results in the creation of additional sorption sites, which is considered the primary reason for the potentially higher moisture content (MC) observed in reaction wood. In addition to internal stress development, previous drying significantly influence the subsequent mechanical behavior of wood, even in water-saturated conditions and (Dudiak 2025). Also study of authors Miyoshi *et al.* (2015) demonstrated that water-swollen wood subjected to prior drying exhibited increased lateral tensile failure strain and reduced elastic modulus compared to control samples. These changes were attributed to increased molecular mobility (fluidity) and alterations in the microstructural state of wood polymers, particularly in the amorphous zones. These findings indicate that drying history does not only affect moisture gradients and stress development during processing, but also modifies the intrinsic deformation behavior of wood at the cellular level. Based on the citated work Sujan *et al.* 2015 the characteristic hygrothermal (HT) behavior of tension wood (TW) specimens treated at temperatures of 80, 100, and 120°C was compared. Deformation in both the longitudinal and tangential directions, measured after 10 cycles of 10-minute HT treatments at the respective temperatures, revealed that the deformation consisted of an initial recovery phase followed by continuous deformation. In the longitudinal direction, both the initial recovery and the continuous deformation exhibited contractive behavior, whereas in the tangential direction, these phases were expansive. A multiple comparison test conducted to evaluate the temperature dependence of hygrothermal recovery (HTR) indicated that the parameters defining the trend lines differed significantly across temperature treatments. Notably, at 80°C, the initial recovery was significantly smaller, nearly negligible, while the continuous contraction was considerably greater than at 100°C and 120°C. Additionally, a distinct change in behavior was observed between 80°C and 100°C. Also, similar observations are shown by authors Yamamoto *et al.* 2022; Placet *et al.* 2007 that moisture desorption causes a large scale of volumetric shrinkage of matrix component in the G-layer. This enables the Cellulose microfibril (CMF) that had been stretched to be recovered. In other words, the drying process allows the G-fiber to longitudinally contract due to the concerted effect of the remaining tensile stress in the Cellulose microfibril and the shrinking stress of the matrix substance in the G-layer. Hydrothermal treatment has a significant effect on the morphological changes that occur in the cell wall of tension wood. Stress relaxation is reflected by a change in dimensions in the longitudinal direction. The authors Čunderlík *et al.* (1995) dealt with the influence of hydrothermal treatment by steaming on the relaxation of growth stresses in tension reaction wood. Experiments show that the temperature and time of steaming significantly affect the longitudinal contraction of tension reaction wood.

The main objective of the experiment conducted on long boards under industrial conditions was to analyse the development of warp in boards containing tension and normal wood. Process optimization strategies focused on minimizing shape deformations through different technological approaches, namely the combination of steaming and kiln drying with applied load, as well as steaming and kiln drying without load.

MATERIAL AND METHODS

The measurements were conducted under operating conditions. The blanks used measured 65 mm (*width*) × 55 mm (*thickness*) × 2000 mm (*length*). We focused on selecting blanks without visible wood defects that could negatively affect longitudinal warping particularly false heartwood, rot, knots or dote and thus lead to distorted results. Suitable logs were selected based on macroscopic characteristics, primarily increased woolly surface (Fig. 1) and the initial value of longitudinal warping determined prior to the cross-cutting process.

Fig. 1 Woolly surface and normal surface of beech blanks

The selection of blanks consisted of targeted and random sampling. From the targeted selection, 20 blanks showing reaction wood were selected based on macroscopic characteristics, and 20 normal blanks were selected for each stack separately. The random selection involved randomly selecting 100 pieces of lumber for each cell separately. Based on the random selection, we evaluated the proportion of reaction wood in the stack and the resulting longitudinal warping. The placement and number of lumber pieces were identical in both stacks. Two stacks were prepared from the selected sawn timber pieces (Fig. 2). Stack no. 1 (steamed blanks) was steamed prior to the drying process and then dried, while Stack no. 2 was only dried (unsteamed blanks).

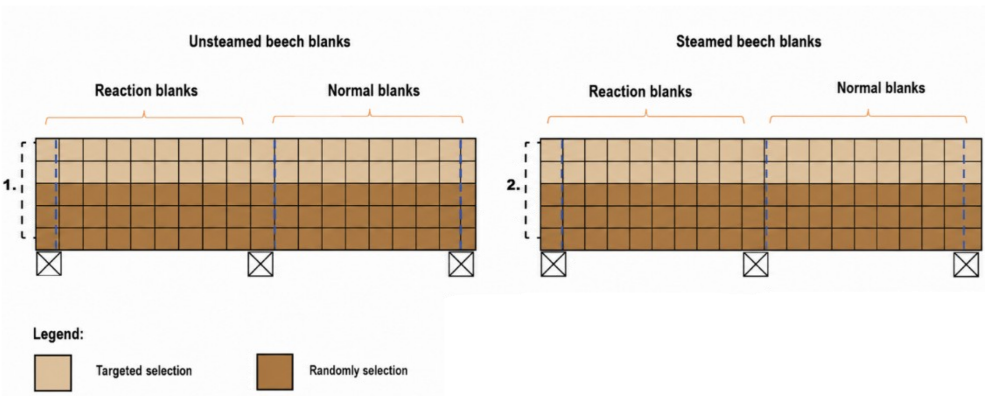

Fig. 2 Stacking layout of blanks in a stack

As part of the operational measurement, a pressure steaming process was applied to the first stack in order to determine the effect of steaming on the size of longitudinal warping in blanks containing reaction wood. The steaming process was carried out in a VYVOS steaming device with a volume of 63 m³. Steaming took place in three consecutive stages. In the first stage, the material was heated to 108 °C for 3.5 hours.

The second stage took place at 60 °C for 2.5 hours, and the third stage at 108 °C for 1 hour. The total steaming time was 7 hours. The drying process took place in an ICD 140 SP dryer manufactured by Incomac.

The stacks were placed in the upper layers of the dryer. The drying process was divided into two phases. The first drying phase ranged from the initial wood moisture content to approximately the equilibrium moisture content (EMC). During this phase, the drying temperature was maintained at a constant 45 °C.

The equilibrium moisture content of the drying environment was regulated based on the current wood moisture content so that the drying gradient did not exceed 3. In the second drying phase, when the wood moisture content fell below FSP, the temperature was increased to 65 °C. Drying proceeded at a constant drying gradient, corresponding to the equilibrium moisture content values.

Moisture measurements were performed using a Greisingert GMH 3850 resistance moisture meter. Measurements were taken on every second blanks before drying, after steaming, and after drying.

Under operating conditions, the longitudinal warping of the logs and ways to reduce it were analysed, given their sufficient length. Blanks containing reaction wood exhibit increased susceptibility to longitudinal warping due to their different physical properties compared to normal wood. As part of this study, bow warping, crook warping, and their combination were evaluated (Fig. 3).

Fig. 3 Different types of longitudinal warping a.) bow b.) crook

The measurements were taken on a straight surface, monitoring the maximum warping at the length centre of the lumber (1000 mm). The measurement point was precisely marked to ensure consistency between individual measurements. The maximum warping was determined using a sliding scale. Testing was conducted on blanks that were specifically selected to ensure a comprehensive comparison. To minimize longitudinal warping, the blanks were placed in the stack so that their orientation corresponded to the direction of the resulting warping, and the crossbars were spaced closer together. The test specimens examined included both reaction wood and normal wood and were placed in both stacks (*targeted selection*).

The proportion of reaction wood in the examined blanks was assessed using a chemical reagent applied to the end surfaces of randomly selected blanks. For this purpose, a special reagent was applied that allows for the identification of tension wood (Fig. 4). The chemical reagent used is the result of our own research and innovation, described in detail in the paper by Vilkovská *et al.* (2024). The reagent's function is based on its chemical interaction with the structure of tension wood: $ZnCl_2$ causes the cellulose macromolecules to swell, thereby destroying the hydrogen bonds between cellulose chains and simultaneously reducing the crystallinity of the cellulose.

The coating was applied to the wood samples placed in both chambers prior to the drying and steaming processes. The presence of reaction wood was indicated by a dark red to purple color.

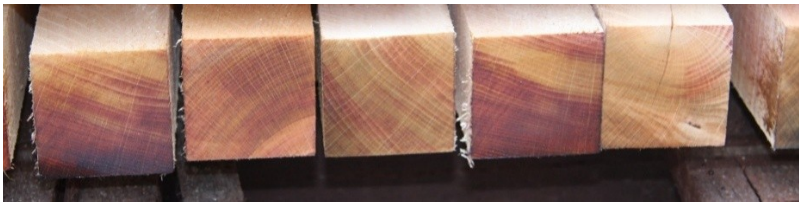

Fig. 4 Identification of tension wood on the fronts of beech blanks

RESULTS AND DISCUSSION

The actual drying process under operating conditions is illustrated in Fig. 5. The graph shows the drying environment temperature (°C), the equilibrium moisture content (%), and the drying curve characterizing the decrease in material moisture content throughout the process (%). A two-stage drying mode was used, with control based on the current moisture content of the blanks. In the first stage, when the moisture content was above the fibre saturation point (FSP), the drying chamber temperature was maintained at 45 °C. After the moisture content fell below the FSP, the temperature was increased to 65 °C. The drying curve showed an almost linear trend, with moisture losses in the wood being relatively uniform and gradual. The total duration of the drying process was 28 days.

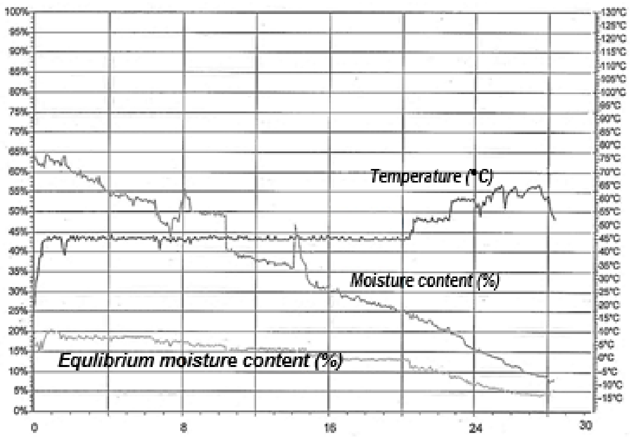

Fig. 5 Drying process under operating conditions

For the first stack, moisture content was measured before drying, after steaming, and after drying. For the second stack, measurements were taken before and after drying only. The tables also include the average moisture content values and the variance of the final moisture content. In Stack 1 (steaming + drying), the initial moisture content of reaction wood blanks before drying averaged 66.4%, with a variance of 36.1%. After the steaming process, a substantial equalization of moisture content occurred, resulting in an average value of 55.4% and a variance of 8.2%. Following drying, the moisture content stabilized at an average of 7.4% with a minimal variance of 1.6%. Normal wood blanks in Stack 1 exhibited lower variability already before drying, with an average moisture content of 62.3% and a variance of 7.1%. After steaming, the average moisture content was 55.9% (variance 6.8%), and after drying it reached 6.8% (variance 1.0%). Thus, the steaming process significantly reduced the initial variability in moisture content. In Stack 2 (drying only), the initial moisture content of reaction wood blanks averaged 53.8% with a variance of 15.16%, whereas normal wood blanks showed a higher average moisture content of 56.8% with a comparable variance of 14.9%. After drying, the moisture contents of both groups became virtually identical: reaction wood blanks reached an average value of 7.4% (variance 1.19%), while normal wood blanks reached 7.5% (variance 0.93%). Based on the obtained results, it can be concluded that the differences in initial moisture content between reaction wood and normal wood blanks were eliminated during the drying process. Under industrial operating conditions, no significant effect of differences in moisture content or of the varying proportion of reaction wood within the blanks on the drying process or on the final moisture content of the material was demonstrated.

Several authors have investigated the influence of drying kinetics, which depend on the anatomical structure of wood. Tarmian *et al.* (2012), Rahimi *et al.* (2011), and Sayar *et al.* (2013) compared diffusion coefficients of normal and reaction beech wood samples using steady-state diffusion measurements by the cup method in the radial direction. The average diffusion coefficients ranged from 0.007 to 0.009 for normal wood and from 0.006 to 0.010 for reaction wood. The resulting diffusion coefficient was found to be higher in tension reaction wood than in normal wood. However, these findings are not fully consistent with the measurements reported by Tarmian *et al.* (2012). According to Gierlinger and Schwanninger (2006), the higher diffusion coefficient can be explained by the chemical composition of tension reaction wood, which is characterized by a higher content of crystalline cellulose and an almost complete absence of lignin. Kúdela and Čunderlík (2012) further noted that diffusion coefficient values depend to a large extent on the method used for their determination.

From a random selection of samples from the first and second stacks, 100 pieces of lumber were evaluated separately for each stack. Subsequently, the proportion of reaction wood was determined. The proportion of reaction wood in the first stack was 38%, whereas in the second stack it reached 50%.

Analysis of Longitudinal Warp in Reaction and Normal Wood Blanks

Based on the results, it can be concluded that the presence of reaction wood had a significant effect on the occurrence and severity of longitudinal warp in beech blanks after drying, while the application of hydrothermal treatment (steaming) partially reduced this phenomenon. Analysis of the randomly selected blanks showed that cupping was the most frequent type of deformation in both reaction and normal wood blanks across both stacks. In the case of reaction wood blanks (Fig 6), bow warping accounted for 47% in the steamed stack and as much as 62% in the non-steamed stack, indicating substantially greater deformation in the absence of steaming. Crook warping occurred less frequently in reaction wood blanks (21% and 28%, respectively), while combined deformation was observed predominantly in the steamed stack (32%) and only minimally in the non-steamed stack

(5%). Straight blanks occurred only rarely among reaction wood samples, confirming the high susceptibility of reaction wood to drying-induced deformation.

This tendency is also associated with longitudinal warp, which is primarily determined by the anatomical structure of reaction wood and differs significantly from that of normal wood.

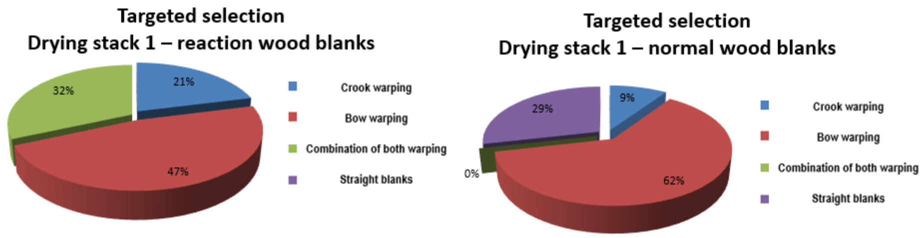

Fig. 6 Analysis of Longitudinal Warp Types for Stacks 1 and 2 (Reaction Wood Blanks)

As shown in Figure 7, bow warping was also the dominant type of deformation in normal wood blanks, accounting for 62% and 63% of the samples in the steamed and non-steamed stacks, respectively. However, a notable difference was observed in the proportion of straight blanks, which was higher in the steamed stack (29%) than in the non-steamed stack (16%). This result suggests a positive effect of hydrothermal treatment on the dimensional stability of normal wood. Combined deformation occurred only rarely, or not at all, in normal wood blanks, indicating a more homogeneous response of wood in the absence of tension wood. These findings further support the conclusion that the presence of reaction wood is a key factor influencing the development of drying-induced deformations and longitudinal warp in beech blanks.

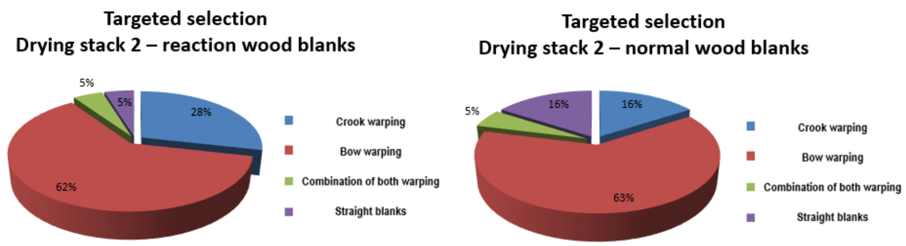

Fig. 7 Analysis of Longitudinal Warp Types for Stacks 1 and 2 (Normal Wood Blanks)

Using Duncan's multiple range test (Table 1), statistically significant differences were evaluated between the type of blank and the drying stacks. In the first stack, a highly significant difference was observed between reaction wood and normal wood blanks, with a significance level of 0.000004 (Table 1). Similarly, in the second stack, a statistically significant difference was also found, with a significance level of 0.00623.

Tab. 1 Duncan test for bow warping

Type of Blanks	Timber stack	Reaction	Reaction	Normal	Normal
		14.302	11.381	1.8518	4.59
Reaction	**1**		0.239549	**0.000004**	**0.000143**
Reaction	**2**	0.239549		**0.000190**	**0.006263**
Normal	**1**	**0.000004**	**0.000190**		0.270204
Normal	**2**	**0.000143**	**0.006263**	0.270204	

In the first stack, Duncan's test confirmed that crook warping differed significantly between reaction wood and normal wood blanks, with a significance level of 0.000143 (Table 5). Side bow occurred with greater intensity in reaction wood blanks. Similarly, in the second stack, the influence of reaction wood was also demonstrated, with a significance level of 0.0054, indicating a statistically significant difference between reaction wood and normal wood blanks (Table 2). These findings are associated with the anatomical and physical heterogeneity of tension wood, which is characterized by an increased proportion of the gelatinous layer (G-layer) and different longitudinal shrinkage behaviour.

Yamamoto *et al.* (2005) concluded that the increased cellulose content in reaction wood, together with weaker bonding between the G-layer and the S_2 layer, leads to greater swelling of the remaining cell wall layers. This creates additional sorption sites and is considered one of the main reasons for the potentially higher moisture content observed in reaction wood.

The results also suggest that hydrothermal treatment may partially reduce the internal stresses generated during tree growth and associated with the presence of reaction wood, thereby contributing to improved dimensional stability of the material during drying.

Tab. 2 Duncan test for crook warping

Type of Blanks	Timber stack	Reaction	Reaction	Normal	Normal
		11.625	7.997	2.0558	0.9215
Reaction	**1**		0.138164	**0.000143**	**0.000026**
Reaction	**2**	0.138164		**0.015181**	**0.005364**
Normal	**1**	**0.000143**	**0.015181**		0.642921
Normal	**2**	**0.000026**	**0.005364**	0.642921	

ANOVA revealed that the type of blank had a statistically significant effect on the evaluated parameters. Duncan's multiple range test was subsequently used to determine the significance boundaries of the effects of both the blank type and the stacking arrangement (kiln stack). Based on the statistical evaluation, Duncan's test confirmed that, in both the first and second stacks, the type of blank (reaction wood vs. normal wood) entering the drying and production process significantly influences the final quality of the dried material, resulting in lower or higher levels of bowing and cupping deformation.

According to Čunderlík *et al.* (1995), during steaming in saturated steam, the longitudinal shrinkage of reaction wood increases linearly with increasing temperature up to approximately 80 °C. Above this temperature threshold, contraction increases rapidly up to temperatures of 140–150 °C. Studies investigating the effects of hydrothermal treatment have shown that it has a significant impact on the morphological changes occurring in the cell wall of tension wood during the treatment process. Stress relaxation is manifested by dimensional changes in the longitudinal direction. Čunderlík *et al.* (1995) specifically investigated the effect of hydrothermal treatment by steaming on the release of growth stresses in tension reaction wood. Their experiments demonstrated that both steaming temperature and duration have a substantial effect on longitudinal shortening (longitudinal shrinkage) of tension reaction wood. In contrast, normal wood samples exhibited no measurable longitudinal shortening. According to Clair *et al.* (2001), longitudinal shortening after one hour of hydrothermal treatment at 80 °C should be approximately 0.3%. The explanation for the observed longitudinal shortening can be found in the works of Placet *et al.* (2002) and Tejada *et al.* (1998), who reported that the structure of the cell wall undergoes qualitative changes following hydrothermal treatment. Furthermore, the application of high temperatures causes greater degradation of highly developed tension wood, resulting in increased longitudinal shortening of the material. These findings are in good agreement with the results reported by Čunderlík *et al.* (1995). From a technological perspective, the proper arrangement of blanks within the stack and the use of smaller spacing between stickers also proved to be important factors, potentially contributing to a partial reduction in deformation. Nevertheless, the results confirm that the decisive factor influencing the occurrence of longitudinal warp is the presence of reaction wood itself. In addition, the chemical identification of tension wood using the reagent proposed by Vilkovská *et al.* (2024) proved to be a suitable method for the rapid selection of potentially problematic blanks prior to processing. This approach may have practical significance for optimizing lumber grading and sorting procedures under industrial operating conditions.

CONCLUSIONS

Currently, European beech accounts for the highest proportion of trees in Slovak forests, but its quality is low. Therefore, it is necessary to find ways to optimize European beech (*Fagus sylvatica* L.) a tree species whose quality is determined by the structure and properties of the wood as well as the presence of defects (false heartwood, water stain, reaction wood) and thereby significantly increase processing efficiency. In conclusion, based on measurements under operational conditions, we can state the following:

- Greater variability in initial moisture content was observed in the treated samples compared to the untreated ones. The pressurized steam treatment significantly reduced this variability, and after subsequent drying, the differences between the treated and untreated samples were no longer apparent. The final moisture content values were comparable in both groups, and the differences can be considered negligible.
- Pressure steaming contributed to the intensification of growth stress release, which manifested as a combination of bow and crook warping. From a technological standpoint, this combination of deformations is undesirable, as it negatively affects the subsequent machinability and dimensional stability of the material.
- A comparison of the results between the first and second stacks revealed higher values of longitudinal warping in the first stack (steaming + drying). Based on these findings, it is recommended to optimize the stacking method for sawn timber, particularly by reducing the distances between the stacking strips, which will ensure a more uniform distribution of load during drying and limit deformations.

The workability of reaction wood is determined not only by its proportion in the blanks but also by the initial degree of warping and the presence of a woolly surface. These macroscopic characteristics can be identified even before the cross-cutting process, which allows for timely material selection and optimization of the technological process.

ACKNOWLEDGMENTS

This work was supported by the Slovak Research and Development Agency under contract no. APVV-21-0049. This work was supported by the Scientific Grant Agency of the Ministry of Education, Science, Research and Sport of the Slovak Republic and the Slovak Academy of Sciences project VEGA no. 1/0092/26.

LITERATURE

1. Brischke C, Alfredsen G. Wood-water relationships and their role for wood susceptibility to fungal decay. Appl Microbiol Biotechnol. 2020 May;104(9):3781-3795. doi: 10.1007/s00253-020-10479-1. Epub 2020 Mar 6. Erratum in: Appl Microbiol Biotechnol. 2021 Aug;105(14-15):6121. doi: 10.1007/s00253-021-11408-6.
2. Clair, B., Thibaut, B., 2001. Shrinkage of the gelatinous layer of Poplar and Beech Tension wood, IAWA Journal, Roč. 22, s. 121-131
3. Čunderlík, I., Kúdela, J., Bluskova, G., 1995. Relaxation of stresses in streamed beech tension wood. In: Lesotechnicesko Obrazovanie v Bulgarii., Sofia, s. 199-205.
4. Gierlinger, N., Schwanninger, M. 2006. Chemical imaging of poplar wood cell walls by confocal Raman microscopy. Plant Physiol, Roč. 140, s. 1246-1254
5. Placet, V., Passard, J., Perre, P. 2007. Viscoelastic properties of green wood across the grain measured by harmonic tests: hardwood versus softwood and normal wood versus reaction wood. Holzforschung, Roč. 61, s. 548-557
6. Rahimi, S., Faezipour, M., Tarmian, A. 2011. Drying of internal-check prone poplar lumber using three different conventional kiln drying schedules. Journal of the Indian Academy of Wood Science. Roč. 8, č. 1, s. 6-10
7. Tarmian, A., Remond, R., Dashti, H., Perré, P. 2012. Moisture diffusion coefficient of reaction woods: Compression wood of (Picea abies L.) and Tension wood of (*Fagus sylvatica* L.) Wood Science Technology, Roč. 46, č. 1, s. 405-417
8. Tejada, A., Okuyama, T., Yamamoto, H., Yoshida, M., Imai, T., Itoh, T. 1998. Studies on the softening point of wood powder as a basis for understanding the release of residual growth stress in logs. Forest Product Journal, Roč. 48, s. 84-90
9. Fu, Z.; Chen, J.; Zhang, Y.; Xie, F.; Lu, Y. Review on Wood Deformation and Cracking during Moisture Loss. Polymers 2023, 15, 3295. https://doi.org/10.3390/polym15153295
10. Sujan, K.C., Yamamoto, H., Matsuo, M. *et al.* Is hygrothermal recovery of tension wood temperature-dependent?. Wood Sci Technol 50, 759–772 (2016). https://doi.org/10.1007/s00226-016-0817-1
11. Sujan KC, Yamamoto H, Matsuo M, Yoshida M, Naito K, Shirai T (2015) Continuum contraction oftension wood fiber induced by repetitive hygrothermal treatment. Wood Sci Technol 49:1157–1169
12. Vidholdová Z, Dudiak M and Slabejová and Eva Výbohová G (2026) Hydrothermal Modification of Beech Wood. Wood Science and Processing Engineering [Working Title]. IntechOpen. Available at: http://dx.doi.org/10.5772/intechopen.1015232.
13. Yamamoto, H., Sujan, K.C., Matsuo-Ueda, M. *et al.* Microscopic mechanism of contraction of tension wood G-fiber due to boiling. Cellulose 29, 7935–7954 (2022). https://doi.org/10.1007/s10570-022-04742-z
14. Yamamoto, H., Abe, K., Arakawa, Y., Okuyama, T., Gril, J., 2005: Role of the gelatinouslayer (G-layer) on the origin of the physical properties of the reaction beech wood of Acersieboldianum. Journal of Wood Science 51: 222-233.
15. Kúdela, J., Čunderlík, I., 2012: Bukové drevo štruktúra, vlastnosti, použitie. (Beech woodstructure, properties and utilization). Technical University in Zvolen,152 pp. ISBN 978-80-228-2318-0
16. Dudiak, M. Evaluation of the Process of Steaming Beech Sapwood and False Heartwood with Saturated Water Steam in Terms of Acidity Changes and Color Wood. *Forests* 2025, *16*, 864. https://doi.org/10.3390/f16050864

17. Placet V, Passard J, Perre P (2007) Viscoelastic properties of green wood across the grain measured by harmonic tests in the range 0–95 °C: hardwood vs. softwood and normal wood vs. reaction wood. Holzforschung 61:548–557
18. Vilkovská, T., Klement, I., Vilkovský, P., Čunderlík, I., and Geffert, A. (2024). "Chemical reagent for detecting tension wood in selected tree species," BioResources 19(3), 4335-4351.
19. Yin, Qin, and Hong-Hai Liu. 2021. "Drying Stress and Strain of Wood: A Review" Applied Sciences 11, no. 11: 5023. https://doi.org/10.3390/app11115023
20. Miyoshi, Y., Kiryu, T., Kojiro, K. *et al.* Effects of drying and/or quenching histories on lateral tension deformation properties of water-swollen wood. J Wood Sci 61, 525–528 (2015). https://doi.org/10.1007/s10086-015-1496-5

Spoločnosť AREKO, s.r.o. a Technická univerzita vo Zvolene majú dlhodobú spoluprácu v rámci dodávania záznamových a meracích prístrojov, senzorov, softvéru a kalibrácií. V rámci drevárskej fakulty sa prístroje využívajú napr. na katedre drevených stavieb pre výskum vlhkostných a tepelných vlastnosti drevených konštrukcií, tepelno-technických vlastností okien na báze dreva, energetickej náročnosti stavieb a kvality vnútorného prostredia drevostavieb.

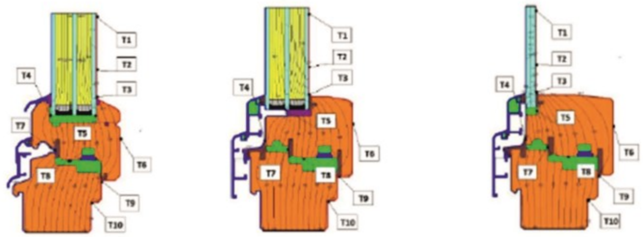

Využívané sú prístroje ako ALMEMO typ MA 5690 – 1 , snímač teploty, vlhkosti a tlaku vzduchu FHAD46C0, snímač koncentrácie CO2 FYA600CO2, snímač koncentrácie formaldehydu vo vzduchu FYA600CH2O, ALMEMO METEO-MULTISENZOR FMD760, ALMEMO 202 a iné. Pomocou prístrojového vybavenia Areko bol zrealizovaný napr. aj výskum vplyvu konštrukcie drevených a drevo-hliníkových okien na povrchové teploty.

V súčasnosti prebiehajú v dlhodobom horizonte výskumy vlhkostných a tepelných vlastností obalových konštrukcií na báze dreva v referenčnom výskumnom objekte v areáli TU vo Zvolene, ako aj na reálnych obývaných stavbách. Taktiež dôležitým prebiehajúcim výskumom je aj mapovanie parametrov obytnej vnútornej klímy ako teplota, vlhkosť, stav CO2 a formaldehydu.

tzv. syndróm chorých budov

CHIP AND CHIPLESS WOODWORKING PROCESSES, 15(1): 133–138, 2026
Zvolen, Technical University in Zvolen, ISSN 1339-8350 (online)

DIGITAL TRANSFORMATION AS A DRIVER OF TECHNOLOGICAL PROCESS MODERNIZATION IN FURNITURE MANUFACTURING

Krzysztof Wiaderek – Barbara Prałat – Dorota Michalak – Tomasz Rogoziński

Abstract
Digital transformation is widely regarded as a means of increasing manufacturing productivity, but information flows in smaller furniture companies often remain descriptive. This study quantifies the time structure of a customized cabinet-production process in an example company. Direct measurements covered three reference cabinets. A digital variant integrating CAD/CAM data, CNC nesting, automated edge banding and drilling, and conveyors was assessed using simulation supported by the technology provider. Within a comparable boundary ending after drilling, information transfer decreased from 28.8 [min] to less than 0.3 [s] per cabinet and material transport from 5.1 [min] to 1.3 [min]. Preparation and machining increased from 4.7 [min] to at most 7.7 [min] because of a broader CNC operation scope; nevertheless, the subtotal fell from 38.6 [min] to at most 9.2 [min], indicating a potential reduction of at least 76.1%. The main modernization leverage therefore lies in data continuity and intralogistics rather than isolated machine-speed improvements. Because the digital state was simulated, the estimated effect requires post-implementation validation.

Key words: *digital transformation; furniture manufacturing; Industry 4.0; process time; CAD/CAM; intralogistics*

INTRODUCTION

The contemporary furniture industry has undergone significant changes in recent decades, with the production of case furniture in particular becoming characterised by a combination of high product variety, short production runs, and customisation. This trend is occurring against a backdrop of mounting pressure to meet production deadlines, maintain product quality, and reduce costs, thereby ensuring the continued competitiveness of the industry. In such circumstances, optimising individual processing operations may not yield a proportional improvement in the system's overall efficiency. The temporal requirements for the delivery of orders are contingent not solely on the velocity of processes such as cutting, edge-banding or drilling, but also on the methodologies employed for the creation of documentation, data transfer, panel layout planning, workpiece identification and inter-operation transport.

Digital transformation is defined in this paper as a coordinated change to production processes, based on data continuity from the order and design model right through to

Poznań University of Life Sciences, ul. Wojska Polskiego 38/42, 60-627 Poznań, Poland
e-mail: krzysztof.wiaderek@up.poznan.pl.

machine programmes and material flow control. The integration of CAD/CAM and production planning systems, the automatic generation of programmes, component identification, CNC machine tools and intralogistics solutions are all encompassed within this framework. This approach corresponds to the concept of the smart factory, in which organisational benefits result from the integration of technologies rather than from the purchase of a single machine (Büchi et al. 2020; Wang et al. 2017).

A review of publications on the timber sector has shown that Industry 4.0 technologies are most commonly used to collect, share and analyse data to support decision-making across the entire value chain (Molinaro and Orzes 2022). In the context of the furniture industry, the significance of integrated real-time data processing is particularly pronounced, as it empowers companies to maintain flexibility in the face of escalating product customisation (Jasińska and Szala 2021; Pech and Vrchota 2022). Concurrently, small and medium-sized enterprises encounter obstacles pertaining to capital, competence and organisational barriers. Consequently, investment decisions should be preceded by an assessment of digital readiness and a measurement of actual bottlenecks (Yi et al. 2021; Červený et al. 2022).

The aim of the study was to determine the effect of digitalisation of information flow, material-handling automation, and the integration of CNC machine tools on the manufacturing lead time of the technological process in a company producing custom-made furniture.

MATERIALS AND METHODS

The study was conducted using a single-case study approach in a representative company employing 20 workers. The company manufactures customised case furniture using a paper-based documentation workflow and a conventional workstation layout. The manufacturing process comprised production preparation, panel cutting, edge banding of narrow surfaces, drilling, carcass assembly, and installation of the rear panel. The primary material was melamine-faced particleboard (MFC) with dimensions of 2800 × 2070 × 18 mm, while the narrow surfaces were finished with 0.5 mm ABS edge banding.

The reference products were three base kitchen cabinets of frame-type construction, with widths of 400 mm (model A), 600 mm (model B), and 800 mm (model C), respectively. Each cabinet carcass consisted of seven wood-based panel components joined in a comparable manner. Cabinet width was treated as the controlled variable, while the material, sequence of operations, machinery, and operators remained unchanged. Production was observed during a single working day, with no changes in workstation staffing. In the panel-cutting experiment, batches corresponding to 10, 9, and 8 complete cabinet carcasses were obtained for models A, B, and C, respectively, from the same number of input panels.

Operation times were recorded using a stopwatch time-study method, based on predefined start and end points for each activity. The following activity categories were distinguished: transmission of order information, material handling, workstation setup and planning, actual machining operations, and assembly activities. Arithmetic means were calculated for repetitive activities, while batch processing times were converted to a per-cabinet basis. Material yield was determined based on the proportion of waste area relative to the total area of two input panels, with a distinction between reusable offcuts and non-reusable waste. The analysis was descriptive in nature; due to the case-study design, no inferential statistical tests were applied.

The modernisation scenario comprised digital transmission of production data, automated panel cutting optimisation, a CNC nesting machining centre, two integrated edge-banding machines, a through-feed CNC drilling centre, component scanning, and conveyor-based material handling. Processing times for the modernisation scenario were determined using a simulation developed in cooperation with the technology supplier. For comparative purposes, a common system boundary was adopted, extending from the transmission of the production order to the completion of the drilling operation. Cabinet assembly, rear-panel installation, and transport to the packaging area were excluded because these operations were not represented symmetrically in both scenarios. The potential reduction in processing time was calculated as:

$$R = \frac{(T_0 - T_1)}{T_0 \times 100\%}$$

Where:
T_0 – processing time for the baseline scenario,
T_1 – processing time for the digital scenario.

RESULTS

The total measured production time for a single cabinet in the base configuration ranged from 58.96 to 60.93 minutes. Changing the body width from 400 to 800 mm had little effect on the total time, as the process was dominated by activities common to the order and independent of the dimensions. The transfer of information between workstations alone took 28.8 minutes per unit, i.e. 59.7–61.7 per cent of the total time. Inter-operation transport took 9.31 minutes per unit (15.3–15.8%), whilst the actual operations took 9.06–10.83 minutes per unit (15.4–17.8%). This indicates that the main bottleneck in the system occurred outside the cutting and assembly zones. The waste data presented in Table 1 were calculated for two sheets of 2800 × 2070 mm board; the batch sizes were 10, 9 and 8 cupboards respectively. The time categories do not account for the entire total, with the remainder comprising, amongst other things, preparation, loading and cutting of HDF for the wall panels.

Table 1. Characteristics of mean production time and material utilisation in the baseline scenario

Cabinet	Width [mm]	Total time [min/unit]	Information flow [min/unit]	Transport [min/unit]	Processing operation [min/unit]	Waste [%]
A	400	58,53	28,8	5,1	9,54	9,59
B	600	59,96	28,8	5,9	9,06	12,19
C	800	60,93	28,8	6,2	10,83	7,53

The proportion of waste after cutting ranged from 7.53 to 12.19 per cent. The highest value was recorded for cabinet B, even though its width was intermediate. This confirms that material efficiency depends on a combination of component dimensions and their arrangement on the sheet, rather than being linearly dependent on the overall dimensions of the piece of furniture. However, the study did not include comparative waste figures for automated nesting; therefore, the quantitative material savings of the digital variant were not estimated.

For the common process boundary up to the completion of drilling, the baseline required 38.59 minutes per unit. Of this, 28.8 [min] was accounted for by information flow, 5.1 [min] by material transport, and 4.7 [min] by planning, preparation and machining. In the digital variant, these values amounted to less than 0.3 [min], 1.3 [min] and less than 7.7 [min], respectively. The total time for the comparable section decreased from 38.6 [min] to less than 9.2 minutes, which corresponds to a potential reduction of over 76.1 per cent. The values for the digital variant shown in Table 2 are upper limits derived from simulation data. Transport to the packaging area (0.33 min), cabinet assembly and rear panel assembly were not included in the comparison.

Table 2 Comparison of the baseline and digital scenarios within the process boundary from production order release to completion of drilling (Cabinet A)

Process block	**Baseline scenario [min/unit]**	**Digital scenario [min/unit]**	**Change [%]**
Information flow	28,8	0,3	Reduktion >99,1
Material transport	5,1	1,3	Reduction 75,5
Planning, preparation and machining	4,7	7,7	Increase to approx. 63,8
Comparable total	**38,6**	**9,2**	**Reduction ≥76,1**

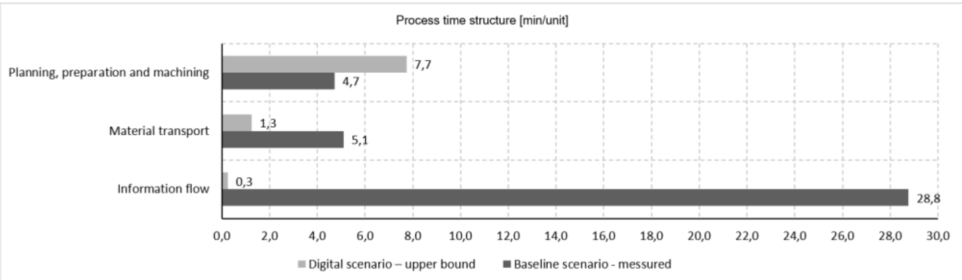

Fig. 1 Process time structure in the baseline scenario and the simulated digital scenario

The preparation and processing time in this scenario increased because the milling operation using nesting technology and the four-sided edge-banding covered a wider scope than the base operations. This result shows that digitalisation does not necessarily shorten every individual operation. System efficiency increases when the reduction in waiting time for data and material movements outweighs the increase in the time taken for selected operations. The simulation for the complete line estimated 1,400 cut-to-size panels per 7.5-hour shift, with a production time of 9.57 minutes to produce a set of Cabinet A components ready for packing. This figure was not directly compared with the full baseline time, which also included the assembly of the cabinet body and the rear panel.

DISCUSSION

The results obtained indicate that the greatest bottleneck in the efficiency of the company under analysis was not the speed of the machine tools, but a lack of continuity in information flow. Paper-based documentation required the technologist and operators to manually collect, interpret and clarify data. This not only resulted in long order-processing times, but also made the process dependent on the knowledge of individual staff members. The introduction of a common CAD/CAM data model, automated parts lists, labels and machine programmes can therefore deliver benefits even before full robotisation is achieved. This is consistent with the conclusion reached by Molinaro and Orzes (2022) that the fundamental role of Industry 4.0 in the timber sector is the integration and processing of data to support decision-making.

Intralogistics was also an important factor. In a comparable section of the production process, transport time was reduced by 75.5 per cent. The demand for transport machinery and equipment is linked to component dimensions, process quality, and workload. The technological demand for equipment cannot be treated as independent investments but must be considered holistically (Jarecki et al. 2021). Conveyors, buffers and the identification of workpieces should be designed in tandem with data flow. Otherwise, a high-speed machine tool may merely shift the bottleneck to the next inter-operational storage area.

A reduction of over 76.1% should be interpreted as a theoretical potential. Firstly, the baseline was measured in an actual plant, whilst the digital variant was obtained through a simulation supported by the equipment supplier. Secondly, the study concerned a single company and a limited group of products. Thirdly, the investment cost, OEE, energy consumption, quality, number of errors and changeover times over the long term were not assessed. For this reason, the results do not constitute causal evidence or a basis for simple generalisation to the entire industry.

Despite the study's limitations, it offers practical value by breaking down the impact of digitalisation into three time blocks. The literature on furniture SMEs emphasises that high costs, a skills shortage and uncertainty regarding benefits limit the uptake of technology (Yi et al. 2021; Červený et al. 2022). For this reason, the recommended R&D pathway should be phased. The first phase covers a digital product data standard, order configuration, CAD/CAM integration and the identification of cutting sheets. The second phase concerns flow measurement, layout redesign and low-cost transport automation. Only the third stage should involve selecting a nesting line and automated centres in line with the actual workload. This approach minimises the risk of automating a process whose information logic remains inconsistent.

Implementation validation should take the form of a before-and-after study. For at least several product families, the following should be recorded: throughput time, value-adding time, waiting time for data, transport time, changeover time, shortages and material consumption. The stability of the results should be assessed over several days and across different operators, and the outcome should be compared with the inputs and the cost of maintaining the system. In future work, it would be worthwhile to extend the model to include intelligent scheduling, which, in the production of customised furniture, can reduce delays and improve resource utilisation (Lu et al. 2025).

CONCLUSIONS

1. In the baseline scenario, lead time was primarily determined by the flow of information: 36.39 min/unit, which accounted for approximately 60% of the total production time for the cabinets under study.
2. In the comparable section leading up to the finish drilling stage, digital data flow reduced the information processing time from 28.8 min/unit to less than 0.3 min/unit, whilst transport automation reduced the transport time from 5.1 min/unit to 1.3 min/unit.
3. The total time for the analysed process stage was reduced by at least 76.1% in the simulation, despite an increase in set-up and machining times. This confirms that the local speed of the machines is not a sufficient measure of system efficiency.
4. The most rational sequence for modernisation comprises: CAD/CAM data continuity, identification and control of the flow, reorganisation of intralogistics, followed by the selection of automated machining cells.
5. The figures for the digital variant require validation in a pilot study following implementation, whilst maintaining consistent process boundaries and measuring quality, costs, material usage and OEE.

REFFERENCES

Büchi G., Cugno M., Castagnoli R. (2020): Smart factory performance and Industry 4.0. Technological Forecasting and Social Change 150, 119790. https://doi.org/10.1016/j.techfore.2019.119790

Červený L., Sloup R., Červená T. (2022): The Potential of Smart Factories and Innovative Industry 4.0 Technologies - A Case Study of Different-Sized Companies in the Furniture Industry in Central Europe. Forests 13(12), 2171. https://doi.org/10.3390/f13122171

Jarecki W., Wieruszewski M., Pałubicki B., Wiaderek K., Matwiej Ł., Orlikowski D. (2021): The parameterization of the demand for machinery as a Dimension-and-Quality function affecting industrial furniture production. MATEC Web of Conferences 338, 01013. https://doi.org/10.1051/matecconf/202133801013

Jasińska K., Szala Ł. (2021): Potential directions for improving production processes in Industry 4.0 conditions based on a Polish furniture enterprise - a case study. Business Informatics 2(60), 27-46. https://doi.org/10.15611/ie.2021.2.03

Lu W., Buck D., Zong F., Guo X., Wang J., Zhu Z. (2025): Enhancing Efficiency in Custom Furniture Production with Intelligent Scheduling Systems. Processes 13(9), 2721. https://doi.org/10.3390/pr13092721

Molinaro M., Orzes G. (2022): From forest to finished products: The contribution of Industry 4.0 technologies to the wood sector. Computers in Industry 138, 103637. https://doi.org/10.1016/j.compind.2022.103637

Pech M., Vrchota J. (2022): The Product Customization Process in Relation to Industry 4.0 and Digitalization. Processes 10(3), 539. https://doi.org/10.3390/pr10030539

Wang L., He J., Xu S. (2017): The Application of Industry 4.0 in Customized Furniture Manufacturing Industry. MATEC Web of Conferences 100, 03022. https://doi.org/10.1051/matecconf/201710003022

Yi L.Y., Ab Latib H., Ratnasingam J., Mariapan M., Choon Liat L., Othman K., Amir M.A., Jegatheswaran N. (2021): Readiness for and adoption of Industry 4.0 among small and medium sized enterprises in the Malaysian furniture industry. BioResources 16(4), 8289-8308. https://doi.org/10.15376/biores.16.4.8289-8308

CHIP AND CHIPLESS WOODWORKING PROCESSES, 15(1): 139–146, 2026
Zvolen, Technical University in Zvolen, ISSN 1339-8350 (online)

ENERGY DENSITY OF CO_2 LASER CUTTING LEADING TO ACCEPTABLE KERF TAPER OF SPRUCE, BEECH AND OAK WOOD

Ivan Ružiak[1] – Ivan Kubovský[1] – Milada Gajtanska[1] – Richard Kminiak[1] – Lukáš Štefančin[1] – Imants Adijans[2] – Oguzhan Der[3] – Luigi Todaro[4] – Valentina Lo-Giudice[4] – Eugenia Mariana Tudor[5]

Abstract
Laser cutting is a widely used wood processing methods owing to its contactless nature, minimal material loss due to its narrow kerf width and low heat affected zone.
Kerf taper produced during wood cutting by wood processing is a negative aspect of woodworking processes because it can adversely affect the subsequent processing of cut materials. In this article we compare kerf taper values of spruce, beech and oak wood at low laser power values up to 130 W with kerf taper at higher powers, versus cutting direction (perpendicular and parallel to wood fibres). Energy density is one of the most important parameters associated with laser parameters, which can characterize the process of laser cutting. Lower energy density values lead to reduced heat affected zones and kerf widths but can also lead to unsuccessful cutting (when wood is not cut during first cycle) and to higher kerf taper which leads to additional preprocessing of sample. On the other side, higher energy density values lead to increase in kerf width and heat affected zones which is negative aspect for next sample processing. Therefore, it is crucial to strike a balance between reduced kerf taper (at high energy densities) and minimized widths of kerf and heat affected zones that are important for next sample processing. In experiment samples of 6mm thickness were used, with nominal laser power 130 W and maximum feed speed 20 mm·s^{-1}.

Key words: *CO_2 laser cutting; energy density; kerf taper; kerf width; spruce wood; beech wood; oak wood.*

INTRODUCTION

Laser cutting belongs to progressive methods of wood material processing, especially for difficult shapes of material with low thickness, thanks to low kerf taper, low material losses and possibility to automatize of cutting process. On the other side, this technology inserts

[1] Technical University in Zvolen, T. G. Masaryka 24, 960 01 Zvolen
e-mail: ruziak@is.tuzvo.sk
[2] Engineering Centre, RTU Rezekne Academy, Atbrivosanas aleja 115, 4601 Rezekne, Latvia
[3] Bandirma Onyedi Eylul University, Maritime Faculty, Balikesir, Türkiye
[4] University of Basilicata, Viale dell'Ateneo Lucano, 10, 85100 Potenza, Italy
[5] Salzburg University of Applied Sciences, Markt 136a, 5431 Kuchl, Austria

into material heat which leads to creation of char layer that can reduce glue joint strength (Igaz *et al.*, 2025).

Recent studies have addressed several complementary aspects of CO_2 laser cutting of beech wood. Rezaei *et al.* (2022) linked processing conditions and moisture-conditioned material to changes in surface anatomy and morphology, while Rezaei *et al.* (2023) showed that laser-induced changes in surface chemistry, wetting, and adhesive penetration influence glued tensile shear strength. Corleto *et al.* (2024) demonstrated that moisture content alters cut-surface quality, and Corleto *et al.* (2025) evaluated how cutting speed, focal-point position, and gas pressure affect roughness, kerf characteristics, and the heat-affected zone. Together, these studies underline that optimization cannot rely on laser power and feed speed alone; wood moisture, anatomy, and the requirements of subsequent bonding must also be considered.

Result of laser cutting of wood in the form of kerf widths and heat affected zones depend on many parameters.

First group consists of parameters of used laser device, the most important are laser power P, feed speed v, diameter of laser beam d. Based on above mentioned laser parameters energy density E for laser working in continuous mode, can be computed in the form $E = P/(v \cdot d)$

Energy density characterizes how much energy is given to 1 mm^2 area of sample and act mainly on the first contact of laser beam with material. (Nukman *et al.*, 2008)

As laser beam is progressing to lower parts of sample, it interacts with wood structure, which lead to different behaviour for coniferous, ring-porous and diffuse-porous wood species. Thus, material properties play also significant role for laser cutting as wood is non-homogenous, anisotropic material. This led to different kerf widths and heat affected zones at first contact of laser beam with material and at opposite side. (Ružiak *et al.*, 2025)

Kerf taper s is defined by equation $s = \frac{WKU - WKL}{H} \cdot 100\%$, where WKU corresponds to cutting kerf width at 1st laser beam contact with material (upper surface in our case), WKL corresponds to cutting kerf width at last beam contact with material (lower surface in our case) and H is thickness of the sample. Lower kerf taper lead to decreased need of sample preprocessing before other technological operations which is welcomed. On other side this parameter does not characterize amount of material removal during laser cutting and therefore it is needed to optimize not only kerf taper but also minimize kerf widths.

Cutting kerf widths WKU and WKL (which are bounded with kerf taper s) for wood materials are significantly affected by energy density values as reported in (Štefančin *et al.*, 2026; Ružiak *et al.*, 2024; Kubovský *et al.*, 2020; Adamčík *et al.*, 2025; Hata, Okabe and Otsuka, 1999). Thus, connection of output parameters WKU, WKL with input parameter energy density E characterize not only creation of kerfs but also value of kerf taper.

As wood is an anisotropic material, variance coefficient of the kerf widths WKU, WKL is higher than for homogeneous materials like polymers or metals, which lead to necessity performing higher amounts of experiments, thus, also to increased time, energy and material demands. To reduce this negative aspect, Nonlinear Regression Models, Artificial Neural Networks, Taguchi design and other Machine Learning Methods are used for modelling of kerf width creation in wood. (Eltawahni, Olabi and Benyounis, 2011; Eltawahni *et al.*, 2013; Nugraha *et al.*, 2024; Ružiak *et al.*, 2022; Ikhsan and Sundin, 2026; Yung *et al.*, 2021).

Other reason for using ML approaches lies in fact that they are able at certain conditions predict changes of kerf widths at higher power values as used laser machine can give. (Ružiak *et al.*, 2022; 2024, 2025; 2026)

In this article we compare how kerf taper *s* is changed with energy density of CO_2 laser for spruce, beech and oak wood as representatives of coniferous, diffuse-porous and ring-porous wood species in cutting direction parallel and perpendicular to longitudinal wood direction. Kerf taper is considered as optimal with maximal value of 2.5%. This value was computed based on the reference tolerance of dimensions in laser cutting equal to 0.15 mm divided by thickness 6 mm, which led to 2.5% maximal kerf taper. Main conclusion of article are minimal energy densities at which kerf taper optimal condition is met.

MATERIAL AND METHODS

Laser cutting of spruce, beech and oak wood was performed at laser power values *P* = 52; 78; 104 and 130 W and at feed speeds *v* = 5; 10; 15; 20 $mm \cdot s^{-1}$. Beam diameter d was equal to 0.151 mm, and focal position of laser was on upper surface. All used wood species were cut in direction perpendicular and parallel to longitudinal anatomical direction.
Energy density of laser *E* was computed based on $E = P/(v \cdot d)$ equation with values for measurement and prediction datasets published in (Ružiak *et al.*, 2025). Energy densities values from experiment are maximal 173 $J \cdot mm^{-2}$. As for beech and oak wood such value of energy density doesn't lead to sufficient value of kerf taper and not to optimal value of the kerf widths ratios WKR = WKL/WKU, ANN prediction was used to find optimal values of *P*, *v* thus also *E*. which was published in (Ružiak *et al.*, 2025).
Former wood samples got dimensions 6 mm (thickness); 70 mm (height) and 500 mm (width). Parameters of kerf widths were determined using Keyence VHX-7000 digital microscope (Keyence Corporation, Osaka, Japan). For each combination of laser power *P* and feed speed *v*, 30 measurements of upper kerf width WKU and lower kerf width WKL were performed.

RESULTS AND DISCUSSION

From average values we have computed kerf taper (*s*) values for spruce wood, beech wood and oak wood. Dependence of kerf taper (*s*) versus energy density (*E*) we present in figures 1 for spruce wood, figure 2 for beech wood and figure 3 for oak wood.

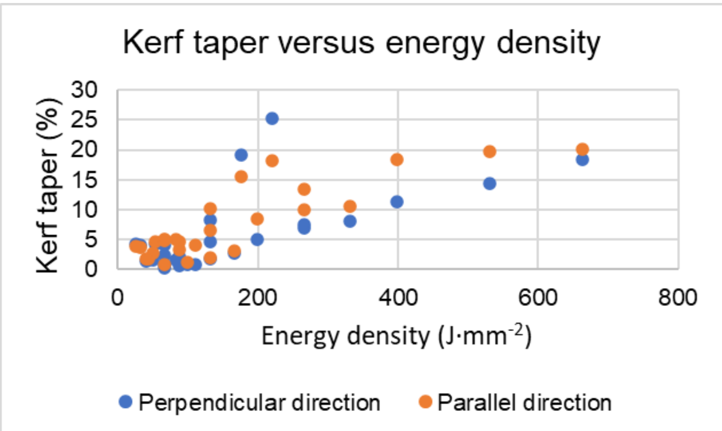

Figure 1. Kerf taper versus energy density for spruce wood cut by CO_2 laser

Average kerf taper for spruce wood cut by CO_2 laser was 5.9 % in perpendicular direction and 7.4 % for parallel direction. Higher value of kerf taper for spruce wood in longitudinal anatomical direction can be contributed to effect of earlywood/latewood differences in density.
Minimal, Maximal and average energy densities which leads to kerf taper lower than 2.5 % are for spruce wood listed in Table 1.

Table 1. *Minimal, maximal and average energy densities leading to acceptable kerf taper*

Cutting direction	Minimal *E*	Average *E*	Maximal *E*
Perpendicular	40	78	133
Parallel	40	77	133

Minimal, average and maximal kerf taper values were then for perpendicular direction (0.2; 1.4; 2.4) % and for parallel direction (0.7; 1.5; 2.0) %. Both results in Table 1 for energy densities and kerf taper values confirm that effect of cutting direction in spruce wood is not very significant as was also found out in (Ružiak *et al*., 2025).

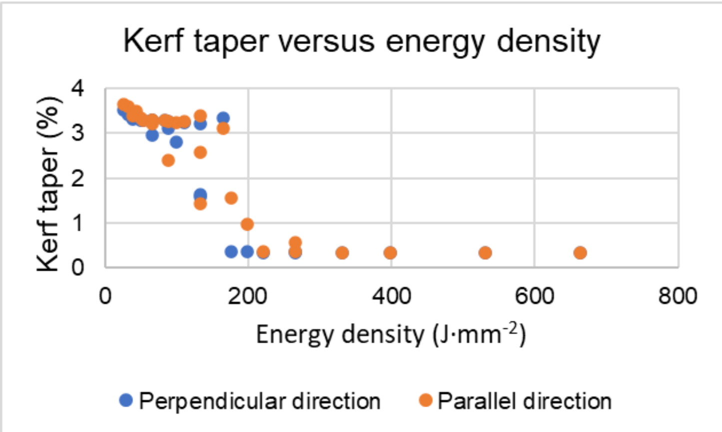

Figure 2. Kerf taper versus energy density for beech wood cut by CO_2 laser

Average kerf taper for beech wood cut by CO_2 laser was 2.2 % in perpendicular direction and 2.3 % for parallel direction.
Minimal, Maximal and average energy densities which leads to kerf taper lower than 2.5 % are for beech wood listed in Table 2.

Table 2. *Minimal, maximal and average energy densities leading to acceptable kerf taper*

Cutting direction	Minimal *E*	Average *E*	Maximal *E*
Perpendicular	133	302	664
Parallel	88	298	664

Minimal, average and maximal kerf taper values were then for perpendicular direction (0.4; 0.6; 1.6) % and for parallel direction (0.4; 0.8; 2.4) %. Both results in Table 2 for energy densities and kerf taper values confirm that effect of cutting direction in beech wood is more significant than for spruce wood (Ružiak *et al*., 2025). On the other hand, kerf taper values for beech wood are significantly lower than for spruce wood but get at higher energy densities values.

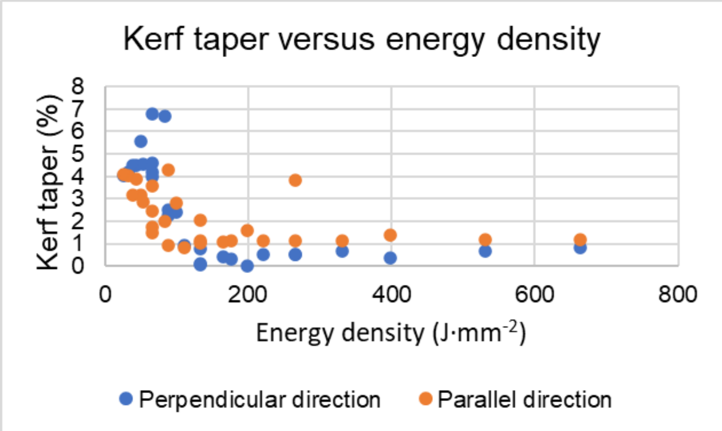

Figure 3. Kerf taper versus energy density for oak wood cut by CO_2 laser

Average kerf taper for oak wood cut by CO_2 laser was 2.4 % in perpendicular direction and 2.2% for parallel direction.
Minimal, Maximal and average energy densities which leads to kerf taper lower than 2.5 % are for oak wood listed in Table 3.

Table 3. *Minimal, maximal and average energy densities leading to acceptable kerf taper*

Cutting direction	**Minimal *E***	**Average *E***	**Maximal *E***
Perpendicular	88	245	664
Parallel	66	213	664

Minimal, average and maximal kerf taper values were then for perpendicular direction (0.02; 0.7; 2.4) % and for parallel direction (0.8; 1.4; 2.4) %. Both results in Table 3 for energy densities and kerf taper values confirm that effect of cutting direction in oak wood is much more significant than for spruce and beech wood as was also found out in (Ružiak *et al.*, 2025).
Similar as for beech wood, oak wood needs higher values of energy densities E for getting good value of kerf taper, than are possible to get by used CO_2 laser. That justify usage of ANN for prediction of cutting kerf values versus laser power P, feed speed v thus also energy density E, which was performed in (Ružiak *et al.*, 2025).
In this paragraph we will compare by graphs differences between species. In figure 4 we compare average kerf taper for spruce, beech and oak wood in both cutting directions. In figure 5 afterwards average energy densities which lead to acceptable kerf taper.

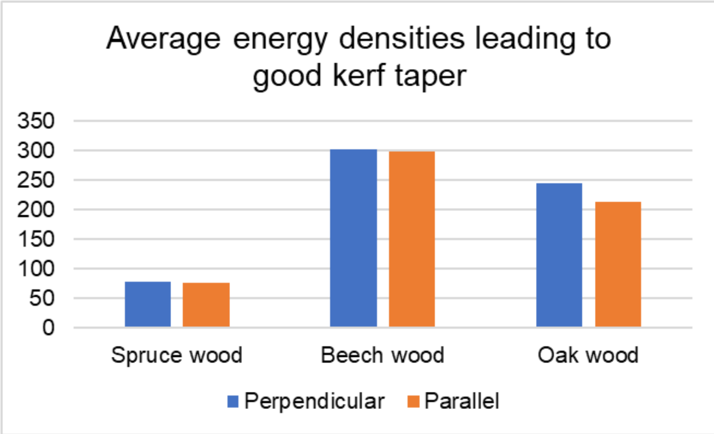

Figure 4. Average kerf taper of spruce, beech and oak wood in both cutting directions

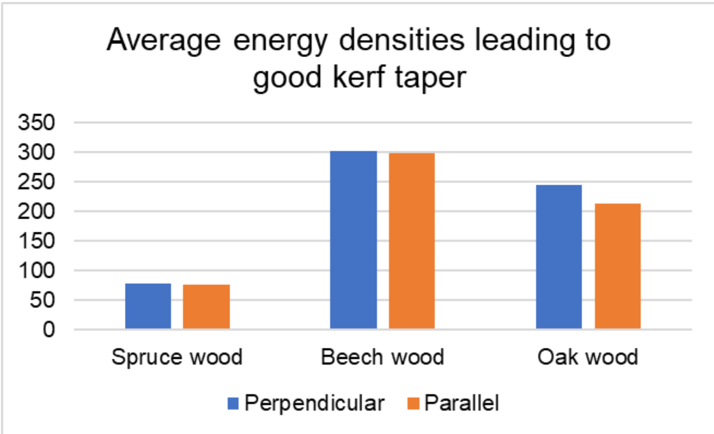

Figure 5. Average energy densities which lead to acceptable kerf taper

From figures 4, 5 it follows:

- Spruce wood with lower density exhibits higher kerf taper which is caused by heat transfer between earlywood and latewood tracheids with significant different densities,
- On other side, spruce wood needs lower values of energy densities to get good value of kerf taper,
- Oak wood as most anisotropic material exhibit most significant differences between optimal energy densities perpendicular and parallel to grain direction.

CONCLUSIONS

From presented results it follows:

- Kerf taper created during spruce wood laser cutting is significantly higher than for more dense beech and oak wood, making optimization of laser cutting as very crucial for next usage of laser cut samples,

- Higher density of wood species causes increase of optimal energy densities but also lower value of kerf tapers together with his variance, thus beech and oak wood is more suitable material for laser cutting,
- On other side higher energy densities can cause higher HAZ area together with charred layer, therefore optimization of laser cutting process is also very important,
- For oak wood as representative of ring-porous species, cutting direction plays most significant role, mainly in the value of the optimal energy density

Acknowledgements
The authors gratefully acknowledge the financial support provided by the VEGA Agency of the Ministry of Education, Research, Development and Youth of the Slovak Republic and the Slovak Academy of Sciences under Grant No. 1/0077/24.

REFERENCES

ADAMČÍK, L., KMINIAK, R., KYSELICA, K., IGAZ, R., KUBOVSKÝ, I. 2025. Optimisation of CO2 laser technological parameters and their impact on the surface quality of cut wood. In Forests 16(5):785. DOI: 10.3390/f16050785.
CORLETO, R., GAFF, M., REZAEI, F., SETHY, A.K., NEMETH, R., VALENTE, F., DITOMMASO, G., TODARO, L. 2024. Effect of moisture content levels on the quality of beech wood cut by CO2 laser. In The International Journal of Advanced Manufacturing Technology 134(1-2):159-169. DOI: 10.1007/s00170-024-14015-7.
CORLETO, R., GAFF, M., SETHY, A.K., KELKAR, B.U., NEMETH, R., DITOMMASO, G., KAMBOJ, G., TODARO, L., REZAEI, F. 2025. Effects of CO2 laser parameters on quality of laser cut beech wood (Fagus sylvatica L.) surface and extent of heat affect zone. In Journal of the Indian Academy of Wood Science 22(1):67-77. DOI: 10.1007/s13196-024-00361-2.
ELTAWAHNI, H.A., OLABI, A.G., BENYOUNIS, K.Y. 2011. Investigating the CO2 laser cutting parameters of MDF wood composite material. In Optics & Laser Technology 43(3):648-659. DOI: 10.1016/j.optlastec.2010.09.006.
ELTAWAHNI, H.A., ROSSINI, N.S., DASSISTI, M., ALRASHED, K., ALDAHAM, T.A., BENYOUNIS, K.Y., OLABI, A.G. 2013. Evalaution and optimization of laser cutting parameters for plywood materials. In Optics and Lasers in Engineering 51(9):1029-1043. DOI: 10.1016/j.optlaseng.2013.02.019.
HATA, K., OKABE, T., OTSUKA, M. 1999. Characteristics of laser machining of MDF. In Journal of the Society of Materials Science, Japan 48(9):1059-1064. DOI: 10.2472/jsms.48.1059.
IGAZ, R., KUBOVSKÝ, I., RUŽIAK, I., RICHVALSKÁ, J. 2025. Analýza pevnosti lepeného spoja dreva po rezaní CO2 laserom [Strength analysis of wood glued joint after CO2 laser cutting]. In Technika a vzdelávanie 14(2):31-35.
IKHSAN, M., SUNDIN, A. 2026. Analysis of the effects of laser cutting process parameters on the kerf width of plywood using the Taguchi method. In METAL: Jurnal Sistem Mekanik dan Termal 10(1):63-69. DOI: 10.25077/metal.10.1.63-69.2026.
KUBOVSKÝ, I., KRIŠŤÁK, Ľ., SUJA, J., GAJTANSKA, M., IGAZ, R., RUŽIAK, I., RÉH, R. 2020. Optimization of parameters for the cutting of wood-based materials by a CO2 laser. In Applied Sciences 10(22):8113. DOI: 10.3390/app10228113.

NUGRAHA, M.D., ISWANDARU, D., DURYAT, HIDAYAT, W. 2024. Optimization of CO2 laser cutting variables of sengon plywood (Paraserianthes falcataria) using response surface methodology. In Journal of Sylva Indonesiana 7(2):97-109. DOI: 10.32734/jsi.v7i02.14850.

NUKMAN, Y., ISMAIL, S.R., MAMAT, A., AHMAD-YAZID, A. 2008. Selected Malaysian wood CO2-laser cutting parameters and cut quality. In American Journal of Applied Sciences 5(8):990-996. DOI: 10.3844/ajassp.2008.990.996.

REZAEI, F., WIMMER, R., GAFF, M., GUSENBAUER, C., FRÖMEL-FRYBORT, S., SETHY, A.K., CORLETO, R., DITOMMASO, G., NIEMZ, P. 2022. Anatomical and morphological characteristics of beech wood after CO2-laser cutting. In Wood Material Science & Engineering 17(6):459-468. DOI: 10.1080/17480272.2022.2134820.

REZAEI, F., GAFF, M., NÉMETH, R., SMARDZEWSKI, J., NIEMZ, P., LI, H., SETHY, A.K., TODARO, L., KAMBOJ, G., DAS, S., CORLETO, R., DITOMMASO, G., BAK, M. 2023. The characteristics of glued tensile shear strength constituted of wood cut by CO2 laser. In Journal of Renewable Materials 11(8):3277-3296. DOI: 10.32604/jrm.2023.028352.

RUŽIAK, I., IGAZ, R., KUBOVSKÝ, I., GAJTANSKA, M., JANKECH, A. 2022. Prediction of the effect of CO2 laser cutting conditions on spruce wood cut characteristics using an artificial neural network. In Applied Sciences 12(22):11355. DOI: 10.3390/app122211355.

RUŽIAK, I., IGAZ, R., KUBOVSKÝ, I., TUDOR, E.M., GAJTANSKA, M., JANKECH, A. 2024. ANN prediction of laser power, cutting speed, and number of cut annual rings and their influence on selected cutting characteristics of spruce wood for CO2 laser processing. In Materials 17(13):3333. DOI: 10.3390/ma17133333.

RUŽIAK, I., KRIŠŤÁK, Ľ., ADIJANS, I., KUBOVSKÝ, I., RICHVALSKÁ, J., ŠTEFANČIN, L., GAJTANSKA, M., TUDOR, E.M., TODARO, L. 2025. Enhancing CO2 laser cutting efficiency for diverse wood species using artificial neural networks. In Forests 16(6):881. DOI: 10.3390/f16060881.

RUŽIAK, I., DER, O., KUBOVSKÝ, I., ADIJANS, I., KUČERKA, M., RICHVALSKÁ, J., GAJTANSKA, M., TUDOR, E.M., TODARO, L., ŠTEFANČIN, L. 2026. Artificial neural network-based optimization of CO2 laser cutting parameters for beech plywood and HDF: A kerf geometry perspective. In Drvna Industrija 77(1):71-80. DOI: 10.5552/drvind.2026.0284.

ŠTEFANČIN, L., IGAZ, R., ADAMČÍK, L., RUŽIAK, I., KUBOVSKÝ, I., KMINIAK, R. 2026. Effects of CO2 laser cutting parameters on kerf width in native wood species. In BioResources 21(3):6463-6481. DOI: 10.15376/biores.21.3.6463-6481.

YUNG, K.C., CHOY, H.S., XIAO, T., CAI, Z. 2021. UV laser cutting of beech plywood. In The International Journal of Advanced Manufacturing Technology 112(3-4):925-947. DOI: 10.1007/s00170-020-06376-6.

CHIP AND CHIPLESS WOODWORKING PROCESSES, 15(1): 147–153, 2026
Zvolen, Technical University in Zvolen, ISSN 1339-8350 (online)

THERMAL INFLUENCE ON VOC EMISSIONS FROM PARTICLEBOARDS INCORPORATING RECYCLED PLASTIC WASTE

Anna Darabošová – Tatiana Bubeníková – Iveta Čabalová

Abstract

The aim of this study was to evaluate the effect of temperature on volatile organic compound (VOC) emissions from three-layer particleboards containing 10% recycled plastic from automotive bumpers. VOC emissions were analysed by HS-GC-MS at 35, 50, 100, and 150 °C. The results showed a strong temperature dependence, with only a moderate increase in emissions between 35 and 50 °C, followed by a substantial rise at 100 and 150 °C. At 150 °C, the total VOC peak area was approximately 114 times higher than at 35 °C. Temperature also affected the chemical composition of the emissions. Monoterpenes, particularly α-pinene and 3-carene, dominated at lower temperatures, while methenamine became the dominant compound at 150 °C. The results confirm that temperature significantly influences both the intensity and composition of VOC emissions from particleboards containing recycled automotive plastics.

Key words: *volatile organic compounds (VOCs); particleboard; recycled automotive plastics; automotive bumpers; temperature; HS-GC-MS*

INTRODUCTION

The use of recycled plastics represents an important direction in current materials research, aimed at reducing environmental impacts and promoting more efficient recovery of waste materials. The production of plastic waste continues to increase, while a substantial proportion of plastics at the end of their service life is still landfilled or used for energy recovery. Although plastics offer several advantageous properties, including low weight, resistance to chemical and environmental influences, and ease of processing, their long-term persistence in the environment represents a serious environmental concern (Wong et al. 2015; Huang et al. 2022).

The automotive industry represents an important source of engineering plastics, with polymeric materials accounting for approximately 20–25% of the weight of non-structural vehicle components. They are widely used in both exterior and interior applications, including bumpers, dashboards, door panels, fuel systems, and electrical components (Prasanth et al. 2021; Adeniyi et al. 2016). At the end of a vehicle's service life, a considerable amount of plastic waste with potential material value is generated. However, its recycling remains technologically challenging due to the diversity and complexity of the

Technical University in Zvolen, T. G. Masaryka 24, 960 01 Zvolen
e-mail: anna.darabosova@is.tuzvo.sk; bubenikova@tuzvo.sk; cabalova@is.tuzvo.sk

polymers used (Froelich et al. 2007). Consequently, increasing attention is being paid to alternative approaches for the material recovery of automotive plastic waste.

One promising approach is the incorporation of recycled plastics into wood-based composites. The use of waste thermoplastics in particleboards provides an opportunity to combine plastic waste recovery with the production of materials suitable for construction and furniture applications. Previous research has demonstrated that the incorporation of plastics can influence the physical, mechanical, and thermophysical properties of wood-based composites while simultaneously contributing to the effective utilization of secondary raw materials (Kazemi Najafi 2013; Gopinath et al. 2020).

In addition to their technical properties, the emission behaviour of these materials should also be considered. Wood-based composites intended for indoor applications can emit volatile organic compounds (VOCs), which may affect indoor air quality and, at elevated concentrations, pose potential risks to human health (Bernstein et al. 2008; Wolkoff 1998; Jones 1999). VOC emissions may originate from the wood component, adhesives, and other materials incorporated into the composite, while their intensity is influenced by several factors, particularly material composition, moisture, and temperature (Hodgson et al. 2003; Roffael 2006). Increasing temperature can promote the release of volatile compounds and may alter both the overall emission level and the relative abundance of individual compounds within the emission profile.

The aim of this study was to evaluate the influence of temperature on volatile organic compound emissions from three-layer particleboards incorporating recycled plastics from the automotive industry. The emission profiles were analysed under different temperature conditions using headspace gas chromatography coupled with mass spectrometry (HS-GC-MS), with particular attention to changes in overall VOC emissions and the relative abundance of individual identified compounds.

MATERIAL AND METHODS

Three-layer particleboards were manufactured from spruce (*Picea abies* L.) particles and recycled polypropylene (PP) obtained from recycled automotive bumpers. The bumper waste was cleaned, mechanically shredded, and sieved to obtain a particle fraction of 1–4 mm. The recycled plastic was incorporated into the core layer at a 10% proportion, while the surface layers consisted exclusively of wood particles. Urea-formaldehyde (UF) resin (Kronores CB 1100 F) was used as the adhesive, together with ammonium nitrate as a hardener and a paraffin emulsion. The prepared particle mats were cold-prepressed at 1 MPa and subsequently hot-pressed at 230 °C and 5 MPa for 5 min.

Volatile organic compound (VOC) emissions were analysed using headspace gas chromatography coupled with mass spectrometry (HS-GC-MS). For each analysis, 0.5 g of the particleboard sample was placed in a 20 ml headspace vial and hermetically sealed. To evaluate the effect of thermal exposure on the emission profile, the samples were analysed at four temperatures: 35, 50, 100, and 150 °C, with an incubation time of 60 min at each temperature. Three replicate samples were analysed under each temperature condition. The samples were designated RAB-35, RAB-50, RAB-100, and RAB-150, according to the applied temperature.

The measurements were performed using an Agilent 7890A GC/5975C MSD system equipped with an Agilent 7697A Headspace Autosampler. VOC separation was carried out on an HP-5MS capillary column (30 m × 0.25 mm × 0.25 μm) using helium as the carrier gas at a constant flow rate of 1.0 mL min^{-1}. The GC temperature programme ranged from

40 to 270 °C, while mass spectra were recorded over the range of 45–500 amu. Individual VOCs were identified by comparing the acquired mass spectra with the NIST17 mass spectral library. Changes in VOC emission profiles at the individual temperatures were subsequently compared to evaluate the effect of temperature on emissions from particleboards containing recycled plastic waste from automotive bumpers.

RESULTS, DISCUSSION

The HS-GC-MS analysis demonstrated a pronounced effect of temperature on the emission of volatile organic compounds from particleboards containing recycled plastic from automotive bumpers. The total VOC peak area increased considerably with increasing temperature (Figure 1). At 35 °C, the total peak area was 235,501 a.u., increasing to 345,794 a.u. at 50 °C. A substantially greater increase was observed at 100 °C, where the total peak area reached 4,185,374 a.u., while at 150 °C it increased to 26,878,226 a.u. At the highest temperature, the total peak area was therefore approximately 114 times higher than at 35 °C. While the increase between 35 and 50 °C was relatively moderate, a pronounced rise in emission intensity occurred at higher temperatures, with the most substantial change observed between 100 and 150 °C.

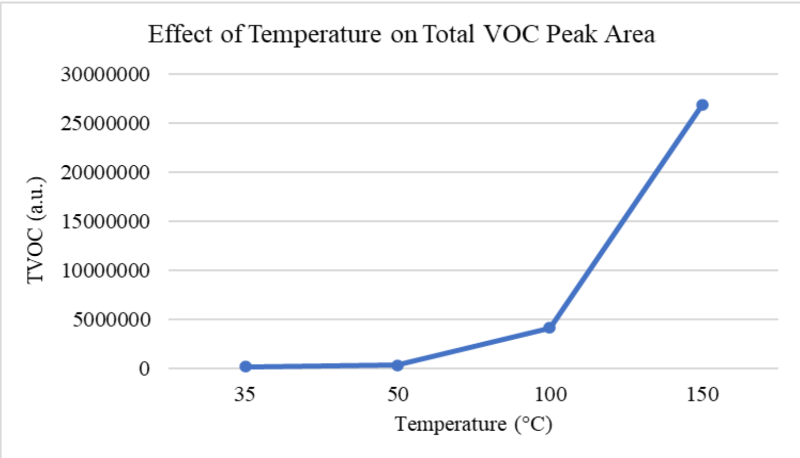

Figure 1. Effect of temperature on the total VOC peak area of particleboards containing recycled automotive bumper waste

Increasing temperature affected not only the overall emission intensity but also the chemical composition of the emission profile (Table 1). At 35 °C, the VOC profile was characterized mainly by the presence of α-pinene and 3-carene. These compounds are monoterpenes commonly associated with softwood and represent important naturally emitted VOCs from wood and wood-based materials. The occurrence of α-pinene, β-pinene, 3-carene, and other terpene compounds in emissions from wood materials has been reported in several previous studies (Kim et al. 2006; Brown 1999; Yrieix et al. 2010; Hyttinen et al. 2010). Thus, at the lowest investigated temperature, the emission profile was characterized predominantly by volatile compounds typical of the wood component of the composite.

Table 1. Relative abundance of selected VOCs in particleboard emissions at different temperatures (% of TVOC)

VOC	RAB-35	RAB-50	RAB-100	RAB-150
	Relative contribution to TVOC (%)			
Toluene			1.18	1.45
Hexanal			4.99	
Furfural			0.65	2.58
γ-Terpinene			0.68	
α-Thujene				1.13
α-Phellandrene			0.88	
α-Pinene	11.13	29.78	48.42	8.55
Camphene			1.46	0.75
Dehydrosabinene				1.80
Benzaldehyde			1.88	5.95
Mesitylene				1.18
p-Cymene			1.42	0.95
Sabinene				0.94
β-Pinene		3.89	2.21	0.94
α-Methylstyrene				0.94
2-Pentylfuran			1.84	2.46
3-Carene	5.25	11.00	9.87	2.21
o-Cymene			1.04	1.08
Limonene			1.86	1.44
Naphthalene			0.78	2.88
Methenamine				19.34

At 50 °C, the emission profile continued to be characterized primarily by monoterpenes. α-Pinene remained the dominant compound, while 3-carene and β-pinene were also among the major identified VOCs. Compared with 35 °C, the overall character of the emissions therefore remained relatively similar, although an increase in the total peak area was accompanied by changes in the relative abundance of individual terpene compounds. The results obtained at 35 and 50 °C indicate that under moderate thermal conditions, the emission profile of the investigated particleboards remained relatively stable and was strongly characterized by monoterpenes.

More pronounced changes were observed at 100 °C. Along with the sharp increase in the total VOC peak area, the spectrum of substantially represented compounds became broader. α-Pinene remained the dominant compound, with 3-carene also showing considerable relative abundance. In addition to monoterpenes, hexanal, benzaldehyde, and 2-pentylfuran were identified, together with other terpene compounds such as β-pinene, limonene, camphene, and p-cymene. Thus, although the emission profile at 100 °C remained strongly influenced by terpenes, the presence of oxygen-containing VOCs became more evident.

The occurrence of hexanal at elevated temperature is consistent with the temperature-dependent emission behaviour of wood-based materials reported in previous studies. Jiang et al. (2017) observed increasing aldehyde emissions from particleboards with increasing temperature, with hexanal and pentanal among the relevant compounds. The substantial increase in the total peak area at 100 °C may be associated with enhanced volatilization and release of compounds from the material at elevated temperature. At the same time, higher temperatures may promote processes that contribute to changes in the chemical composition of the overall emission profile.

The most pronounced changes were observed at 150 °C. At this temperature, not only was the highest total VOC peak area recorded, but the character of the emission profile also changed substantially. In contrast to the lower temperatures, α-pinene was no longer the dominant compound, and methenamine showed the highest relative abundance. Other important identified compounds included benzaldehyde, naphthalene, furfural, 2-pentylfuran, and 3-carene. Several additional terpene, aromatic, and aliphatic compounds were also present (Table 1). The emission profile at 150 °C was therefore considerably more complex than those observed at lower temperatures.

The temperature-dependent behaviour of α-pinene provides a clear indication of the changing emission profile. Its relative abundance increased progressively from 35 to 100 °C, reaching its highest contribution at 100 °C. At 150 °C, however, its relative abundance decreased considerably and methenamine became the dominant compound. This decrease in the relative abundance of α-pinene should not be interpreted automatically as a reduction in its absolute emission, since the total VOC peak area at 150 °C was several times higher than at 100 °C. The values presented in Table 1 represent the relative abundance of individual compounds as a percentage of TVOC and therefore primarily reflect changes in the overall chemical composition of the emission profile.

The predominance of methenamine at 150 °C may be associated with chemical processes occurring within the material under more intensive thermal exposure. Van Den Velde et al. (2009) suggested that methenamine formation may be related to reactions involving formaldehyde and nitrogen-containing compounds. At the highest temperature, compounds such as benzaldehyde, furfural, and 2-pentylfuran also became more prominent. Their occurrence, together with the changing relative abundance of monoterpenes, indicates the increasing importance of thermally induced transformations at elevated temperatures. Changes in VOC profiles resulting from thermal exposure have also been reported for softwood, including changes in terpene abundance and the formation of additional volatile compounds (Pohleven et al. 2019).

Overall, increasing temperature resulted in a substantial rise in VOC emission intensity and changes in the chemical composition of the emission profile. While monoterpenes dominated at lower temperatures, the profile became more complex at 150 °C, with methenamine emerging as the dominant compound.

CONCLUSION

The results of this study confirmed that temperature has a significant effect on both the intensity and composition of VOC emissions from particleboards containing recycled plastic derived from automotive bumpers. A relatively moderate increase in the total VOC peak area was observed between 35 and 50 °C, whereas considerably higher emissions occurred at 100 and 150 °C. The highest emission intensity was recorded at 150 °C, where the total VOC peak area was approximately 114 times higher than at 35 °C. In addition to the quantitative increase in emissions, increasing temperature also resulted in substantial changes in the VOC profile. At lower temperatures, the emissions were dominated mainly by monoterpenes, particularly α-pinene and 3-carene. At 100 °C, α-pinene remained the predominant compound, while the presence of oxygen-containing compounds, including hexanal, benzaldehyde, and 2-pentylfuran, became more evident. The most pronounced change in VOC composition occurred at 150 °C, when methenamine became the dominant compound and benzaldehyde, furfural, and 2-pentylfuran were among the more prominent VOCs. These findings demonstrate that elevated temperature not only increases the overall release of volatile compounds but also substantially alters their relative composition. The results provide important information on the thermal emission behaviour of particleboards incorporating recycled automotive plastic and highlight the importance of temperature when evaluating the VOC emission characteristics of such composite materials.

REFERENCES

1. Adeniyi, A.; Agboola, O.; Sadiku, E.R.; Durowoju, M.O.; Olubambi, P.A.; Reddy, A.B.; Ibrahim, I.D.; Kupolati, W.K. Thermoplastic-Thermoset Nanostructured Polymer Blends. In *Design and Applications of Nanostructured Polymer Blends and Nanocomposite Systems*; Thomas, S.; Shanks, R.; Chandrasekharakurup, S., Eds.; William Andrew Publishing: Boston, MA, USA, 2016; pp. 15–38.
2. Bernstein, J.A.; Alexis, N.; Bacchus, H.; Bernstein, I.L.; Fritz, P.; Horner, E.; Li, N.; Mason, S.; Nel, A.; Oullette, J.; Reijula, K.; Reponen, T.; Seltzer, J.; Smith, A.; Tarlo, S.M. The health effects of non-industrial indoor air pollution. *J. Allergy Clin. Immunol.* 2008, *121*, 585–591. https://doi.org/10.1016/j.jaci.2007.10.045.
3. Brown, S. Chamber Assessment of Formaldehyde and VOC Emissions from Wood-Based Panels. *Indoor Air* 1999, *9*, 209–215. https://doi.org/10.1111/j.1600-0668.1999.t01-1-00008.x.
4. Froelich, D.; Maris, E.; Haoues, N.; Chemineau, L.; Renard, H.; Abraham, F.; Lassartesses, R. State of the art of plastic sorting and recycling: Feedback to vehicle design. *Miner. Eng.* 2007, *20*, 902–912. https://doi.org/10.1016/j.mineng.2007.04.020.
5. Gopinath, K.P.; Nagarajan, V.M.; Krishnan, A.; Malolan, R. A critical review on the influence of energy, environmental and economic factors on various processes used to handle and recycle plastic wastes: Development of a comprehensive index. *J. Clean. Prod.* 2020, *274*, 123031. https://doi.org/10.1016/j.jclepro.2020.123031.
6. Hodgson, A.; Beal, D.J.; McIlvaine, J. Sources of formaldehyde, other aldehydes and terpenes in a new manufactured house. *Indoor Air* 2003, *12*, 235–242. https://doi.org/10.1034/j.1600-0668.2002.01129.x.
7. Huang, S.; Wang, H.; Ahmad, W.; Ahmad, A.; Vatin, N.I.; Mohamed, A.M.; Deifalla, A.F.; Mehmood, I. Plastic Waste Management Strategies and Their Environmental Aspects: A Scientometric Analysis and Comprehensive Review. *Int. J. Environ. Res. Public Health* 2022, *19*, 4556. https://doi.org/10.3390/ijerph19084556.
8. Hyttinen, M.; Masalin-Weijo, M.; Kalliokoski, P.; Pasanen, P. Comparison of VOC emissions between air-dried and heat-treated Norway spruce (*Picea abies*), Scots pine (*Pinus sylvesteris*) and European aspen (*Populus tremula*) wood. *Atmos. Environ.* 2010, *44*, 5028–5033. https://doi.org/10.1016/j.atmosenv.2010.07.018.
9. Jiang, C.; Li, D.; Zhang, P.; Li, J.; Wang, J.; Yu, J. Formaldehyde and volatile organic compound (VOC) emissions from particleboard: Identification of odorous compounds and effects of heat treatment. *Build. Environ.* 2017, *117*, 118–126. https://doi.org/10.1016/j.buildenv.2017.03.004.
10. Jones, A.P. Indoor air quality and health. *Atmos. Environ.* 1999, *33*, 4535–4564. https://doi.org/10.1016/S1352-2310(99)00272-1.

11. Kazemi Najafi, S. Use of recycled plastics in wood plastic composites – A review. *Waste Manag.* 2013, *33*, 1898–1905. https://doi.org/10.1016/j.wasman.2013.05.017.
12. Kim, S.; Kim, J.-A.; Kim, H.-J.; Kim, S.-D. Determination of formaldehyde and TVOC emission factor from wood-base composites by small chamber method. *Polym. Test.* 2006, *25*, 605–614. https://doi.org/10.1016/j.polymertesting.2006.04.008.
13. Pohleven, J.; Burnard, M.D.; Kutnar, A. Volatile Organic Compounds Emitted from Untreated and Thermally Modified Wood—A Review. *Wood Fiber Sci.* 2019, *51*, 231–254. https://doi.org/10.22382/wfs-2019-023.
14. Prasanth, S.M.; Kumar, P.S.; Harish, S.; Rishikesh, M.; Nanda, S.; Vo, D.-V.N. Application of biomass derived products in mid-size automotive industries: A review. *Chemosphere* 2021, *280*, 130723. https://doi.org/10.1016/j.chemosphere.2021.130723.
15. Roffael, E. Volatile organic compounds and formaldehyde in nature, wood and wood based panels. *Holz Roh Werkst.* 2006, *64*, 144–149. https://doi.org/10.1007/s00107-005-0061-0.
16. Van Den Velde, S.; Van Steenberghe, D.; Van Hee, P.; Quirynen, M. Detection of Odorous Compounds in Breath. *J. Dent. Res.* 2009, *88*, 285–289. https://doi.org/10.1177/0022034508329741.
17. Wolkoff, P. Impact of air velocity, temperature, humidity, and air on long-term VOC emissions from building products. *Atmos. Environ.* 1998, *32*, 2659–2668. https://doi.org/10.1016/S1352-2310(97)00402-0.
18. Wong, S.L.; Ngadi, N.; Abdullah, T.A.T.; Inuwa, I.M. Current state and future prospects of plastic waste as source of fuel: A review. *Renew. Sustain. Energy Rev.* 2015, *50*, 1167–1180. https://doi.org/10.1016/j.rser.2015.04.063.
19. Yrieix, C.; Dulaurent, A.; Laffargue, C.; Maupetit, F.; Pacary, T.; Uhde, E. Characterization of VOC and formaldehyde emissions from a wood based panel: Results from an inter-laboratory comparison. *Chemosphere* 2010, *79*, 414–419. https://doi.org/10.1016/j.chemosphere.2010.01.062

ACKONWLEDGEMENT

This work was supported by the Slovak Research and Development Agency under the Contract no. APVV-22-0034; and by the Ministry of Education, Research, Development and Youth of the Slovak Republic under the Contract no. VEGA 1/0027/24 and the project UNIVNET "University Research Association for Waste Recovery, especially from the Automotive Industry" No. 0201/0082/19.